ROYAUME DU MAROC
Université Mohammed V - RABAT -
جامعة محمد الخامس – الرباط –
Faculté des sciences
كلية العلوم
CENTRE D'ETUDES DOCTORALES - SCIENCES ET TECHNOLOGIES

N° d'ordre :3199

THESE

En vue de l'obtention du : ***DOCTORAT***

Centre de Recherche : CENTRE DE RECHERCHE DES SCIENCES DES MEDICAMENTS, POLE DE COMPETENCES PHARMACOCHIMIE
Structure de Recherche : LABORATOIRE DE CHIMIE ORGANIQUE HETEROCYCLIQUE
Discipline : Sciences de la Matière
Spécialité : Chimie-physique des matériaux

Présentée et soutenue le : 20/04/2019 par :

Marya RAJI

Elaboration des composites et des nanocomposites à base d'argile marocaine

JURY

ECHAABI Jamal	*PES*	*École Nationale Supérieure d'Électricité et de Mécanique Casablanca*	***Président/ Rapporteur***
BENSSALAH Mohammed Ouadi	*PES*	*Faculté des Sciences, Université Mohammed V, Rabat*	***Rapporteur/ examinateur***
DRAOUI Khalid	*PES*	*Faculté des Sciences, Université Abdelmalek Essaadi, Tétouan*	***Rapporteur/ examinateur***
BOUHFID Rachid	*PhD*	*Directeur de la recherche à la Fondation MAScIR, Rabat*	***Co-encadrant de thèse***
QAISS Abou El Kacem	*PhD*	*Directeur du centre composites nanocomposites à la Fondation MAScIR, Rabat*	***Co-encadrant de thèse***
ESSASSI El Mokhtar	*PES*	*Faculté des Sciences, Université Mohammed V, Rabat*	***Directeur de thèse***

Année Universitaire : 2018-2019

✉ Faculté des Sciences, avenue Ibn Battouta, BP. 1014 RP, Rabat –Maroc
☎ 00212(05) 37 77 18 76 🖷 00212(05) 37 77 42 61 ; http://www.fsr.um5.ac.ma

Je dédie ce travail à

Mes parents et mes chers frères,

Mon époux et à mes beaux enfants.

AVANT-PROPOS

Les recherches qui ont fait l'objet de cette thèse de doctorat ont été réalisées dans le cadre d'une thèse de doctorat à la Faculté des Sciences de Rabat, Université Mohammed V (laboratoire de Chimie Organique Hétérocyclique) en collaboration avec la Fondation MAScIR (Moroccan Foundation for Advanced Science, Innovation and Research) au sein de l'Institut des Nanomatériaux et Nanotechnologies (NANOTECH) (centre des Composites et Nanocomposites) concernant élaboration des composites et des nanocomposites à base d'argile marocaine sous la direction de Mr **El Mokhtar ESSASSI**, **Mr Abou El Kacem QAISS** et **Mr Rachid BOUHFID**. Ce travail n'aurait pu aboutir sans la contribution de nombreuses personnes. Je les remercie sincèrement.

Tout d'abord, je tiens à remercier infiniment **Mr. El Mokhtar ESSASSI**, PES à l'université Mohammed V, d'avoir accepté la direction de ce travail et pour l'aide qu'il a toujours su m'apporter avec enthousiasme tout au long des années de thèse. Je lui suis très reconnaissante pour sa patience, ses conseils et ses remarques constructives m'ont été de précieux piliers dans la réalisation de ce travail.

J'adresse mes vifs et sincères remerciements à mon co-encadrant de thèse, **Mr Abou El Kacem QAISS**, autant que directeur du centre composites et nanocomposites au sein de la fondation MAScIR, pour la qualité des nombreux conseils, l'engagement, la disponibilité, l'orientation, l'encouragement, aussi leur esprits responsables, critiques et rigoureux tout au long de mon travail. Grace à ses aides j'ai pu réaliser ce travail.

Je tiens à témoigner toute ma reconnaissance et mes sincères remerciements à **Mr Rachid BOUHFID,** directeur de la recherche au sein de la fondation MAScIR et autant que co-encadrant de thèse, pour sa patience, sa disponibilité et surtout ses judicieux conseils chimiques, qui ont contribué à alimenter ma réflexion et aussi diriger mes recherches.

Mes remerciements vont aussi au **Mr. Jamal ECHAABI,** PES à École Nationale Supérieure d'Électricité et de Mécanique de Casablanca, pour avoir accepté de participer au jury de cette thèse et de présider mon jury de thèse de doctorat. Je lui adresse mes remerciements les plus respectueux ainsi d'avoir accepté de juger ce travail comme rapporteur.

Je remercie également le **Mr. Mohammed Ouadi BENSALAH**, PES à l'université Mohammed V premièrement pour l'aide et le soutien qui m'a apporté et deuxièmement pour le temps consacré à la lecture de ce rapport pour le juger en tant que rapporteur de thèse et examinateur.

Je tiens à exprimer mes sincères reconnaissances au **Mr. Khalid DRAOUI,** PES à université Abdelmalek Essaadi de Tétouan d'avoir accepté de juger ce travail comme rapporteur et examinateur.

Je remercie également **Mr Hamid ESSABIR** pour sa gentillesse, le partage des connaissances scientifiques, sa collaboration, et son esprit d'équipe ainsi que son aide documentaire et ses encouragements.

Je remercie aussi du fond du cœur mon mari **Mehdi AIT DAHI** en tant que technicien de laboratoire de mise en œuvre à MAScIR pour son aide et sa disponibilité durant la réalisation de la partie expérimentale de ce travail. Il faut reconnaître que je n'en serai pas arrivé à ce point sans son soutien et son aide précieuse et qui m'a apporté beaucoup de joie durant ma vie de doctorante.

Je remercie vivement pour le soutien financier : les dirigeants de MAScIR et en précisément **Mme. Hanane BAYAHYA** pour son support et soutient tout au long de cette période de thèse.

Un grand merci pour mes parents, mon frère et mes sœurs pour leurs encouragements et leurs soutiens.

Pour terminer, je voudrais exprimer mes remerciements à toutes les personnes, qui de loin ou de près ont participé au bon déroulement de ce travail et ainsi à mes collègues de centre composites et nanocomposites.

RESUME

Le présent travail a été réalisé dans le cadre d'une thèse de doctorat à la Faculté des Sciences de Rabat, Université Mohammed V-Agdal (laboratoire de Chimie Organique Hétérocyclique) en collaboration avec la Fondation MAScIR (Moroccan Foundation for Advanced Science, Innovation and Research) au sein de l'Institut des Nanomatériaux et Nanotechnologies (NANOTECH) (centre des Composites et Nanocomposites) concernant élaboration des composites et des nanocomposites à base d'argile marocaine.

Nous avons envisagé l'élaboration de nouveaux composites et nanocomposites à base de plusieurs types d'argile (kaolinite, illite, perlite, montmorillonite, sépiolite et halloysite), connus pour leurs propriétés spécifiques et possédant également une densité faible, un coût faible. Nous avons modifié chimiquement les particules d'argiles par l'intercalation des molécules chimique (surfactant) ou par l'utilisation des agents de couplage, puis l'exfoliation des feuilletés d'argile durant la mise en œuvre des nanocomposites. Des études des propriétés mécaniques, thermiques et rhéologiques ont été également effectuées. De même, la capacité d'absorption d'eau a été examinée.

Mots Clés : composites, argile, fonctionnalisation, propriétés mécaniques, propriétés rhéologiques.

ABSTRACT

The present work was done as part of a doctoral thesis at the Faculty of Sciences of Rabat, Mohammed V-Agdal University (Laboratory of Heterocyclic Organic Chemistry) in collaboration with the MAScIR Foundation (Moroccan Foundation for Advanced Science, Innovation and Research) within the Institute for Nanomaterials and Nanotechnologies (NANOTECH) (Composites and Nanocomposites Center) for the elaboration of composites and nanocomposites based on Moroccan clay.

We have considered the development of new composites and nanocomposites based on several types of clay (kaolinite, illite, montmorillonite, sepiolite and halloysite), known for their specific properties and also having a low density, a low cost. We chemically modified the clay particles by intercalation of the chemical molecules (surfactant) or by the use of coupling agents, then the exfoliation of the clay sheets during the implementation of the nanocomposites. Studies of mechanical, thermal and rheological properties were also carried out. Similarly, the water absorption capacity was examined.

Keywords: composites, clay, chemical modification, mechanical properties, physicochemical properties.

TABLE OF CONTENTS

Chapitre I

Literature Review

Chapitre II

Effect of clay structure and particle content on thermoplastic composites properties: mechanical, thermal, rheologic and hygroscopic properties.

Chapitre IV

Effect of clay-intercalation process on the thermoplastic nanocomposites' properties: mechanical, thermal, and optical properties.

LIST OF FIGURES

LIST OF TABLES

ABREVIATIONS

OMC : Organic matrix composites
CMC : Ceramic matrix composites

MMC: Metal matrix composites

PP: polypropylene

HDPE: high density polyethylene

SEBS-g-MA: Styrene-(ethylene-butene)-styrene triblock copolymer grafted with maleic anhydride

SEM: Scanning electron microscopy

WAXD: Wide-angle X-ray diffraction

FTIR: Fourier transforms infrared spectra

TGA: Thermogravimetric analysis

DSC: Differential scanning calorimetry

DMA: Dynamic mechanical analysis

RSA: Rheometer Solid Analysis

XRD: X-Ray Diffraction

BET: Brunauer-Emmett-Teller

BJH: Barrett-Joyner Halenda

LOI: Loss on ignition

ΔHm: melting enthalpies

Tm: Melting temperatures

Tc: crystallizing temperatures

APTES : 3-aminopropyltriéthoxysilane

VTMS : vinyltriméthoxysilane

MMT-Na: Montmorillonite

SEP: Sepiolite

Hallo: Halloysite

PA6 : polyamide 6

DMSO dimethylsulfoxide

MeOH: methanol

CTAB: cetyltrimethyl ammonium bromide

TEOS : triethoxy(octyl)silane

NaOH: sodium hydroxide

Introduction, Originalité et Objectifs

INTRODUCTION GENERALE

Au cours des dernières années, la majorité des recherches sur les matériaux a été orientée vers les matériaux composites basés sur des charges naturelles pour le renforcement des matrices polymériques [1]. Ces matériaux composites, présentent un grand intérêt dans le domaine de l'automobile, l'emballage alimentaire, la construction et dans des applications électriques [1]. En raison de leurs caractères spéciaux, les charges naturelles sont renouvelables avec un faible coût et une faible densité, ce qui permet de réduire par la suite le poids des matériaux composites [3]. Dans les matériaux composites à matrice polymérique, le renforcement naturel peut être organique ou inorganique [9]. Les charges organiques utilisées sont les fibres naturelles, telles que les fibres de coco, les coquilles d'argan, doum, les fibres de chanvre, les fibres d'Alfa, les fibres de pomme de pin [4-7], etc. Les charges inorganiques sont à titre d'exemple, le graphène, le carbonate de calcium, l'argile [8-9] …etc. L'utilisation de l'argile comme charge pour les polymères, peut réduire le coût des matériaux. En plus, les argiles n'ont pas des effets indésirables sur l'environnement [8].

Les propriétés globales des composites renforcés par des argiles ne sont pas influencées que par les caractéristiques d'argile utilisées (Taille ; forme ; structure), du pourcentage des charges, ainsi que leur dispersion [12-13] et distribution dans la matrice thermoplastique, mais aussi par les procédés de fabrication utilisés et l'adhésion interfaciale entre les polymères et la surface des particules d'argile [11]. Pour disperser les particules d'argile dans la matrice polymère, différentes techniques peuvent être utilisées comme le procédé des sols gels, la polymérisation in situ, et le mélange à l'état fondu [14]. Ce dernier est le plus utilisé pour élaborer les composites avec une grande homogénéité, une grande dispersion et une meilleure distribution des charges. En plus, le malaxage à l'état fondu a un coût effectif qui intéresse les industries de plasturgie [15]. D'une autre façon, la polarité des grains d'argile est une factrice importante pour résoudre le problème l'adhésion entre les particules et la matrice polymère. L'argile est hydrophile ; alors que le polymère est d'une nature hydrophobe. Les méthodes chimiques les plus appropriées pour la modification de la surface de l'argile sont l'utilisation d'acides aminés, les sels d'alkyle ammoniums organiques, ou phosphonium organique [16-18]. En plus, pour des polymères sans groupes fonctionnels polaires tels que le polypropylène (PP) et polyéthylène (PE), on applique couramment les techniques de greffage des groupements fonctionnels polaires où on ajoute des polymères greffés au cours du traitement afin d'améliorer l'affinité entre l'argile hydrophile et le polymère hydrophobe.

ORIGINALITÉS

L’originalité de ce travail se décompose en quatre points principaux :

- L’utilisation de différentes structures d'argile à différentes dimensions pour élaborer de nouveaux composites et nanocomposites à base de polymère thermoplastique avec des propriétés physico6chimiques spécifiques.
- L'utilisation de différentes morphologies d'argile à l'échelle microscopique et nanométrique pour préparer des composites et les nanocomposites thermoplastiques.
- Utilisation d'un procédé chimique pour la purification de l'argile.
- Préparation d'argile intercalée à base des argiles gonflant et non-gonflant.

OBJECTIFS

Les différents objectifs fondamentaux de cette thèse sont :

- La valorisation des roches argileuses prélevées des gisements marocains comme renfort dans les matières plastiques et l'identification des différents types d'argile.
- L'amélioration des propriétés optiques et thermiques des argiles marocaines ou commerciales par purification mécanique ou chimique ou bien par l'utilisation de fonctionnarisation chimique.
- Étude de l'effet de l'incorporation d'argiles de structure soit cristalline ou amorphe et de différentes morphologies (nano-fibres, nano-feuilles, nanotubes, sphère) avec et sans modification chimique dans les matrices polymères à différents taux de charge pour améliorer les propriétés mécaniques et rhéologiques des composites.
- Préparation d'organo-argile à base d'argile gonflants ou non-gonflants utilisant différentes molécules chimiques pour améliorer l'adhérence de surface entre les particules et la matrice polymère.
- De plus, étudier l'effet de la méthode de mise en œuvre sur les propriétés des composites et l'utilisation de la masse fondue comme processus vert pour avoir une bonne distribution et dispersion des particules d'argile dans la matrice et pour avoir une exfoliation partielle des organo-argiles afin de diminuer les particules taille au niveau nanométrique.
- Par ailleurs, l'examen des propriétés hygroscopiques des composites par modélisation.
- Et enfin, améliorer les propriétés globales des composites et nanocomposites.

Introduction, Originality and Objectives

GLOBAL INTRODUCTION

In recent years, natural-based composites for polymeric matrix reinforcement were an easy and effective recipe to obtain new materials with desired properties [1]. These composite materials have a great interest in the field of automotive, food packaging, construction and electrical applications [1]. Due to their special characteristics, natural fillers are renewable with low cost and low density, which in turn reduces the weight of composite materials [3].

In composite materials, natural reinforcement can be organic or inorganic [9]. The organic fillers used are natural fibers, such as coconut fibers, argan shells, doum, hemp fibers, Alfa fibers, pine cone fibers [4-7], and so on. Inorganic fillers are, for example, graphene, calcium carbonate, clay [8-9], etc. The use of clay as a filler for polymers can reduce the cost of materials, with less weight, low moisture absorption, and the low density. In addition, clays do not have undesirable effects on the environment [8].

The overall properties of clays reinforced composites are not only influenced by the general characteristics of the used clay (Size, shape, structure), the percentage of fillers, and their dispersion [12-13] and distribution in the thermoplastic matrix. Also, by the manufacturing processes used and the interfacial adhesion between the polymer's matrix chains and the clay particles surfaces [11]. To disperse the clay particles in the polymer matrix, different techniques can be used such as the solution intercalation, in situ polymerization, and melt-mixing [14]. The latter is the most used to develop the composites with a great homogeneity, a great dispersion and a better distribution of the fillers. In addition, melt blending has an effective cost that is of interest to the plastics industry [15]. In another way, the polarity of the clay particles is an important factor in solving the problem of adhesion between the particles and the polymer matrix. Clay is hydrophilic; while the polymer is of hydrophobic nature. The most appropriate chemical methods for modifying the surface of the clay by using different organic molecules such as amino acids, organic alkyl ammonium salts, or organic phosphonium [16-18]. In addition, for polymers without polar functional groups such as polypropylene (PP) and polyethylene (PE), the grafting techniques of the polar functional groups are commonly applied, in which graft polymers are added during the treatment in order to improve the affinity between the hydrophilic clay and the hydrophobic polymer.

ORIGINALITIES

The originality of this work is divided into four principals' points:

- The use of different clay structures at different dimensions to prepare new structured composites and nanocomposites based on the thermoplastic polymer with specific physicochemical properties.
- The use of different clay structure at microscale and nanoscale dimension to prepare the thermoplastic composites and nanocomposites
- Use of chemical process for clay purification
- Preparation of intercalated clay based on the swelling and non-swelling clay.

OBJECTIVES

The different basic objectives of this thesis are:

- The valorization of clay rocks extracted from Moroccan regions in plastic materials and the identification of the different types of clay.
- The improvement of the optical and thermal properties of Moroccan or commercial clays by mechanical or chemical purification or by the use of chemical functionalization.
- Studied the effect of the incorporation of clays of crystalline or amorphous structure and of different morphologies (nano-fibers, nanosheets, nano-tube, spherulite) with and without chemical modification into the polymer matrices at different loading rates to improve the mechanical and rheological properties of the composites.
- Preparation of organo-clay based on swelling or non-swelling clays using different chemical molecules to enhance the surface adhesion between particles and polymer matrix
- In addition, study the effect of the method of implementation on composites properties and the use of melt compounding as a green process to have a good dispersion distribution of clay particles and to have a partials exfoliation of organo-clays in order to decrease the particles size to the nanoscale level.
- Furthermore, the examination of the hygroscopic properties of composites by modeling.
- And finally, enhance the overall properties of the composites and nanocomposites.

Chapitre I

Literature Review

Résumé

Ce premier chapitre comprend trois axes. Le premier regroupe les classes des matériaux composites selon le type de la matrice utilisée et la morphologie ou la forme du renfort. Dans la seconde partie, les méthodes de préparation des composites polymères comprennent trois stratégies principales ; intercalation en solution, intercalation avec polymérisation in situ et l'intercalation par voie fondue. La dernière partie traite les différentes structures d'argiles et les différentes structures des composites polymère-argile en tenant compte la structure d'argile utilisée.

I.1. Introduction

The composite materials are the result of a combination of at least two phases where the reinforcement element and the matrix are integrated in order to improve the properties of the composites. The use of composite materials is slowly emerging from the realm of advanced materials [1–3], allowing them to invade more and more space both in the academic and industrial fields such as automotive, wind energy, aeronautics, and civil applications...etc. [4,5]. These kind of materials are replacing conventional materials due to their interesting performances like as improved mechanical, thermal and electrical properties and also to offset the high price of the matrices [6–9]. Several studies have shown that the composites materials filled by natural or synthetic loading are provided several advantages over other materials such as good durability, high corrosion resistance, and low density [10–12]. However, The key culprits to the lack of their structural properties were the manufacturing approach [9], shaping and mainly the state of interphase links [13]. There are also numerous factors that have a direct impact on the mechanical behavior of composite materials, such as active mechanisms of various constitutive elements [14], for example: the volumetric fraction [15–17], morphology [18,19], distribution [20], dispersion [21,22] and the state of interfaces and content's dispositions [23]. Accordingly, these microscopically elements are the influenced factors on the composite material properties.

In general, the particles reinforcement can be synthetic or natural as mentioned before [24] [8]. Typical examples are layered materials such as graphite [25], silicate [2], graphene, and some kind of clays [26]), or fiber-like materials such as carbon nano-tubes and nano-fibers [4], sepiolite [2], or cellulose nano-fibers [11]. Although the inorganic natural fillers are currently dominating the plastic industry, the use of clays is still growing because they have shown the effectiveness of enhancing of polymer composite properties [10,27]. As like mechanical properties enhancement [28] and thermal stability improvement [29], decreases also the gas and liquid permeability [2,30] are shown to improve the flame retardancy [31], without affecting the optical properties of the base polymer [27]. Generally, clay particles are naturally hydrophilic [32]. This character makes them difficult to mix and interact with most polymer matrices, which are hydrophobic [33]. For these reasons, clays must be surface treated before their incorporation into a polymer matrix to make high-quality composites by ensuring good dispersion-distribution and great interfacial adhesion between clay surface and polymer chain [34]. Clay surface can be modified using different kind of organic compounds based on the attachment of these latter to the clay particles by the different way is in depend on clay structure. The most commonly used are alkyl ammonium [35], sulfonium [36], and phosphonium [37] ions.

Therefore, the chapter covers the different classes of composites materials and the different routes of composites preparation. And in the last part to do this, this content deals with two parts, the first one focuses on clays, their structures, their properties and the processes allowing to modify the clay surfaces to make it adequate to that of the matrix polymer chains. In the second part, the different polymers-clays structures are discussed in depth.

I.2. Classification of composite materials

A composite material or simply composite, from Latin composĭtus, is a complex material made of an assembly of two or more distinct phases (matrix phase and dispersed phase) [2], and having majority properties significantly different from those of any of the constituents [38]. The primary phase is the matrix named continuous phase characterized by more ductile and less hard [39]. The secondary phase called dispersed phase is the reinforcing phase embedded within the matrix, generally stronger than the primary phase and it is the responsible for enhancing one or more properties of matrix [40–42]. The main advantages of composite materials in structural applications that have the following characteristics [43].

- Composite is a multi-phase material consist of two or more physically distinct components and mechanically separable materials [44].
- Composite are made by mixing the components in a controlled way to achieve an uniform dispersion of the constituents leading to an optimum properties [45].
- Composite mechanical properties are superior to the properties of each individual components and in some cases uniquely different from the properties of their constituents [46].

Composite materials have been widely used in the practical applications because of their many advantages: high strength and modulus to weight ratio, easy processability and cost effective. furthermore, their flexibility in material and structure design [47].

I.2.1. Classification in accordance with the type of matrix material.

The choice of the matrix is driven by their industrial application depending upon many factors such as resistance to atmospheric agents or the operating environment, mechanical properties and cost [48]. The matrix plays two key roles in composite materials: first, transferring the load to the reinforcement and secondly protect the reinforcement against chemical attacks and adverse environmental effects [49]. The matrix may serve also as a barrier to crack propagation. Composites can be grouped into three categories depending upon the matrix:

- **Organic matrix composites (OMC),**

Polymer Matrix Composites are composed of two distinct categories of polymers that are generally considered [50]: thermoplastics and thermosetting [51]. The difference between them all depends on a curing or crosslinking reaction that either does or does not occur during the molding process.

  - Thermoset matrix are not recyclable because of their irreversible cross-linking process. Their easy implementation allows, in particular, the production of large parts. The thermoset matrix like as (Unsaturated Polyester (UP), Epoxy (EP))
  - Thermoplastic matrix are recyclable polymers that can soften under the effect of temperature as like (Polycarbonate (PC), Polyvinylchloride, Nylon, Polysterene).

- **Ceramic matrix composites (CMC),**

Ceramic Matrix Composites are composed of a ceramic matrix and embedded fibers of other ceramic material (dispersed phase) [52].

- **Metal matrix composites (MMC)**

Metal Matrix Composites are composed of a metallic matrix [53,54] (aluminum, magnesium, iron, cobalt, copper) and a dispersed ceramic (oxides, carbides) or metallic (lead, tungsten, molybdenum) phase

While the two last composites types (MMC) and (CMC) are suited for industrials applications in which hardness, thermal stability, high-temperature or corrosion resistance are critical, their use is limited by the high manufacturing costs. The most widely used composites are those based on a polymeric matrix because they often used as lightweight metal replacements and have the advantages of being lightweight, stiff, and strong, low density, their simplicity of manufacture and generally their relatively low manufacturing costs [55]. Considering the huge range of potential polymer matrix materials that can be combined with a number of different reinforcement types, which themselves can be arranged in various different architectures, the range of OMCs becomes apparent.

I.2.2. Classification in accordance with the type and form of reinforcements

Reinforcements are strong materials with a particular morphology that is incorporated into the matrix to improve composite's physical properties [56]. The different reinforcements used in composites have different properties and so affect the properties of the composite in different ways

[57]. Consequently, the properties of composites are a function of the properties of this dispersed phase, its relative amounts, and its morphology, which mean that the composites can be classified according to their types of reinforcements [58,59]. They are thus divided into four categories:

I.2.2.1. Fiber reinforcements

The reinforcements of this type of composites are in the form of fibers. The length of the fibers is much greater than the dimensions of its cross-section [60,61]. According to their applications, the fibers used take two form, see figure (I-1):

- **Short-fiber reinforced composites.** Short-fiber reinforced composites consist of a matrix reinforced by a dispersed phase in form of discontinuous fibers (length < 100*diameter) [62,63].
    - Composites with random orientation of fibers.
    - Composites with preferred orientation of fibers.

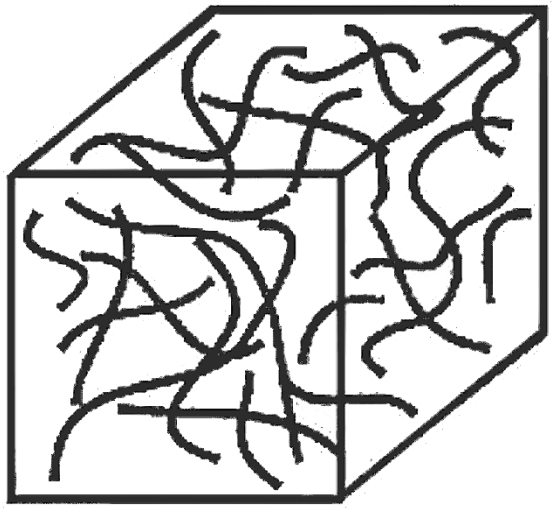

Figure I-1: short fiber reinforced composite

- **Long-fiber reinforced composites.** Long-fiber reinforced composites consist of a matrix reinforced by a dispersed phase in form of continuous fibers, see figure (I-2).
    - Unidirectional orientation of fibers.
    - Bidirectional orientation of fibers (woven).

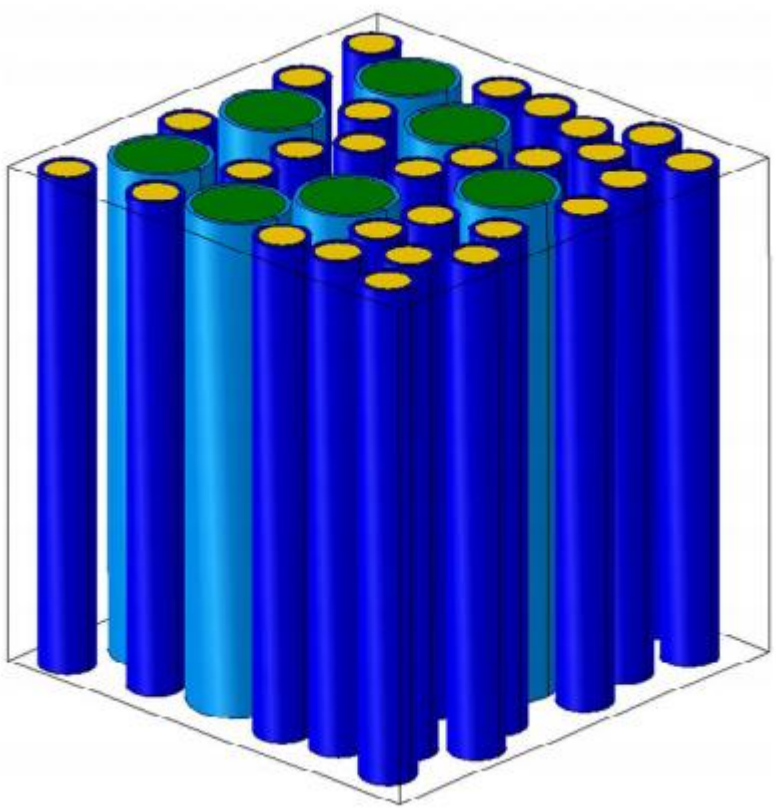

Figure I-2 : long fiber reinforced composite

I.2.2.2. Particulate reinforcements

The reinforcement is considered as hard particles dispersed in the less rigid matrix if all its dimensions are approximately equal and small in front of the other dimensions of the material [21,64,65] , see figure (I-3).

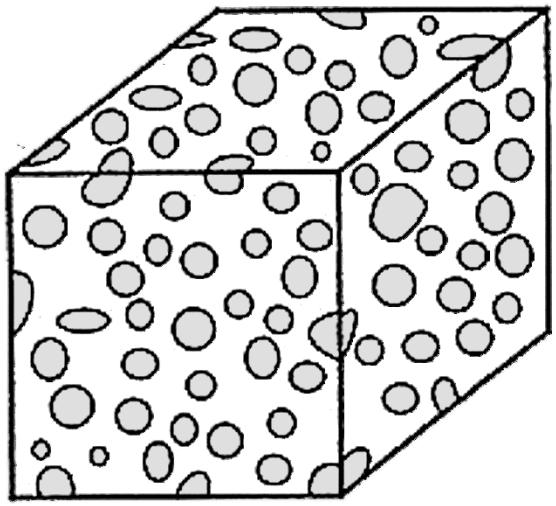

Figure I-3: particulate composite

I.2.2.3. Flake reinforcements

The flakes have a very small dimension compared to the other dimensions [66]. However, the flakes can be arranged in parallel so as to have more uniform properties in the plane, see figure (I-3). Classification based on geometry of reinforcement:

- Composites with random orientation.

The dispersion of this type of reinforcement is generally random

- Composites with preferred orientation.

Dispersed phase of these materials consists of two-dimensional flat platelets (flakes), laid parallel to each other, see figure (I-4).

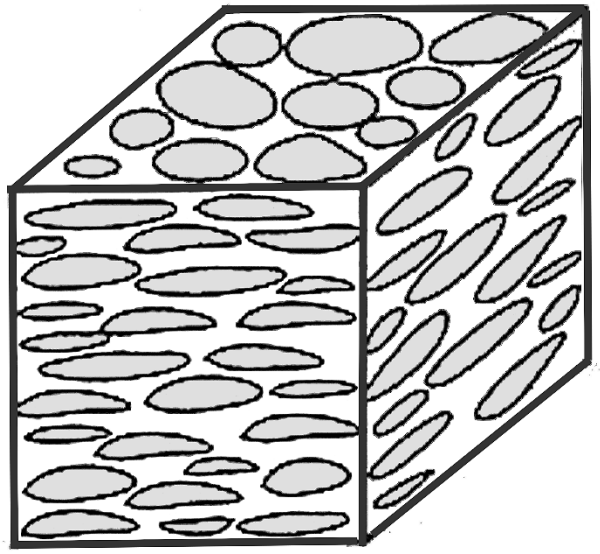

Figure I-4: flake composite

I.2.2.4. Hybrid Composite Materials (More than one element of distinct reinforcements)

Several recent studies have shown that the combination of two or more types of reinforcement in the same matrix makes it possible to improve the mechanical and thermal properties of the composite [67–69]. It may be a combination of the reinforcing elements of different shapes and/or natures, as in the case of hybrid composite reinforced by the clay particles and the natural fibers [70–72].

In principle, it appears that in order to have a valuable hybrid composite material the reinforcement elements must not exceed two types. These materials can bring new functionalities and can therefore meet technical and/or economic requirements in an efficient way than conventional composite materials [73], see figure (I-5).

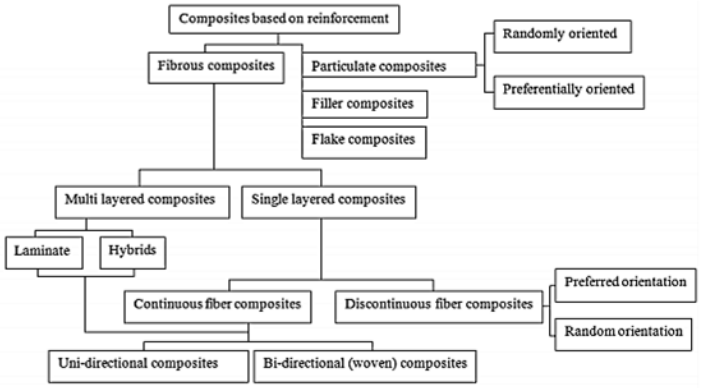

Figure I-5 : composites classifications in depending on reinforcements [73]

I.3. Polymer composites preparation

Polymer matrix composites can be prepared either by a chemical or mechanical process. The homogeneous dispersion of charge in the polymer matrix is one of the real problems encountered in polymer nanocomposite fabrication. In general, the majority of fillers have a tendency to aggregate and form micron size filler cluster, which deteriorates the overall properties of composites. Many attempts have been made to disperse fillers uniformly and homogeneously into a polymer matrix, different techniques were proposed such as solution intercalation [74,75], in situ polymerization [64,76], and melt blending [77,78]. The latter is the most commonly used process since several parameters can be controlled to improve homogeneity and get good dispersion/distribution [6,28]. Melt blending is also cost-effective and quite attractive for polymer processing industries. In the case of the composite with nano-charge that might at a very lower mass fraction, instead of mixing individual additives, it could be using a masterbatch to good pre-disperse the charge [79]. The masterbatch is a very concentrated mixture of reinforcement dispersed in the used polymer matrix prepared by first mixing the particles reinforcement with a polymer at high concentration rate to obtain a masterbatch, which is thereafter diluted to the desired content [80,81].

I.3.1. In-situ polymerization

In-situ polymerization is a conventional technique used for both thermoplastic and thermoset composites synthesis. This process has been applied for the swelling the fillers into polymer matrix, and then a curing agent is added to initiate the polymerization [82,83]. The mixture is generally polymerized either using radiation, heat, initiator diffusion or by organic initiator.

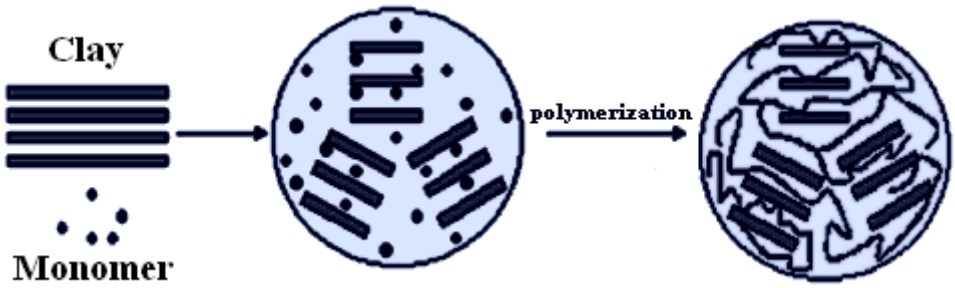

Figure I-6 : In-situ polymerization process

I.3.2. Solution intercalation

Solution intercalation is based on a solvent system in which the common solvent or solvent mixture is used to disperse the clay particles and then the polymer or pre-polymer is solubilized using the same solvent [84].

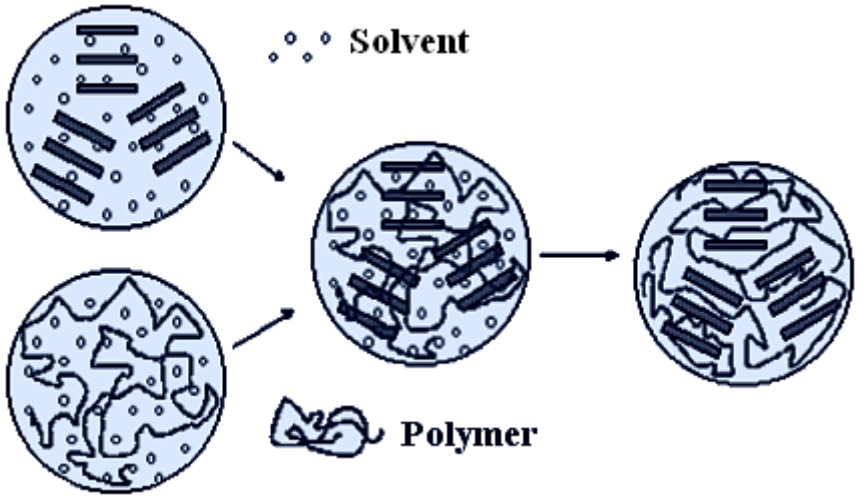

Figure I-7 : Solution intercalation process

I.3.3. Melt compounding

This method involves blending a molten thermoplastic with reinforcement particles , then annealing at a temperature above the glass transition temperature of the polymer to form a composite using the shear stress (hydrodynamics force) [84].This procedure is the most commonly used process since several parameters can be controlled to improve homogeneity and get good dispersion/distribution. Melt blending is also cost-effective and quite attractive for polymer processing industries.

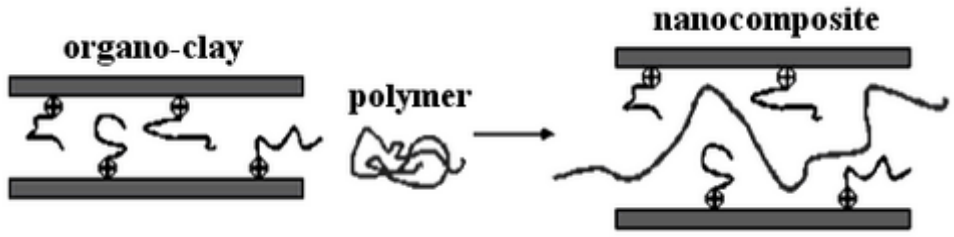

Figure I-8 : Melt compounding process

I.4. Polymer-Clay Composites

The development and progression of environmentally friendly/green nanocomposites materials, will not only benefit on the plastic industry, but would lead to reduce the percentage of the expensive polymer used in the manufacture of materials, such as polypropylene, polyethylene, polyacrylic, polyester and epoxies etc. They are hazardous to the environment, non-degradable and take a long time to decompose, which generates huge many environmental problems associated with their disposal, including damage to the environment eco-system, water supplies, and sewer systems as well as to the lakes, rivers and streams. Furthermore, they are non-renewable; and their high price and unstable with impending depletion of petroleum resources [85].

The incorporation of natural particles in the polymer composites can reduce their production cost, through the substitution of small amount of polymer by a cheap and abundant resource may be organic or inorganic include layered materials such as graphite, and some clay types, or fiber-like materials namely carbon tubes and fibers, cellulose fibers or other types of clay [86]. Among these particles loading, the different kinds of clay reinforcement have been proven an unavoidable synergistic impact on the overall performance of the composites, due to its special structure, which is most thermally stable and is arranged on the micrometric or nanometer scale with a high aspect ratio and/or an enormously large surface interface with the polymer. In this regard, the low cost, less weight, low moisture absorption and the low density makes the clay an attractive alternative to organic or petrochemical-based loading [87].

I.4.1. Clay structure

The clay has become a class of organic-inorganic hybrid materials with potential uses in polymer composites, as rheological modifiers, gas absorbents, flame retardancy and drug delivery carriers... To fully understand the effect of clay reinforcement on the polymer matrix properties, it is important to highlight the clay definition and their structure. The term clay mineral is difficult to define. From chemical point of view, this term signifies a class of the broad category of hydrated

phyllosilicates, likewise, based on geo- logical knowledge, this clay making up the fine-grained fraction of rocks, sediments, and soils. Far from this definition which create some ambiguity until the moment, and for roughly speaking, clay minerals are essentially hydrous aluminosilicates with very fine particle size and a general chemical formula (Ca, Na, H)(Al, Mg, Fe, Zn)$_2$(Si, Al)$_4$O$_{10}$(OH)$_2$−xH$_2$O, where x represents the variable amount of water [88]. Generally, the clay minerals may be broadly classified into two categories: natural and synthetic clays Include Montmorillonite, Hectorite, sepiolite, laponite, saponite, rectorite, bentonite, vermiculite, biedellite, kaolinite, chlorite, as a natural clays and the synthetic one such as various layered double hydroxides, synthetic Montmorillonite, Hectorite, etc. [89,90].

Generally, the structures of clay minerals are composed of alternating of tetrahedral silica sheets "SiO_2" and alumina octahedral layers "AlO_6" in different ratios. Firstly, 1:1 when one octahedral sheet is linked to one tetrahedral sheet as Kaolinite, Halloysite [91,92]. Secondly, 2:1 this structure created from two tetrahedral sheets sandwiching an octahedral sheet such as Montmorillonite and Sepiolite [64,93]. Finally the proportion of 2:1:1 (chlorite), this latter are not always considered as clay, sometimes being classified as a separate group within the phyllosilicates [76]. One side of this lamella remains linked to each other through common oxygen atoms, seen figure (I-9).

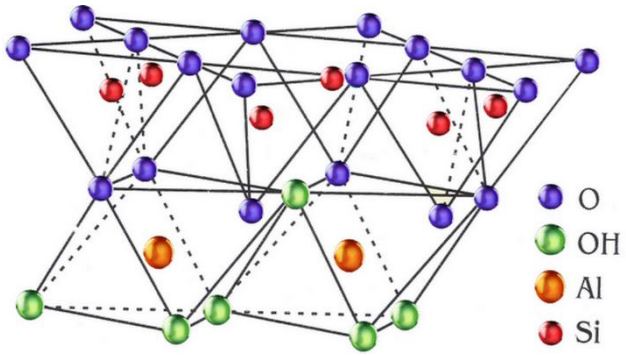

Figure I-9 : clay structure

Clay, sometimes being classified as a separate group within the phyllosilicates. One side of this lamella remains linked to each other through common oxygen atoms and generally has a physical dimension may be about one nm in thickness and the lateral dimension is varied from 30 nm to several micrometers or even larger, depending on particular silicate, due to an isomorphic substitution of alumina cation (Al3+) within the silicate layers [94]. In consequently, the clay platelet undergoes a structural rearrangement to give different structures (nano-fibers, nano-tubes, and plate-like filler), see figure (I-10).

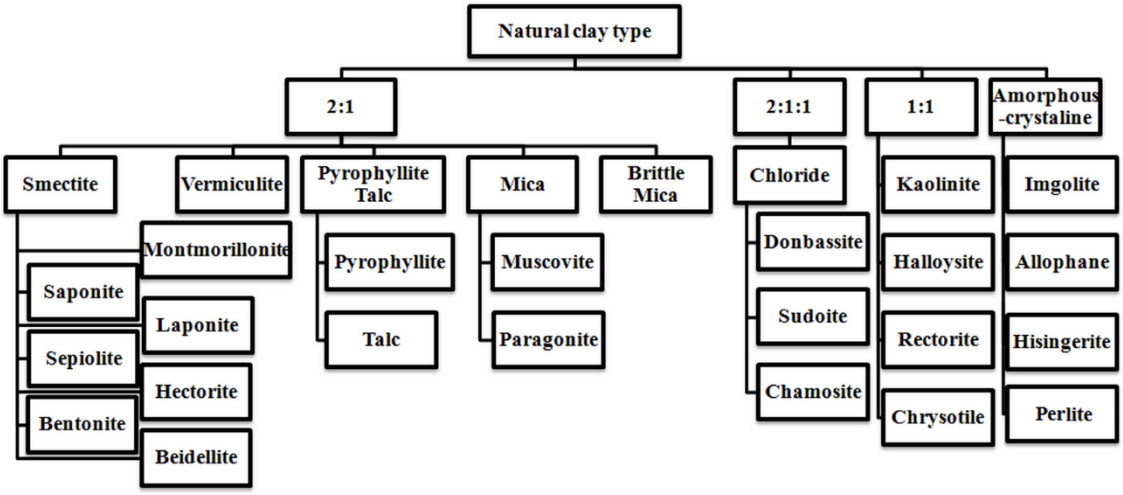

Figure I-10 : Natural clay type

I.4.2. Structure polymer-Clay composites

Depending on the composite's components (polymer matrix, surfactant cations, and coupling agents) and the manufacturing methods (in-situ polymerization, solution intercalation, and melt intercalation), three possible types of nanocomposites structure can be obtained. The literature commonly refers to three types of conventional composites morphology: flocculated, intercalated, and exfoliated composites [95]. Figure (I-11) illustrate the different clay dispersion into polymer matrix.

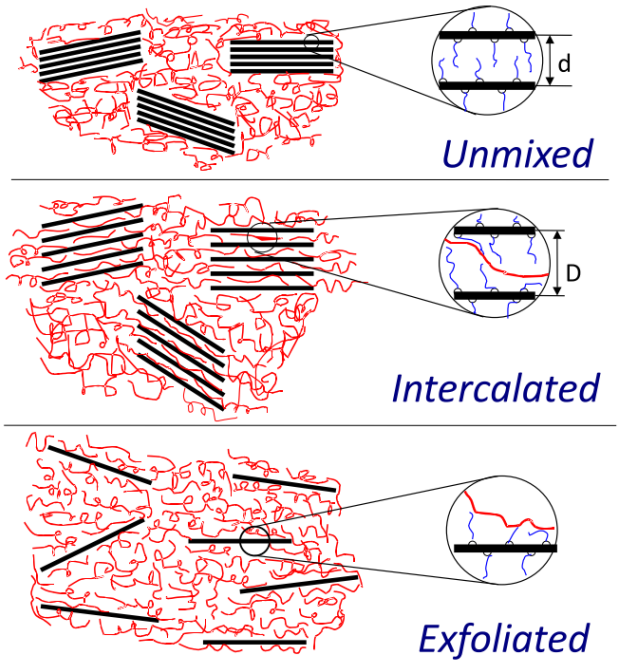

Figure I-11 : the different states of dispersion of clays in polymers

I.4.2.1. Flocculated composites,

flocculated composites called also microcomposite (immiscible or conventional) composite is obtained when the polymer chains are not at all intercalated between the clay sheets, which testifies to a phase-separated composite formation [96]. This type of composite maintains the immiscibility between the macromolecular chains of polymer and inorganic clay. In this case, a minimal reinforcement by the clay particles will be obtained and, thus, the enhancement in the composite properties is negligible [97].

I.4.2.2. Intercalated nanocomposites

The intercalation nanocomposite is the state in which the polymer molecule chains diffuse into the inter-galleries of the clay structure in such a way that the interlayer spacing between clay sheets is expanded up to several times the original value with a repeat distance of a few nanometers [98]. This intercalation facilitate the penetration of the polymer chains into the interlayer galleries of the clay, then the properties of the intercalated composites improved as compared to the conventional composite [99].

I.4.2.3. Exfoliated nanocomposites

Exfoliated or fully delaminated nanocomposites are the preferred configuration, in which the clay sheets are completely and uniformly separated and dispersed in a continuous polymer matrix to the individual 1 nm thick layers [73]. Such a structure allows the maximum reinforcement because of the proper clay distribution and the miscibility of clay sheets resulting in a large surface area. The structure and properties of the resulting nanocomposites can be altered by controlling the polymer-clay interactions. However, there is usually some degree of combined intercalated and exfoliated clay [88].

I.5. Conclusion

Polymer-clay composites are increasingly utilized in many engineer applications because they offer many enhanced properties and various advantages over traditional composites materials such as improved mechanical, thermal and electrical properties and also to offset the high price of the matrices offered by the specifics properties of clay particles like as good durability, high corrosion resistance, and low density [10–12]. Several studies have provide that there is numerous factors that have a direct impact on the mechanical behavior of composite materials, such as active mechanisms of various constitutive elements [14], for example: the volumetric fraction [15–17], morphology [18,19], distribution [20], dispersion [21,22] and the state of interfaces and contents dispositions [23,100]. In this chapter, we have reviewed the different classes of composites materials, their different routes of composites preparation. Besides, we have reviewed the clays structures, their properties and their different polymers-clays structures.

Chapitre II

Effect of clay structure and particle content on thermoplastic composites properties: mechanical, thermal, rheologic and hygroscopic properties.

Résumé

Ce chapitre est consacré à l'étude de l'effet de la structure argileuse ; cristalline (illite) ou amorphe (perlite) sur le comportement général des composites à base des polymères thermoplastiques. Généralement, nous avons produire des nouveaux composites de polymère avec des propriétés spécifiques via un procédé d'extrusion à l'état fondu à différentes teneurs en particule qui ne dépasse pas 40 % en poids. Les résultats montrent que l'utilisation de 20 % en poids des particules soit d'illite de formule chimique ($Al_2Fe_2K_3Mg_2O_{36}SI_4H_{12}$) ou bien de la perlite d'une formule proche de celle d'illite ($Al_2Fe_2K_2MgO_{12}SiCaNa_2$) donne des composites à des propriétés thermiques et mécaniques très élevées. Par ailleurs, l'utilisation d'un agent de couplage qui est SEBS-g-MA peut donner des meilleurs résultats parce qu'il peut améliorer l'adhérence à l'interface argile-matrice polymérique.

M. Raji et al, Polymers and Polymer Composites. 2016;16(2):101–13

M. Raji et al. Composites Part B: Engineering. 2019

Part 1

Morphological, Thermal, Mechanical, and Rheological Properties of High-Density Polyethylene Reinforced with Illite Clay

Résumé

Ce travail a permis d'évaluer l'impact de l'Illite (argile naturelle marocaine) sélectionnée comme renfort pour l'amélioration des propriétés de la matrice polymérique polyéthylène haute densité (PEHD) et de déterminer l'efficacité d'agent de couplage SEBS-g-MA. Les composites ont été fabriqués par le procédé d'extrusion à l'état fondu puis ont été moulés en utilisant l'injection à diverses teneurs en argile. Les propriétés morphologiques, thermiques, mécaniques et rhéologiques ont été mesurées à partir des échantillons produits, les résultats ont montré que l'adhérence à l'interface particules-matrice polymérique était améliorée avec l'ajout d'agent de couplage entraînant une augmentation du module de Young, et une résistance à la traction plus élevée. Néanmoins, la valeur maximale pour les composites sans SEBS-g-MA (augmentation du module de 57%) a été obtenue à 20 % en poids comparé à 15 % en poids pour les composites avec SEBS-g-MA (augmentation du module de 45 %). D'autant plus, la stabilité thermique des composites augmentait également avec la teneur en argile, en particulier lorsque l'agent de couplage était ajouté. Enfin, les tests d'absorption d'eau ont révélé que les composites avaient une plus forte tendance à absorber l'eau lorsque la teneur en argile augmentait, mais l'utilisation d'un agent de couplage a considérablement réduit ce problème.

Mot clé : Illite; polyéthylène haute densité; d'agent de couplage; rhéologiques.

M. Raji et al, Polymers and Polymer Composites. 2016;16(2):101–13

II.1. Abstract

In this work, Illite (natural Moroccan clay) was selected to reinforce high density polyethylene (HDPE) and to determine the efficiency of SEBS-g-MA as a coupling agent. The composites were prepared by extrusion followed by injection molding of various clay contents (5-40% wt.). From the samples produced, the morphological, thermal, mechanical, and rheological properties were measured. The results showed that interfacial adhesion was improved with coupling agent addition leading to increased Young's modulus, as well as higher tensile strength, and strain at yield. Nevertheless, the maximum value for the composites without SEBS-g-MA (57% modulus increase) was obtained at 20% wt. compared to 15% wt. for the composites with SEBS-g-MA (45% modulus increase). The thermal stability of the composites also increased with clay content, especially when the coupling agent was added. Finally, water absorption tests revealed that the composites have a higher tendency to absorb water with increasing clay content, but the use of a coupling agent substantially reduced this problem.

II.2. Introduction

In recent years, composite materials based on synthetic and/or natural fillers have gained interest to reinforced polymer matrices [95]. These materials found several applications like automotive [88], aerospace [101], food packing [102], construction [103], and electrical applications [95]. Although synthetic fillers, such as carbon or glass fibers [104], have been extensively used to reinforce polymers in terms of modulus and strength [92], they usually have high costs, high density, as well as health and safety issues [93]. In contrast, natural fillers are renewable with lower density and lower cost. In this case, both final part density and raw material cost is reduced [94]. Natural reinforcements can be of organic or inorganic nature [95, 96]. For example, high-density polyethylene (HDPE) reinforced with chemically modified coir fibers [97], and polypropylene (PP) reinforced by Moroccan hemp fibers were studied [98]. On the other hand, inorganic fillers like natural talc [99], calcium carbonate [96], and clays [101, 102] have been used. Generally, natural fillers are added to polymer matrices to improve their mechanical [66] and thermal properties [88, 94]. However, mechanical properties are highly function of interfacial adhesion between the phases [103], as well as filler size, loading, and dispersion-distribution [104]. To get good filler dispersion into a polymer matrix, different techniques were proposed such as sol-gel casting [105], in-situ polymerization [106], and melt blending [107]. The latter is the most commonly used process since several parameters can be controlled to improve homogeneity and get good dispersion/distribution [95]. Melt blending is also cost-effective and quite attractive for

polymer processing industries [66]. Using clay into polymers can reduce material cost and is valuable for industrial production and practical application as initially developed by Toyota automotive [108], and followed by applications like fuel tanks [109]. Fillers polarity is also an important factor controlling adhesion as clay is hydrophilic while most polymers are hydrophobic [110]. This is why different approaches have been developed to improve interfacial properties. The most popular chemical methods for clay surface modification are amino acids [111], organic ammonium salts [112], or tetra organic phosphonium [113] to modify the surface polarity and improve adhesion with the polymer. Moreover, for polymers without any polar functional groups such as PP, it is common to graft polar functional groups or add grafted polymers (copolymers/coupling agents) during processing to improve the affinity between the hydrophilic clay and the hydrophobic polymer [101].

In this study, polymer composites based on polyethylene were produced using a local variety of clay (Illite) as natural filler. This choice was made as to valorize abundant and unexploited Moroccan natural resources. Some studies evaluated the possibility to manufacture clay/polymer composites [66], which showed that this type of clay was more effective than talc to improve the mechanical and thermal properties of PP [100]. Here, the effect of clay content (5, 10, 15, 20, 25, 30, 35, and 40% wt.) is studied. Also, styrene-(ethylene-butene)-styrene triblock copolymer grafted with maleic anhydride (SEBS-g-MA) is proposed as a coupling agent to improve the properties of these composites. Scanning electron microscopy (SEM), Fourier transform infrared spectroscopy (FTIR), and differential scanning calorimetry (DSC) are used to complete the mechanical properties taken in tension. Finally, dynamic mechanical thermal analysis (DMA) and melt rheology are used to get more information on the effect of clay and coupling agent contents.

II.3. Experimental details

II.3.1. Materials

High density polyethylene (HDPE) (extrusion grade HD F0455), with a density of 0.95 g/cm^3 and a melting temperature of 135°C, was purchased from SODEVIC (Morocco). The natural clay used in this work is Illite, which is a natural resource from the center of Morocco (Rhamna) (density of 2.1±0.2 g/cm^3). Clay purification was done in our laboratory before composite manufacturing. A clay suspension was prepared by mixing 10 g of clay with 500 mL of water in a 1 L beaker for 24 h [100]. The suspension was filtered through a 100 µm sieve and dried at 110°C for 24 h. Then, the material was crushed and sieved at 1 mm and the particle size distribution was analyzed by laser granulometry as described below. The results showed that 90% of the clay particles have a size below 40 µm. Styrene-(ethylene-butene)-styrene triblock copolymer grafted with maleic

anhydride (SEBS-g-MA) was used as a coupling agent. This grafted copolymer was purchased from Shell (Kraton FG-1901X) and contains 1.4-2% wt. of MA with 29.5% wt. of styrene. In this study, HDPE/Illite will be noted as the binary composite while HDPE/SEBS-g-MA/Illite will be noted the ternary one.

II.3.2. Composites preparation

Polymer composites reinforced with various amounts of clay (Illite) were prepared either by compounding HDPE with clay for the binary composites or HDPE (HDPE/SEBS-g-MA (8% wt.) with clay for the ternary composites. Various clay concentrations (5, 10, 15, 20, 25, 30, 35, and 40% wt.) were prepared using a Leistritz ZSE-18 twin-screw extruder (Leistritz, Germany) with D = 18 mm and L/D = 40. The polymer and clay particles were added via two feeders. The temperature of the seven sections of the extruder barrel, and that of die (4 mm), was set at 170,170,180,180,180,180,180, and 170°C, respectively [115]. The strands coming out of the extruder were cooled in a water bath and pelletized (Thermo Fisher, UK) into pellets of 2-3 mm in length. All the specimens were molded using an Engel e-Victory injection molding machine with a 40 tons platen force. The process temperature was fixed at 190°C in the barrel and 180°C at the nozzle, while the mold was maintained at 45°C [116].

II.4. Characterization

II.4.1. Granulometry

The clay particle size distribution was measured by laser granulometry via a Malvern Mastersizer 3000 (Horiba instruments). The sample was analyzed in the dry state using an ultrasonic bath. The particle size distribution was determined based on the diffraction and absorption of a laser beam and expressed as a function of the volume occupied by the particles.

II.4.2. Morphological characterization

II.4.2.1. Scanning Electron Microscopy (SEM)

Scanning electron microscopy (SEM) was used to determine the morphology of the clays and to investigate clay dispersion/distribution in the polymer matrix. To obtain clean and accurate fractures, all the composite samples were cryofractured under liquid nitrogen. Then, the exposed surface was covered with Au/Pd to be examined with a JEOL JSM 840A scanning electron microscope at 15 kV with different magnifications.

II.4.3. Structural properties

II.4.3.1. X-Ray Diffraction (XRD)

Wide-angle X-ray diffraction (WAXD) was used to identify the chemical composition and crystallographic structure of the clay. The data were obtained on a Bruker D8 Discover using the Cu K□ radiation (k = 1.54184 nm) and a GADDS detector. The samples were consolidated in an aluminum holder and scanned at 45 kW from 0.5° to 90° of 2θ. The diffraction patterns were analyzed using X'Pert High Score software.

II.4.3.2. Fourier transform infrared spectroscopy (FTIR)

Fourier transforms infrared spectra (FTIR) of the clay and the composites were recorded using ABB Bomem FTLA 2000-102 spectrometer (ATR: Specac Golden Gate). The spectra were obtained with an accumulation of 16 scans with a resolution of 4 cm^{-1}.

II.4.4. Thermal Analysis

II.4.4.1. Thermogravimetric analysis (TGA)

The thermal degradation of the clay and composites was evaluated by thermogravimetric analysis (TGA) using a Q500 from TA Instruments. Roughly, 20 mg of each sample was placed in a platinum pan and heated under air from room temperature up to 700°C at a heating rate of 10°C/min.

II.4.4.2. Differential scanning calorimetry (DSC)

Differential scanning calorimetry (DSC) analysis was carried out using a Q100 from TA Instruments. The samples, weighing about 5 mg, were placed in an aluminum crucible to be heated, cooled, and heated from -80°C to 400°C at a heating rate of 20°C/min. The degree of crystallinity (Xc) was determined from the melting enthalpy values as [99]:

$$X_c = \frac{\Delta H_m}{(1-\alpha)\Delta H_m^0} \qquad \text{(II-1)}$$

where ΔH_m is the melting enthalpy of the specimens (J/g), ΔH_m^0 is the enthalpy value for a theoretically 100% crystalline HDPE (291.6 J/g), and $(1-\alpha)$ is the weight fraction of polymer in the composites.

II.4.5. Mechanical properties

II.4.5.1. Tensile testing

Tensile tests of three specimens for each type of composites were performed according to ISO 527-1:2012 [117]. The tests were performed on a universal testing machine INSTRON 8821S (Instron, USA) at a crosshead speed of 5 mm/min using a five kN load cell. Tensile properties such

as Young's modulus, tensile strength, and strain at yield of the composites were obtained from the stress-strain curves.

II.4.5.2. Dynamic mechanical analysis (DMA)

The dynamic mechanical properties were measured using a Rheometer Solid Analysis (RSA), according to ASTM D 4092-01 [118]. Due to the stiffness of the studied materials, a dual cantilever configuration was used. The samples dimensions were 45 x 5.5 x 2 mm^3. First, a strain sweep test was performed at 1 Hz. Then, frequency sweeps from 0.015 to 15 Hz with a strain of 10-4 (linear viscoelastic regime) were performed.

II.4.6. Dynamic rheological measurements

Oscillatory melt rheology tests were performed on an MCR 500 (Physica) rheometer equipped with a CTD600 device. The measurements were carried out at 200°C under small amplitude oscillatory shear mode using 25 mm parallel plate-plate geometry with 2 mm thick samples. Frequency sweeps between 500 and 0.05 Hz were performed at a strain of 5% (linear viscoelastic regime).

II.4.7. Water absorption

Composite samples having dimensions of 25 mm in diameter and 2 mm in thickness were immersed in distilled water (pH 7) at room temperature. For each measurement, the specimens were removed from the water bath and surface water was wiped off using paper towels. Weight was measured after different time period to get its variation. Water absorption was determined using the weight gain as:

$$(\%)\ Weight\ gain = \frac{(Wf - Wi)}{Wi} \times 100 \qquad \text{(II-2)}$$

where Wi is the initial weight of the specimen after drying at 80°C for 48 h, and Wf is the weight after specific water immersion time [119].

II.5. Results and discussion

II.5.1. Morphological characterization

II.5.1.1. Scanning Electron Microscopy (SEM)

SEM analysis as presented in Figure (II- 1) gives information on the clay state of dispersion and distribution, as well as the effect of SEBS-g-MA addition. From Figure II-1 (20% clay), it is clear that the morphology of Illite clay particles is lath-shaped and platy particles [120]. Based on these images, the width and thickness of 50 particles can be measured to get an average particle width of 1.02 µm with an average particle thickness of 0.30 µm.

As expected, the addition of a coupling agent increases the HDPE/clay particles adhesion where much less gaps/voids can be seen at their interface, as these are associated with poor bonding between HDPE and clay particles. Any crack/failure in the composite will start from these voids leading to premature material failure [73, 121]. It is also clear from Figure II-1 that the reinforcing clay particles are uniformly dispersed inside the matrix and no clear filler aggregates can be observed, an indication that the melt compounding conditions were optimum to manufacture these composites and should lead to good composite properties [66].

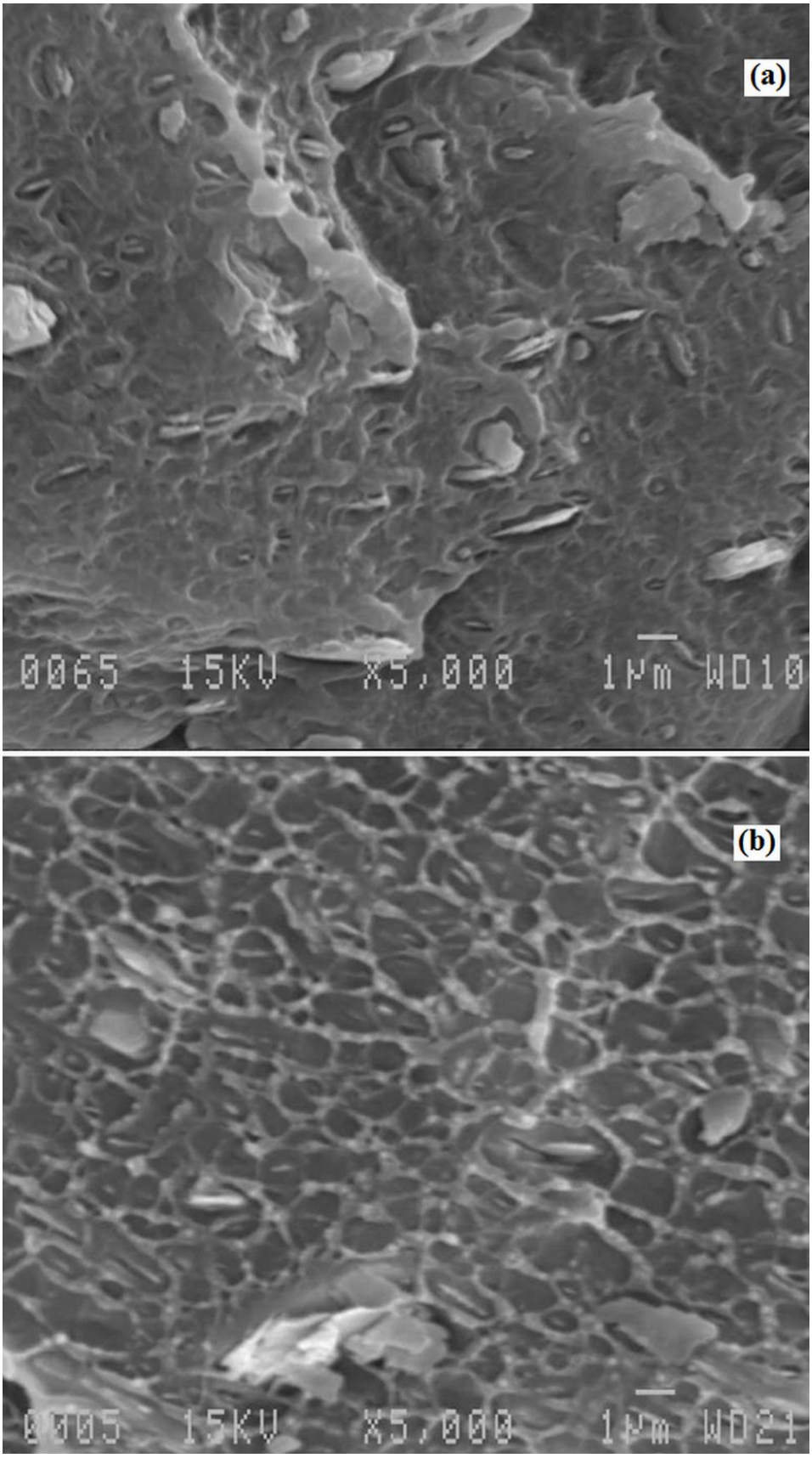

Figure II-1-: SEM images of the (a) HDPE/clay and (b) HDPE-SEBS-g-MA/clay (20%).

II.5.2. Structural properties

II.5.2.1. X-Ray Diffraction (XRD)

The crystallographic structure and composition for Illite were carried out by X-ray diffraction. Figure II-2 shows the XRD pattern of the neat Illite showing that the peaks are mainly located between 20° and 70° which are characteristics of Illite: $(K,H_3O)(Al,Mg,Fe)2(Si,Al)_4O_{10}$ $[(OH)_2,(H_2O)]$ [122]. Illite also contains some associated clay minerals such as quartz (SiO_2), dolomite ($MgCa(CO_3)_2$), and calcite ($CaCO_3$). This mixture of minerals at different content plays an important role on the overall structural and physical properties of Illite.

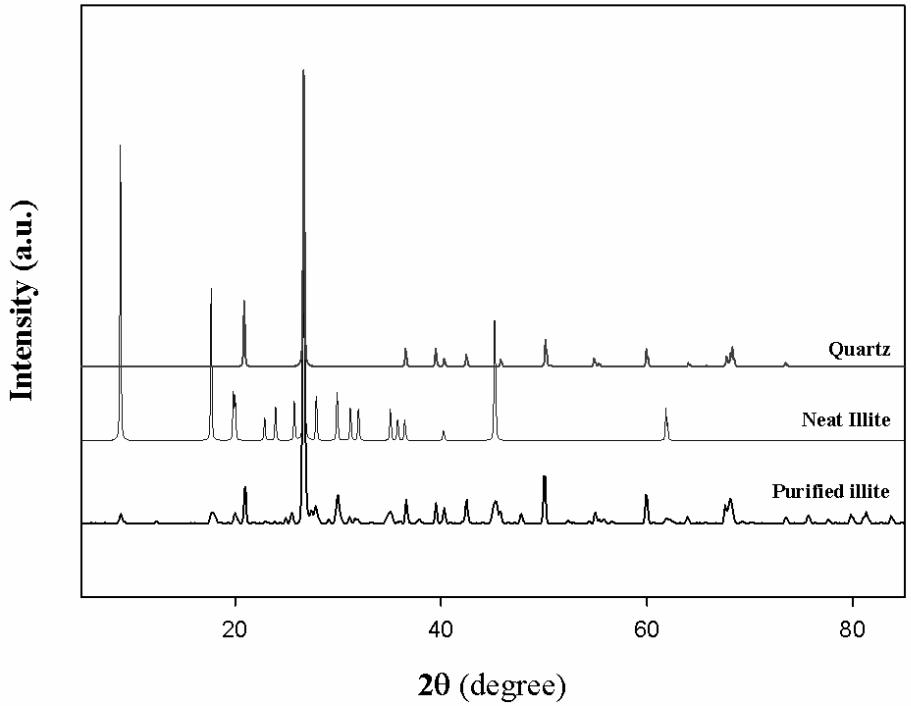

Figure II-2 : XRD spectra of Illite

II.5.2.2. Fourier transform infrared spectroscopy (FTIR)

Figure II-3 shows the spectra in the 4000-400 cm^{-1} range for raw Illite, as well as purified Illite and the manufactured composites. FTIR spectroscopy analysis was used to characterize and compare the purified Illite versus the untreated one (raw Illite).

Raw and purified Illite curves show a bands at 3640 cm^{-1} [123], which corresponds to O-H stretching of the structural hydroxyl group. The band at 1428 cm^{-1} corresponds to the C-O stretching vibration characteristic of calcite [124], while the band located near 1000 cm^{-1} corresponds to the Si-O stretching vibration [125]. The band at 918 cm^{-1} corresponds to Al-OH deformation [126, 127], while the bands at 798 cm-1 and at 456 cm^{-1} correspond to Si-O-Si

vibration and Si-O-Si deformation, respectively [128]. The bands at 757 cm^{-1} and 631 cm^{-1} result from Si-O deformation perpendicular to the optical axis and Si-O deformation parallel to the optical axis, respectively [129]. The band at 541 cm^{-1} is associated to Al-O-Si deformation [130].

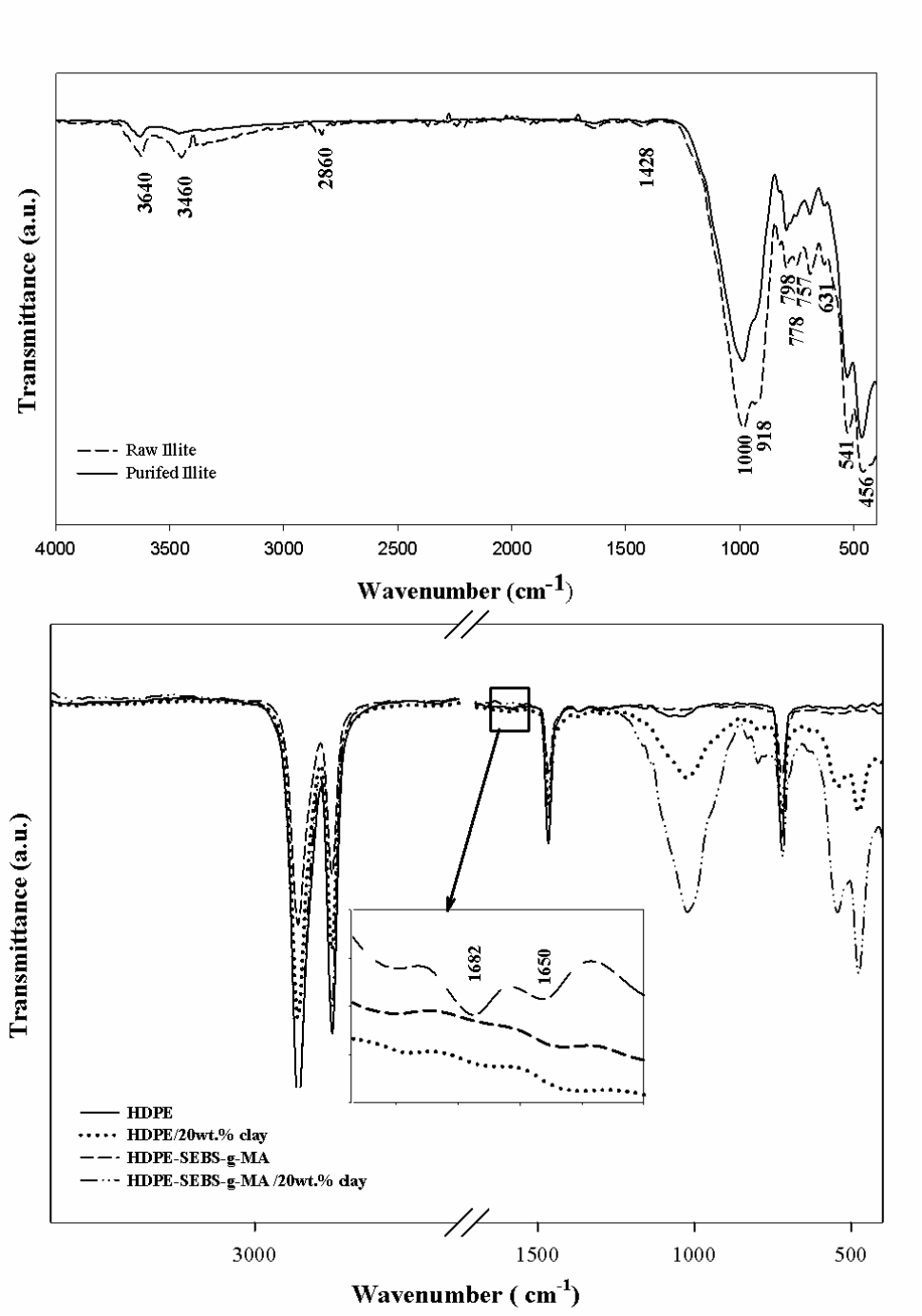

Figure II-3 : FTIR Spectrum of: a) raw illite powder and purified one, b) illite composites with and without coupling agent

For the purified Illite curve compared to the raw one, the transmittance bands located at 3460 cm^{-1} and 1646 cm^{-1} disappeared, which was attributed to O-H deformation [126], as well as O-H stretching of water [125] respectively, after drying. In addition, the bands around 2860 cm^{-1},

corresponding to C-H stretching vibrations, have intensified which can be associated to the removal of organic matter by washing/filtration during the purification process.

Figure II-3b shows the spectra of the binary and ternary composites. Comparing the spectra of HDPE with the composites, the most prominent HDPE bands are easily observed in all spectra, but a combination of bands from both HDPE and Illite components are seen in the composites. Furthermore, the composites with coupling agent have two extra bands at 1650 cm^{-1} and 1682 cm^{-1} (see the magnified area). These bands are characteristics of the formed ester bonds between the O-H groups of the filler and the maleic anhydride functions grafted on the coupling agent [116]. This clearly indicates that the reaction took place. Thus, good wettability of the particles by the matrix is expected leading to good interfacial interactions.

II.5.3. Thermal properties

II.5.3.1. Thermogravimetric analysis

The thermogravimetric (TGA) and differential thermogravimetric (DTG) curves of Illite are shown in Figure II-4. It can be observed that Illite lost only 6% of its weight up to 950°C, showing its good thermal stability. Nevertheless, the slight thermal decomposition of Illite occurred in four steps. The first step between 50 and 150°C is associated to the release of adsorbed and interlayer water [131], while the second step between 450 and 650°C corresponds to the dehydroxylation of the Illite layers [132]. The third step around 570°C is the result of quartz transformation from the alpha to beta phase [132]. Finally, the fourth step around 700°C can be attributed to the final decomposition of the Illite lattice [131].

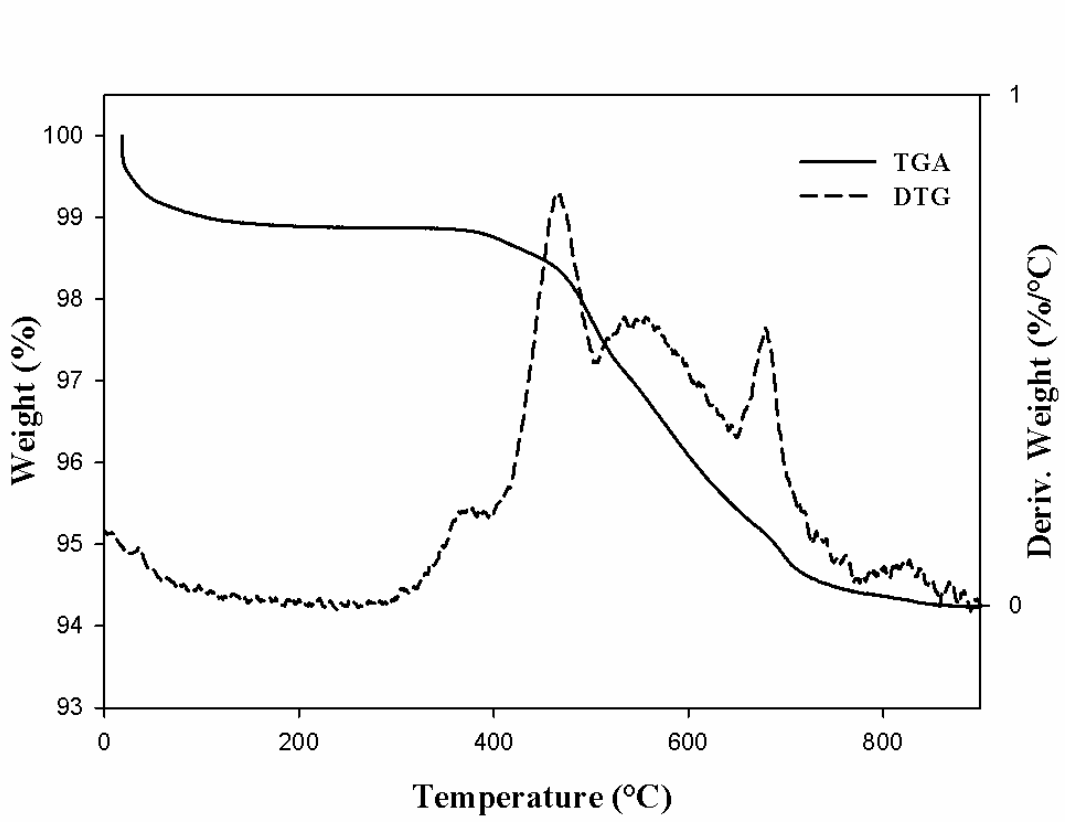

Figure II-4: TGA and DTG curves of purified Illite clay.

Table 0-1 : Thermal degradation of HDPE, HDPE/clay, and HDPE-SEBS-g-MA/clay composites.

Sample	HDPE (wt. %)	HDPE/clay (wt. %)				HDPE-SEBS-g-MA/ Clay (wt. %)			
		10	20	30	40	10	20	30	40
T_{max} (°C)	400	466	465	479	480	464	465	478	482

The thermal analysis of binary and ternary composites was conducted to determine the effect of Illite and coupling agent content on the thermal properties of the composites. Table II-1 quantifies this thermal degradation by using T_{max} defined as the temperature for the maximum rate of mass loss; i.e. the position of the peak in DTG curves (Figure II-5). For binary composites, the use of Illite increased the thermal stability from 400°C for neat HDPE to 480°C and 482°C for the binary and ternary composites (40% wt.), respectively. This increase is due to the high thermal stability of the clay itself as reported in Figure II-4.

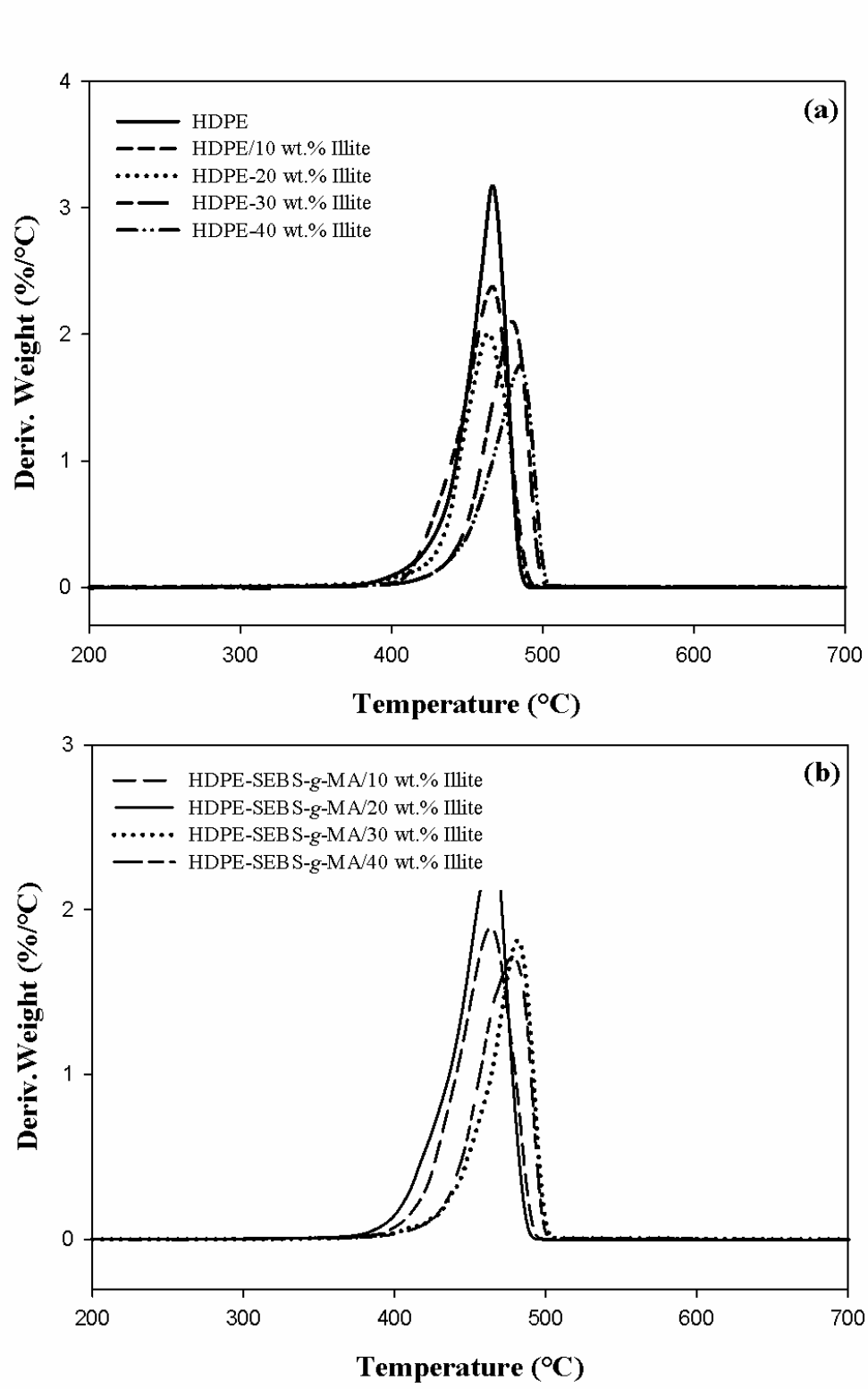

Figure II-5: DTG curves of HDPE, HDPE/clay, and HDPE-SEBS-g-MA/clay composites.

II.5.3.2. Differential scanning calorimetry

Differential scanning calorimetry (DSC) was used to investigate the influence of the clay and the coupling agent on the melting temperature (Tm), specific enthalpy of melting (ΔHm), and temperature of crystallization (Tc). Table II-2 presents the results for the binary and ternary composite systems. For the binary composites, the melting point (Tm) of neat HDPE was 137.7°C, while the melting temperature of the composites with 35% wt. clay content decreased to 132.9°C. The addition of clay influenced the melting temperature of HDPE which might be explained by the reduction of the polymer chain length (thermo-mechanical degradation in melt processing) by addition of the filler at high concentration as higher viscosity (as described later), associated with the presence of solid particles, induce more stresses on the polymer molecules while being processed [100]. Moreover, as clay content increased, crystallization temperature (Tc) increased from 110.5°C for neat HDPE to 121.3°C at 35% wt. This increase indicates faster crystallization of the polymer chains upon cooling. It is well known that solid particles can act as nucleating agents providing sites of low energy to initiate crystallization, thus crystallization can occur faster and at higher temperature [85]. To investigate the influence of fillers on composites crystallization, the crystallinity degree was calculated and reached a maximum (70.3%) at 15% wt. The value decreased beyond this point because more crystallites were formed [101], leading to a steric hindrance effect (decrease of spherulite size at higher contents) [99].

The results also show that ΔHm is more sensitive to clay content. The addition of only 5% wt. of clay to the binary composite increased the ΔHm value because of the heterogeneous nucleation effect. In general, polymer molecular chains can crystallize by themselves through a self-nucleation (homogeneous) effect or by introducing a nucleating agent (heterogeneous) [133].

Table 0-2: DSC results for the binary and ternary composites at different clay content.

Specimen	T_m (°C)	T_c (°C)	ΔH_m (J/g)	X_c (%)
HDPE	137.7	110.5	185.3	63.5
HDPE/5wt.% Illite	133.3	119.9	186.6	67.3
HDPE/15wt.% Illite	133.6	120.0	174.2	70.2
HDPE/35wt.% Illite	132.9	121.3	123.7	25.3
HDPE-g-SEBS-g-MA	133.3	119.3	183.5	62.9
HDPE-g-SEBS-g-MA/5wt. % Illite	134.8	119.9	159.3	57.5
HDPE-g-SEBS-g-MA/15wt. % Illite	133.5	120.2	159.2	64.2
HDPE-g-SEBS-g-MA/35wt. % Illite	132.8	120.4	115.3	60.8

Comparing the results between the binary and ternary composites in Table II-2, it is clear that the coupling agent has a significant effect on the thermal properties of these composites. The results also show that the melting temperature for the neat ternary composite decrease from 137.7°C to 133.6°C, while the crystallization temperature (Tc) increase from 110.5°C to 119.3°C. The ΔHm of the ternary composite was lower than the binary composites. This can be explained by the ester bonds formed in the ternary system leading to good interfacial adhesion. It is important to notice that the crystallinity of the ternary composites is lower than their binary counterparts. This indicates that the introduction of SEBS-g-MA has a negative effect on HDPE crystallization probably due to chain entanglement, which modifies locally their mobility and rearrangement; i.e. distortion of the crystal structure resulting from the interactions between HDPE and SEBS-g-MA [134].

II.5.4. Mechanical properties

II.5.4.1. Tensile properties

To investigate the effect of filler and coupling agent content, the mechanical properties of the composites were evaluated in tension to get their Young's modulus, tensile strength, and strain at yield. The variation of Young's modulus for the binary and ternary composites as a function of clay loading is presented in Figure II-6a. The Young's modulus is shown to increase with clay loading up to a maximum, and then decreases with increasing clay content. This decrease at high clay content indicates the formation of agglomerates creating some defects in the composites. The results show that the maximum Young's modulus for the binary system (970 MPa) is reached at 20% wt., which corresponds to a 57% increase over neat HDPE (650 MPa). On the other hand, the ternary system achieves its maximum at lower clay content (15% wt.) with a slightly lower value (899 MPa). This reduction, after SEBS-g-MA addition, can be attributed to the low elastic modulus of the rubber blocks used to graft MA (7.2 MPa based on our measure); i.e. the elastomeric nature of SEBS (copolymer) leads to a more ductile behavior of the ternary composites compared to binary ones, thus decreasing the rigidity of the composites [66,135].

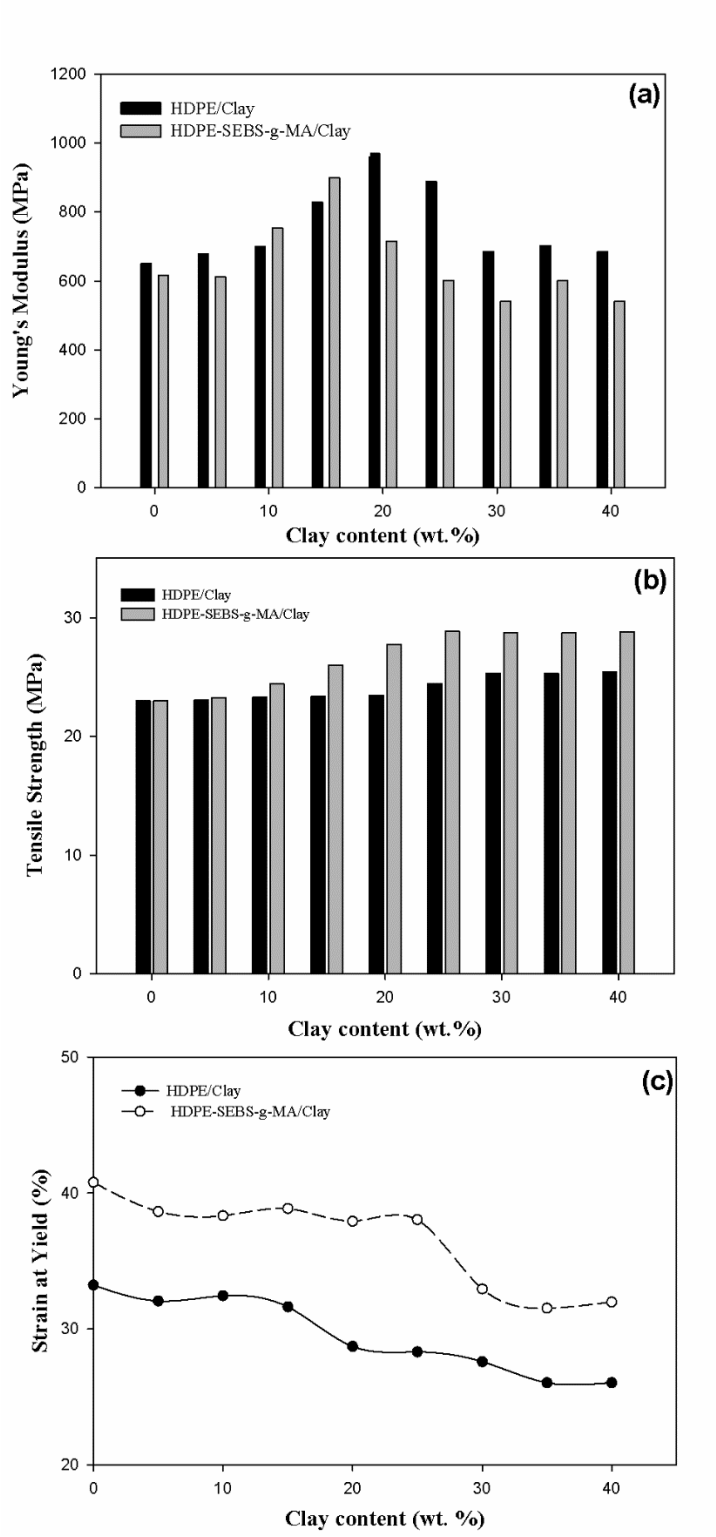

Figure II-6: Tensile properties of neat HDPE, HDPE/clay, and HDPE-SEBS-g-MA/clay composites as a function of clay content: a) Young's modulus, b) tensile strength, and c) strain at yield.

Figure II-6b shows the effect of clay and coupling agent on the tensile strength of the composites. This figure clearly indicates that the tensile strength values increase from 23.6 MPa to 29.6 MPa and from 26.7 MPa to 32.1 MPa for the binary and ternary composites, respectively. It can be

concluded that the tensile strength values of both composite systems gradually increase with increasing clay content. In this case, the addition of the coupling agent leads to higher tensile strength. This difference can be explained by the improved interfacial adhesion between the particles and the matrix. It is important to notice that the interactions between the HDPE matrix and clay increased with increasing clay content. There are physical entanglements between HDPE and the EB part of SEBS-g-MA on one side, and chemical interaction (ester bonds) between the hydroxyl groups of clay with the MA groups of the coupling agent as confirmed by FTIR (see Figure II-3). Both types of interactions are responsible for better interfacial stress transfer [126].

The strain at yield is reported in Figure II-6c and the results show a linear decrease with increasing clay content for both composite systems (similar slopes) giving a decrease of 22% at 40% wt. clay. This result indicates the loss of ductility of a ductile matrix with rigid particles addition [136]. This reduction indicates lower plastic energy in the composites compared to the neat polymer matrix [135]. However, for compatibilized systems, higher values were obtained. This behavior can again be associated to the elastomeric nature of the SEBS blocks giving more ductility to the ternary composites and improving its plastic energy absorption [137].

II.5.4.2. Dynamic mechanical analysis (DMA)

Dynamical mechanical analysis was used to investigate the effect of clay and coupling agent content on the viscoelastic properties of the binary and ternary composites in the solid state. Figure II-7 shows that for both composite systems, the complex modulus increases with clay content due to the presence of rigid particles combined with limited chain mobility slowing down the molecular dynamics [99]. Nevertheless, as reported for the tensile modulus (see Figure II-6a), the complex modulus of the binary composites is higher than for ternary ones, which is again related to the elastomeric nature of the coupling agent used [126]. Nevertheless, E* increases with increasing frequencies for all cases due to the complex viscoelastic behavior of these composites. The variation of applied frequency causes a change in molecular time response of the composites: at low frequencies, the polymer chains have time to relax, while at higher frequency the molecules do not have enough time to relax and present a more solid-like behavior [100, 66].

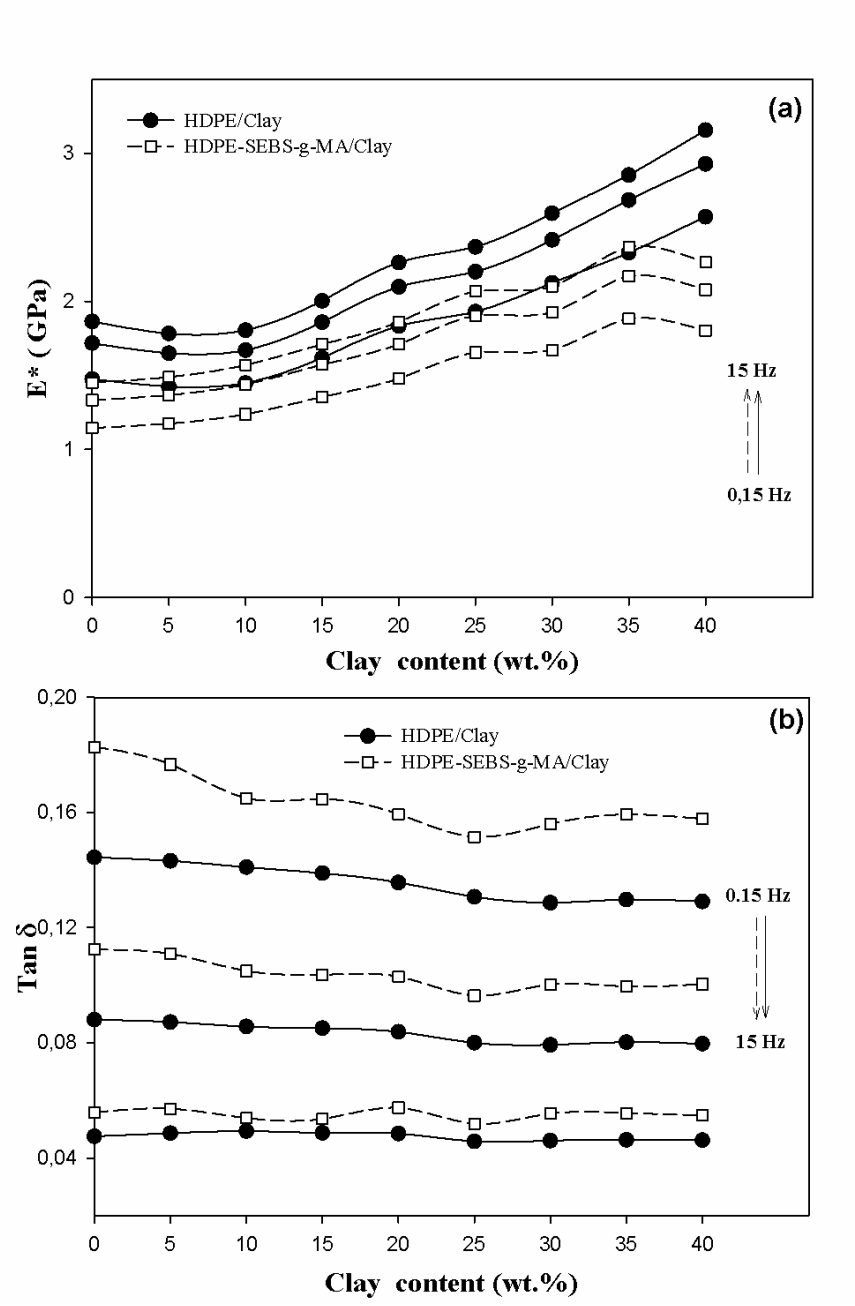

Figure II-7: Complex modulus as a function of clay content at different frequencies for HDPE/clay and HDPE-SEBS-g-MA/clay composites, and b) loss factor (Tan δ) for the same conditions.

One way to better characterize this effect is by looking at the damping factor (tan δ) as presented in Figure II-7b. For both composite systems, tan δ (the ratio between the viscous and elastic components: E''/E') decreases with increasing frequency showing again a more elastic behavior. The curves for each system have similar shape and the low values indicate that the elastic character of the material prevails [138]. In all cases, the coupling agent improved the viscous character of the composites leading to higher tan δ values.

II.5.5. Dynamic rheological measurements

To get more insight on the effect of the parameters studied, the rheological properties of both composite systems were characterized in the melt state to get more sensitivity on the particle and interface effects since the matrix contribution is much lower than in the solid state (see Figure II-7). Rheological measurements are also more sensitive to dispersion state and interaction degree between the components [111]. In addition, the processing behavior of the composites can also be obtained from their rheological characteristics. As seen in figures II-8a, a', the storage modulus (G') of the binary and ternary composite systems increases with increasing clay content and frequency. Nevertheless, the ternary composites have significantly higher storage modulus at low frequency than binary composites, suggesting that the rheological properties of reinforced HDPE were mainly influenced by the addition of the coupling agent. On the other hand, the composites present a plateau at low frequency indicating a transition from a liquid-like to a solid-like viscoelastic behavior. At higher clay content, the elastic character of the material prevails over its viscous behavior [66].

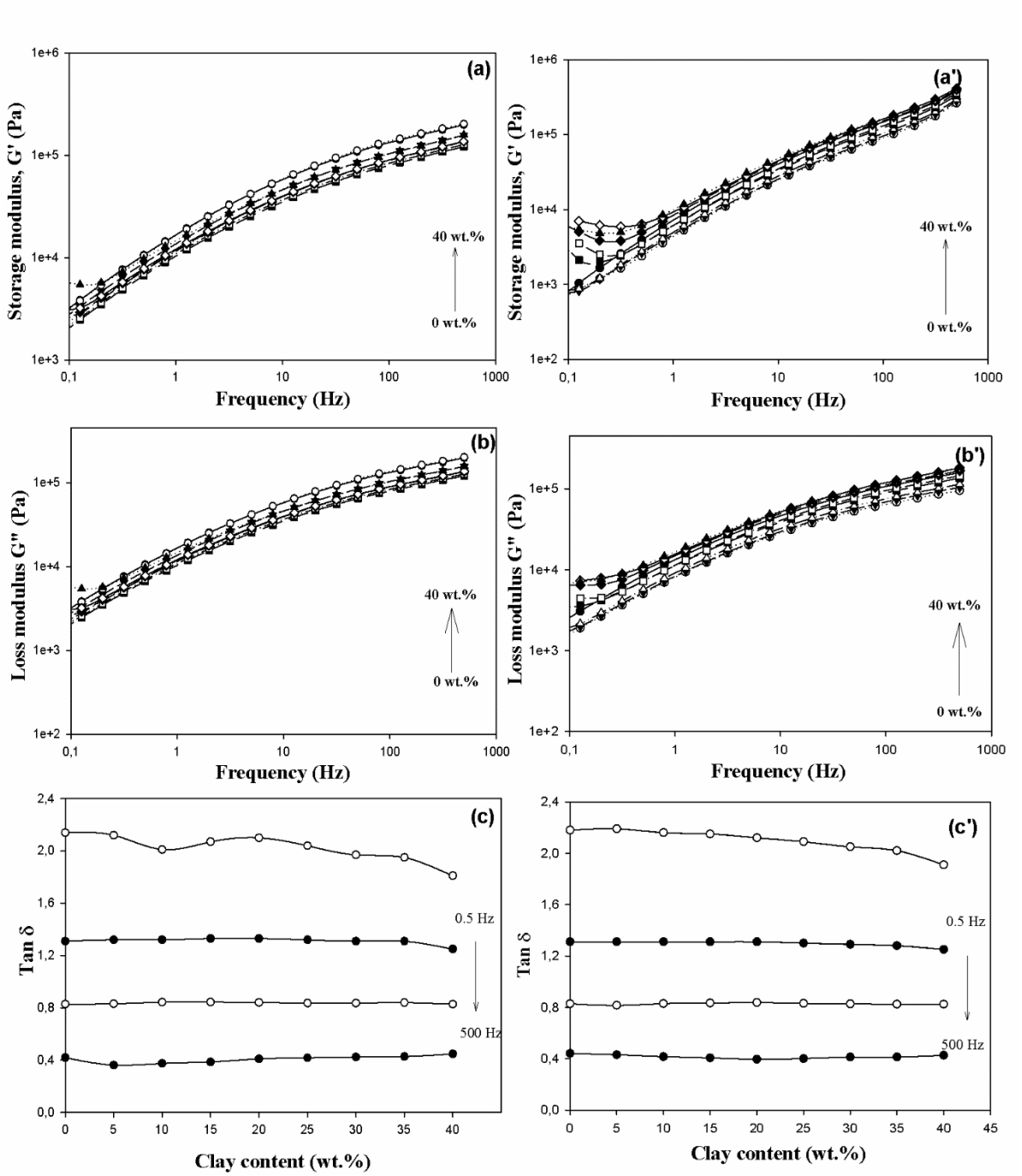

Figure II-8: Rheological properties as a function of clay content for different frequencies: a) storage modulus of HDPE/clay, a') storage modulus of HDPE-SEBS-g-MA/clay, b) loss modulus of HDPE/clay, b') loss modulus of HDPE-SEBS-g-MA/clay, c) damping factor of HDPE/clay, and c') damping factor of HDPE-SEBS-g-MA/clay.

From Figures II-8b, b', it is clear that the loss modulus G" increases with frequency which is in agreement with DMA results (Figure II-7). It is also observed that for both systems (binary and ternary) at high frequency, G' values are higher than G" indicating a more solid-like response in the molten state. This behavior is associated to insufficient time at higher frequency to allow

polymer chains to relax contributing to an increase in the elastic nature of the melt. On the other hand, for ternary composites and at low frequency, the storage modulus results show that the polymer chains have enough time to relax and display a typical terminal behavior [111]. Addition of up to 10% wt. clay increased the storage modulus without changing the viscoelastic behavior, indicating that there is not enough clay to restrain polymer chain relaxation. However, at low frequencies and when the clay content exceeds 10% wt., G' starts to develop a plateau indicative of a transition from a liquid-like to a solid-like viscoelastic behavior [111]. This non-terminal behavior at low frequency can also be attributed to the formation of networks (interactions) between the clay particles and polymer molecules as ester bond were created (see Figure II-3), essential to the formation of an interconnected network structure in the polymer. However, for the binary composites, no changes in the viscoelastic behavior with the use of clay and a lower value compared to the ternary composites were observed. This can be related to good interfacial adhesion inside ternary composites. Figures II-8c, c' show the variation of the damping factor for HDPE/clay and HDPE-SEBS-g-MA/clay composites as a function of clay content and different frequency. The curves have the same trend with particles loading (almost parallel) and the damping factor decreases with increasing frequencies. At a low frequency, neat HDPE and the composites with low clay content exhibit a dominant viscous behavior. However, at higher frequency, the elastic character of the material prevails over the viscous behavior. As expected, the values are higher in the melt state (Figure II-8) than in the solid state (Figure II-7) due to the more viscous behavior nature of the polymer matrix.

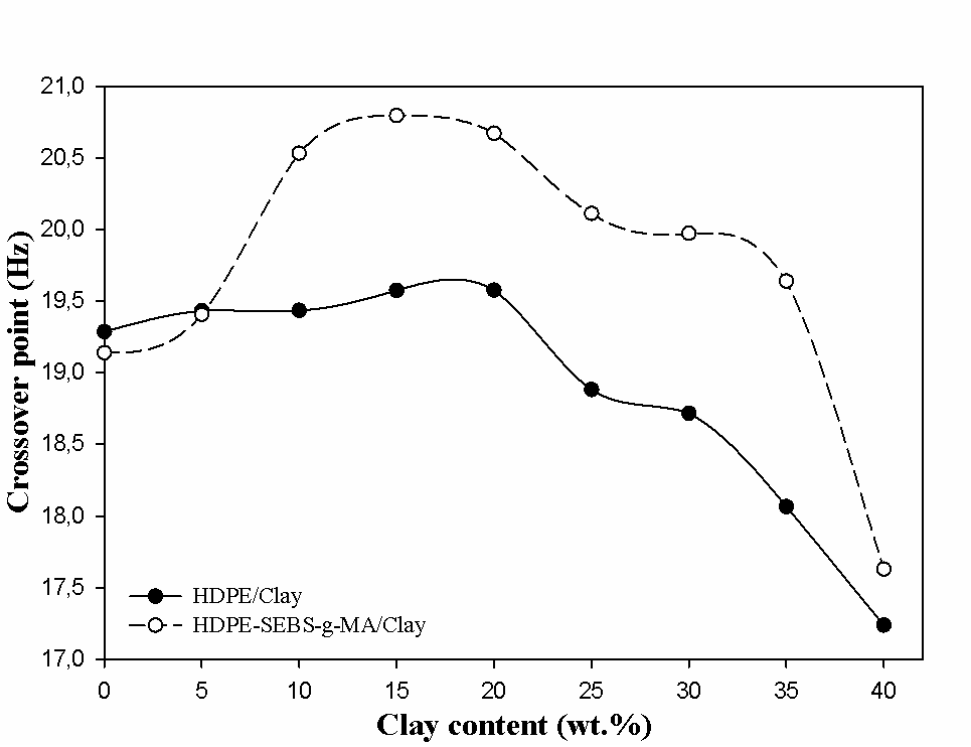

Figure II-9: Crossover point for HDPE/clay and HDPE-SEBS-g-MA/clay composites as a function of clay content.

Figure II-9 shows the crossover frequency (G' = G'') as a function of clay content for both systems. For the ternary composite and at low clay content (less than 15% wt.), the crossover point increases meaning that the viscous behavior prevails over the elastic behavior at higher frequency, and this reduction in composites rigidity can be explained by the rubber character of the coupling agent taking over on the response of the melts leading to a more viscous behavior. At higher clay content (above 15% wt.), the values decrease with clay loading indicating that the elastic behavior prevails over the viscous one. On the other hand, the binary composites curve shows a similar trend, but higher values with a maximum occurring at around 20% wt. clay content are observed. This is mainly due to increased rigidity from the presence a solid particle network with the incorporation of high clay content; clay particles having more effect at higher concentrations. These trends and maximum values are in agreement with the results reported for tensile modulus (Figure II-6) which was measured in the solid state. Finally, the values are higher for the ternary composite because of the coupling agent [66].

II.5.6. Water absorption

Figure II-10 shows the water absorption results of the binary and ternary systems as a function of time and clay content. It can be seen that the rate of water absorption followed a standard trend

with a high initial rate and an equilibrium value at later stage. For example, the equilibrium value for neat HDPE is about 1.5%. However, water absorption increased with Illite content because of its hygroscopic (hydrophilic) nature. On the other hand, the water absorption of the ternary composites was much lower compared to the binary systems due to the presence of SEBS-g-MA. This behavior is the result of improved dispersion and wettability of the clay particles inside the HDPE matrix, as well as increased interfacial adhesion between both phases. There is also the possibility that SEBS-g-MA itself can decrease the diffusion of water molecules in the composites [119]. As expected, the maximum water absorption increases with Illite content which can also be explained by the presence of agglomerates at high loading. However, the use of a coupling agent can significantly reduce this effect because some Illite hydroxyl groups reacted with anhydride groups of the coupling agent lowering the total number of hydroxyl groups available to attract water molecules.

II.5.6.1. Water absorption model

As reported in Figure II-10, water absorption increases with immersion times and clay loading up to an equilibrium value. Fickian models have proposed to evaluate this behavior in reinforced composites as [140]:

$$\frac{M_t}{M_\infty} = kt^n \qquad (3)$$

and

$$\log\left(\frac{M_t}{M_\infty}\right) = \log(k) + n\log(t) \qquad (4)$$

where Mt, M∞, k, and n are the water absorption at time t, the equilibrium water absorption, and model parameters, respectively. Equilibrium values can be obtained on Figure II-10, while the constants n and k are calculated from the slope and the intercept of a log-log plot of Mt/M∞ as a function of time. These values give an idea about the interactions between the polymer and water absorption (k), and information about the type of water absorption behavior (n), which is different for each case as follows.

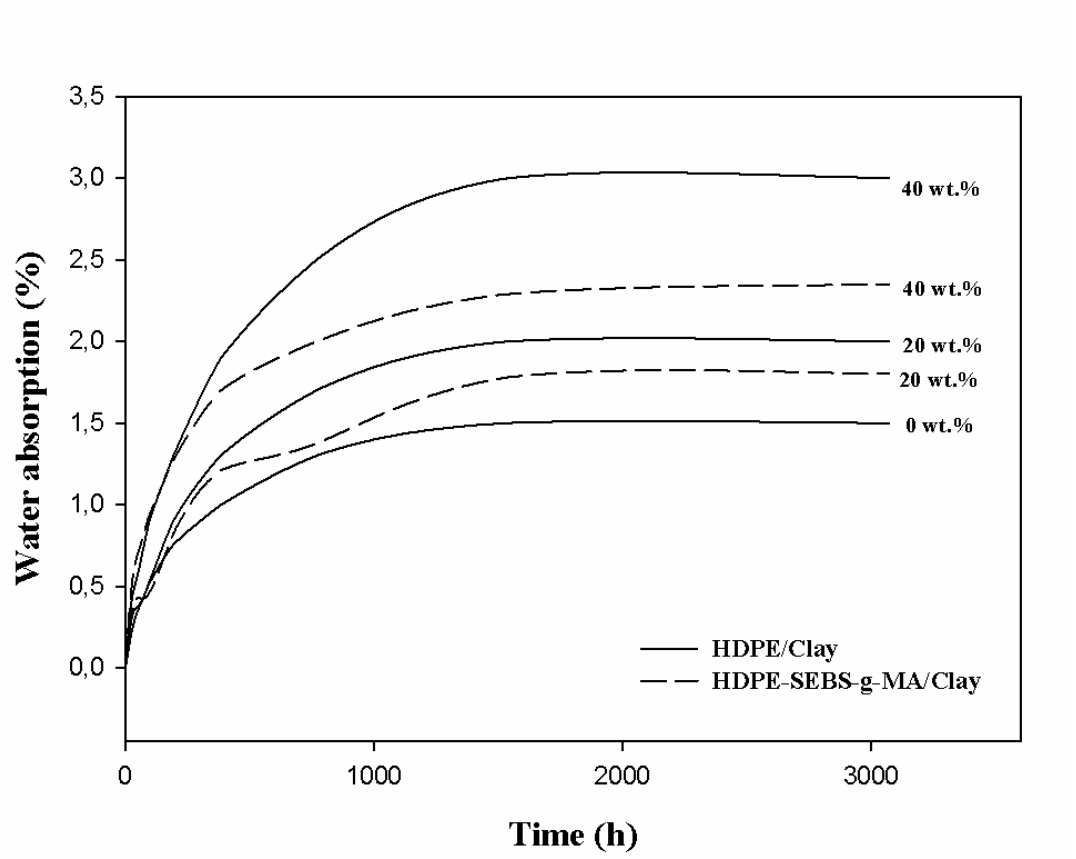

Figure II-10: Water absorption of HDPE/clay and HDPE-SEBS-g-MA/clay composites as a function of time for different clay content.

Table 0-3: Model parameters (Eq.3-4) for water absorption in HDPE/clay and HDPE-SEBS-g-MA/clay composites.

Sample	M_∞ (%)	k (h^{-n})	n (-)	D x 10-14 (m^2/s)
HDPE	1.50	0.0493	0.41	2,48095
HDPE/20% clay	2.00	0.0388	0.44	5,52365
HDPE/40% clay	3.00	0.0377	0.44	7,72756
HDPE-SEBS-g-MA/20% Clay	1.80	0.0493	0.40	4,75189
HDPE-SEBS-g-MA/40% Clay	2.35	0.0853	0.33	6,84401

The results of Table II-3 shows n values are closed to 0.5. Therefore, it can be concluded that the Fickian model is a good approximation for these systems allowing the calculation of a diffusion coefficient (D) for water molecules into the composites via [139]:

$$D = \pi \left(\frac{m\,L}{4\,M_\infty} \right)^2 \qquad (5)$$

where L is the sample thickness, and m is the initial slope of a plot Mt as a function of t½.

Figure II-11 present the diffusion coefficient for the binary and ternary systems as a function of Illite content. As expected, D increases with the clay content and the values are higher for the binary system compared to the ternary one. This behavior is related to the hydrophilic character of the clay particles and their incorporation into polymer matrix increase interfacial area defects (gaps/voids). Once again, the coupling agent slows down water molecules diffusion of the intrinsic properties of SEBS-g-MA as well as better clay encapsulation as reported by SEM (Figure II-1).

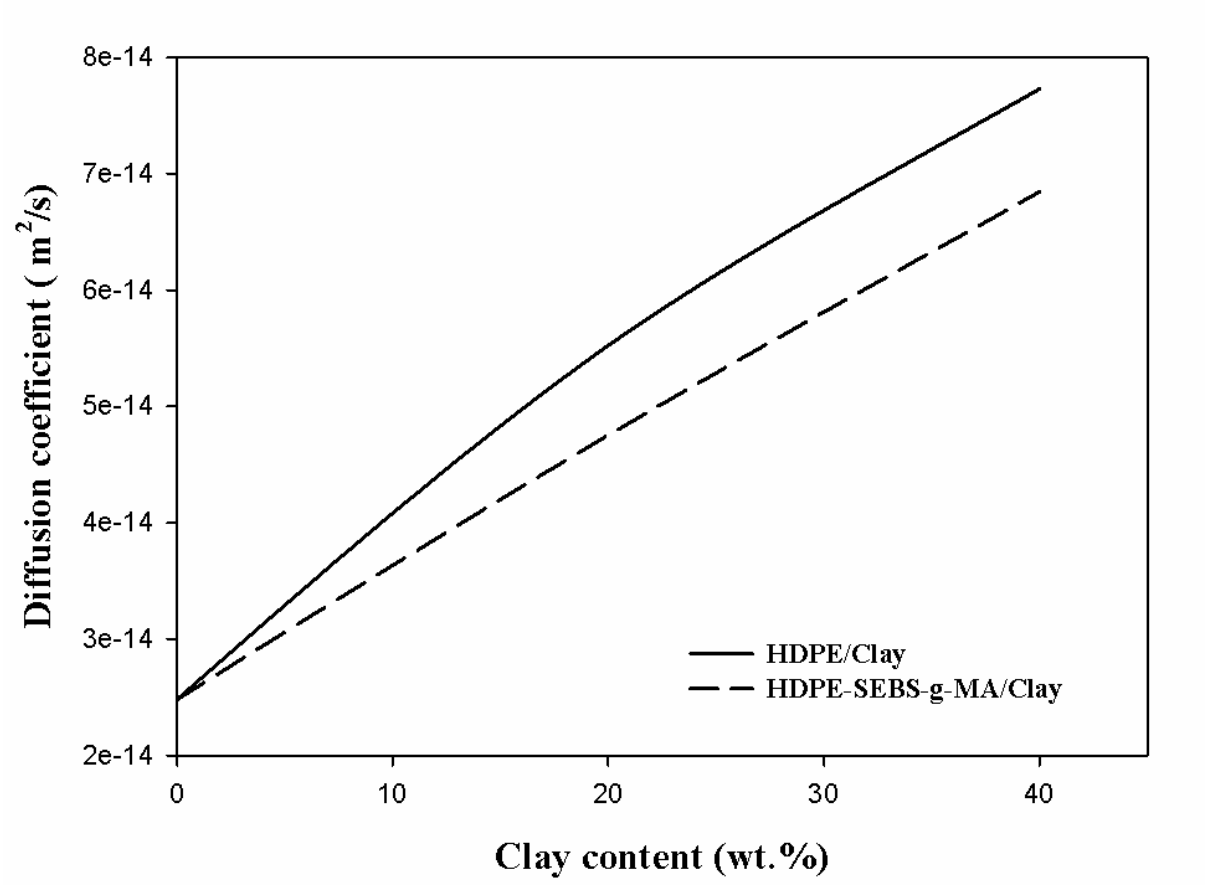

Figure II-11: diffusion coefficient of HDPE/clay and HDPE-SEBS-g-MA/clay composites as a function of clay content.

II.6. Conclusion

This work presented the effect of natural clay (Moroccan Illite) to reinforce high-density polyethylene (HDPE). The clays were purified and grinded into a fine powder to be incorporated in the matrix via extrusion and injection molding to obtain composites at different concentrations (0 to 40% wt.). Furthermore, styrene-(ethylene-butene)-styrene triblock copolymer grafted with maleic anhydride (SEBS-g-MA) was used as a coupling agent to improve the interfacial adhesion as reported from SEM images. The Young's modulus of the composites was significantly increased with increasing filler content, but the maximum value for the binary composites (57% increase) was obtained at 20% wt. compared to 15% wt. for the ternary composites (45% increase). Coupling agent addition mostly increased the tensile strength and strain at yield by increasing interfacial adhesion between the phases. On the other hand, the dynamical mechanical and melt rheological properties showed that the composites become more elastic with clay and coupling agent addition. Finally, the addition of the clay was shown to increase thermal stability and water absorption, but the presence of the coupling agent improved both behaviors.

Acknowledgements

This work was supported by MAScIR (Moroccan Foundation for Advanced Science, Innovation and Research). M.R. would like to thank Mr. Mehdi Ait Dahi for his fruitful technical support and assistance.

Part 2

Utilization of volcanic amorphous aluminosilicate rocks (perlite) as alternative materials in lightweight composites

Résumé

L'objectif de cette étude est de fournir des informations sur l'effet de la structure (brute ou expansée) et de la concentration (0-20% en poids) de perlite (philosilicate amorphe) sur les propriétés morphologiques (SEM), mécaniques (tension), rhéologiques (cisaillement) et thermiques (DSC) des composites à base de polypropylène. Les composites ont été préparés par le procédé d'extrusion bi-vis et mouler par compression. Les résultats montrent que la meilleure dispersion, distribution et meilleure adhésion à l'interface entre les particules et la matrice PP ont été obtenues par l'incorporation des perlites brutes par rapport à la perlite expansée. En général, les propriétés mécaniques et la stabilité thermique du PP ont été améliorées avec l'incorporation de perlite. Par exemple, le module de Young de composites renforcés à la perlite brute a augmenté de 41% (à 15% en poids) par rapport au PP net.

Mot clé : perlite ; propriétés morphologiques ; polypropylène ; stabilité thermique.

M. Raji et al. Composites Part B: Engineering. 2019

II.7. Abstract

The objective of this study is to provide some information on the effect of perlite (volcanic rock) structure (raw or expanded) and concentration (0-20 wt. %) on the morphological (SEM), mechanical (tension), rheological (shear) and thermal (DSC) properties of polypropylene-based composites. The composites were prepared by twin-screw extrusion combined with compression molding. The results show that better dispersion, distribution and interfacial adhesion of the raw perlite in the PP matrix was achieved compared to the expanded perlite. In general, the mechanical properties and thermal stability of PP were improved with perlite addition. For example, the Young's modulus of raw perlite reinforced composites increased by up to 41% (at 15 wt. %) compared to the neat PP.

II.8. Introduction

Over the last decades, the development of new classes of materials was oriented around composite structures to produce more advanced materials for automotive, packaging, and building applications which are in need of high specific properties and low manufacturing costs [3]-[38]. The matrix can be a plastic, a metal, a ceramic or other inorganic material [140]-[105]. Nevertheless, plastic matrices are gaining in interest and can be divided into two main families: thermosets and thermoplastics [141]-[142]. Some advantages such as recyclability, safety, stability, design freedom, and costs are making thermoplastics more attractive for a wide range of applications [59]-[9].

Thermoplastics are typically organic polymers derived from petrochemicals, which have been used for millennia [143]. This is related to their ease of processing, low energy consumption during fabrication and their long-term stability [134]. These materials also have excellent structural performances, although their production generate greenhouse gases emissions (methane and carbon dioxide) causing environmental concerns [120]. To partially solve this problem and extend potential applications, natural fillers have been used to produce the so-call biocomposites. These materials have attracted considerable attention from both scientific and engineering standpoints in the of world material science in general [144].

Reinforcement of a polymer with natural fillers is performed to improve the mechanical properties (modulus and strength) of the matrix as well providing more environmentally friendly materials. But natural reinforcements can also be divided into two main categories: organic or inorganic

fillers such as lignocellulosic fibers [74], calcium carbonate [96], and clays [3]. In the long list of particles, available limited amount of work was devoted to add perlite into plastics [145].

Perlite is a natural amorphous glassy volcanic rock [146], which has a chemical composition equivalent to rhyolite [147]. It has a high silica content (above 70 wt.%) and equilibrium water (2-5 wt.%) [147]. Upon rapid heating up to 850-1150 °C [148], perlite can be expanded to 10-20 times its initial volume due to large volume changes in its softened structure associated with caged water during a liquid-vapor phase transition [149]. The latter is referred to expanded perlite. Both raw and expanded perlites are spherical in shape and are known for their low sound transmission [149], high fire resistance [150], large surface area [151], low moisture retention [148] and low density [151]. Some investigations were reported on the use of perlite as micro-fillers to improve the polymer's mechanical, thermal and rheological properties. For example, Sahraeian et al. [3] studied the properties of low-density polyethylene (LDPE)/perlite nanocomposites, while Arsalani et al. [38] investigated the preparation and characterization of conductive latex based on polyaniline-perlite composites. Similarly, Tian et al. [140] focused on the preparation, characterization and mechanical properties of polylactide/perlite compounds and compared their properties with polylactide/montmorillonite composites.

The objective of this work is to evaluate the effect of perlite structure (raw or expanded) and concentration (0-20 wt. %) on the properties of polypropylene-based composites. Moroccan deposits of perlite can be found in the North-East of Morocco (Nador area) related to the Neogene volcanism activity of this region. The composites are produced by extrusion-compression molding and tested using standard methods.

II.9. Experimental

The polypropylene used as the matrix was a commercial extrusion grade (PPH03BPM) supplied by TASNEE (Saudi Arabia). This polymer has a melt flow index of 3.0 g/10 min obtained using an Extrusion Plastometer (2.16 kg, 190 °C) following ASTM D1238, a density of 0.90 g/cm^3 (ISO 1183), and a melting temperature of 156 °C. The natural (raw) perlite (NP) was obtained from Northern Morocco (Nador) with a dark grey color and a density of 2.90 g/cm^3 as measured by a pycnometer (IsoLab GmbH, Germany). It was easily expanded after grinding when quickly heated at a temperature between 850 and 1200 °C due to the presence of zeolitic water in its structure, forming a lightweight frothy material showing a volume change between 15 and 20 times its original volume. The expanded porous perlite changed to white powdery lumps composed of glassy kernels having a lower density (2.23 g/cm^3).

Composites preparation was as follows. Firstly, natural perlite (NP) and expanded perlite (EP) powders were ground and sieved to less than 0.10 mm. Then, the particles were dry-blended with the virgin polypropylene at different contents (0, 5, 10, 15 or 20 wt.%) to get pre-homogenized mixtures before melt compounding in a lab-scale twin-screw extruder (Haake Minilab II, USA) at 190 °C for 10 min with a screw speed of 60 rpm. The extrudates were pelletized using a cutting mill (Thermo Fisher, UK). Finally, the composites were compression molded in rectangular plates (100 x 70 x 1 mm^3) using a hydraulic hot press (Carver Inc., USA) at 190 °C and 15 tons as required by ASTM D4703 procedure C [152].

The perlite structure, especially the presence of hydroxyls groups in the raw or expanded perlite, was investigated to relate to the final composite properties. Firstly, the perlite mineralogy before and after the thermal expansion was studied by wide-angle X-ray diffraction using a Bruker D8 Discover using the Cu-K□ radiation (51.54184 nm) and a GADDS detector. The BET (Brunauer-Emmett-Teller) (BET) and BJH (Barrett-Joyner Halenda) equations were used to determine the specific surface areas and pores size distribution using a Micromeritics instrument via nitrogen adsorption system. Additionally, the disappearance of hydroxyl groups due to the thermal expansion of the zeolitic water present in natural perlite was confirmed by Fourier transform infrared (FT-IR) spectroscopy in the mid-IR region using an ABB Bomem FTLA 2000-102 spectrometer (ATR: Specac Golden Gate, USA). The spectra were obtained with an accumulation of 16 scans with a resolution of 4 cm^{-1}. Furthermore, the texture and morphology of the natural and the expanded perlite were observed via scanning electron microscopy (JEOL JSM 840A) at 15 kV and different magnifications. The composites specimens (only 15 wt. % presented) were cryofractured under liquid nitrogen and sputter-coated with a thin layer of Au/Pd. The micrographs were used to evaluate the particle dispersion/distribution state in the matrix and to determine the particles/matrix adhesion. Thermogravimetric analysis (TGA) was carried out using a Q5000 (TA Instruments, USA). About 10 mg was placed in platinum pans and heated under air from 50 to 850 °C at 10 °C/min to determine the onset temperature (Tonset) of thermal decomposition, mass loss, and maximum decomposition peak (DTG). Temperature modulated DSC analysis was also performed using around 12 mg of material by means of a model Q100 (TA Instruments, USA) with a heating rate of 10 °C/min from room temperature (25 °C) to 200 °C, cooled down to 50 °C, and reheated to 250 °C. The DSC curves were used to determine the melting (Tm) and crystallizing (Tc) temperature, as well as the melting enthalpy (ΔHm) and rystallinity degree. The mechanical properties of the specimens (8 mm width, 70 mm length and 1 mm thickness) at room temperature (25 °C) were assessed using uniaxial tension on a Tinius Olsen (USA) machine (H10KT) equipped

with a five kN load cell. The tensile properties were evaluated in terms of Young's modulus, strength at yield and strain at yield, which were determined at a crosshead speed of 5 mm/min according to ISO 527-1. At least five repetitions were performed to determine the average and standard deviation. Similarly, shear tests were used to get complementary information about the viscoelastic properties of the samples (8 mm width, 70 mm length, and 1 mm thickness) using frequency sweeps (0.1 to 40 Hz) performed on an ARES-LS (TA Instruments, USA) rheometer operating in the torsion rectangular mode with a strain amplitude of 0.002 (linear viscoelastic region). For each composite, three specimens were tested and the average value reported. From an engineering point of view, studying the viscoelastic properties of polymer composites in the solid and melt states is of great importance to obtain fundamental knowledge such as processability and performance of these materials. So, low amplitude oscillatory shear (SAOS) melt rheology was carried out on an MCR 500 (Physica, USA) rheometer equipped with a CTD600 device to control the temperature using a TC 30 regulator. The measurements were carried out using 25 mm parallel plate geometry with 1 mm thick samples. The data were obtained at a temperature of 190 ˚C (extrusion and molding conditions) for frequency sweeps between 500 and 0.05 Hz and at a strain of 5% (linear viscoelastic regime).

II.10. Results and discussion

The physical characteristics of the perlite particles determined by BET are shown in Table II-4. The BET results show a specific surface area increase from raw perlite (1.1 m^2/g) to the expanded one (2.7 m^2/g). This increase can be associated to pore opening and the development of a more porous structure as the pore volume of raw perlite (1.15 m^2/g) is increased to 2.71 m^2/g for expanded perlite [152]. This change in the pore volume is attributed to the disappearance of surface hydroxyl groups due to the thermal expansion of the zeolitic water present in natural perlite.

Table 0-4: BET results.

Physical characteristics	Raw Perlite	Expanded Perlite
Surface area (m^2/g)	1.10 ± 0.02	2.67 ± 0.01
Pore volume (m^2/g)	1.15	2.71
Pore diameter (nm)	1.70 – 300	1.70 – 300

Figure II-12 compares the FTIR spectra of the natural and expanded perlite. In general, the perlite spectrum is broad and relatively featureless due to the glassy nature of this material. The amorphous and crystalline aluminosilicate phases in natural perlite have four characteristic

absorption bands. The first broadband around 3600-2800 cm^{-1} is likely the -O–H stretching vibration. In particular, the -O–H stretching of free silanol or silanediol groups on the surface of natural perlite is responsible for the relatively sharper feature at 3590 cm^{-1}, while weak H-bonding at 3336 cm^{-1} could occur between neighboring silanols or molecules of adsorbed water or between the silanediol groups of perlite and free water molecules [154]. The second medium intensity band at 1621 cm^{-1} is attributed to the -O–H bending vibration of interlayer water (δH_2O) [25]. The broad intense bands around 1190 cm^{-1} and 1001 cm^{-1} are assigned to out-of-plane and in-plane asymmetric stretching vibration modes of Si─O─Si and Si─O─R in SiO4 tetrahedra, where R can be Si or Al [156]. The FTIR spectra of expanded perlite shows a partial disappearance of the characteristic vibration -O–H functional group corresponding to the frequency νSiO-H in the region of 3600-2800 cm^{-1}. These results show that the thermal treatment modifies the surface of natural perlite through the reduction of surface hydrogen bonding changing thereafter the physical and mechanical properties of the particles, which is in agreement with the results obtained from BET.

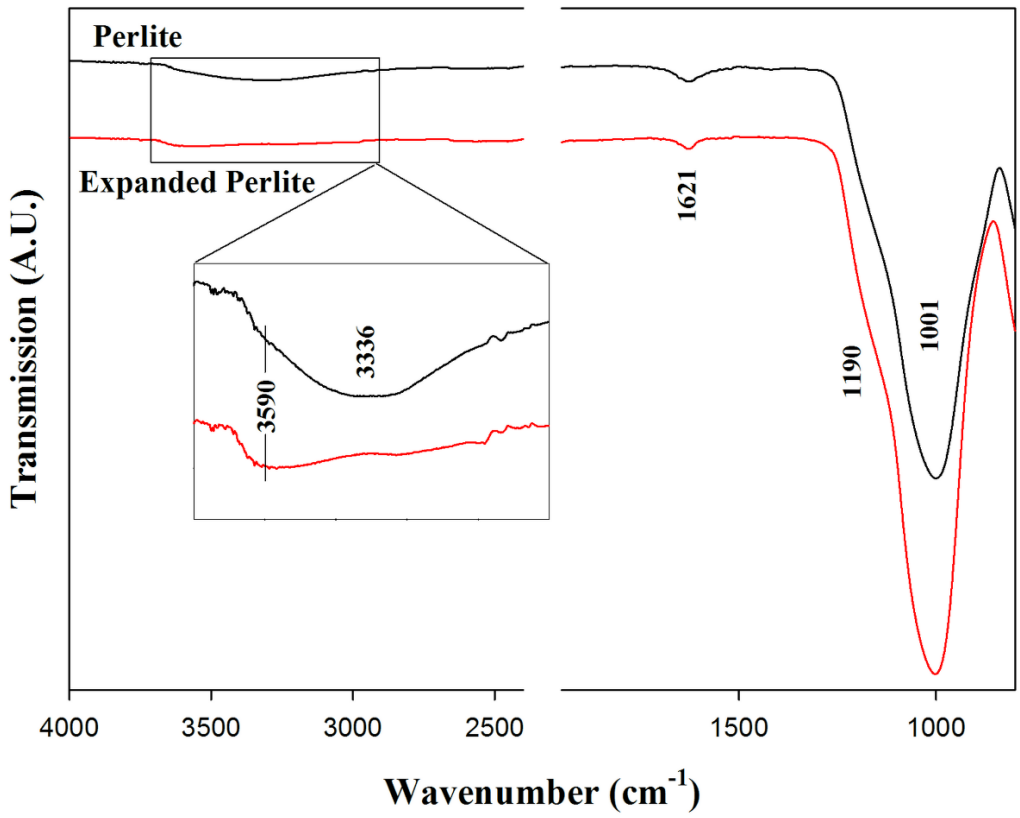

Figure II-12: FT-IR spectra of the raw and expanded perlite.

Loss on ignition (LOI) of both perlite particles was determined by thermogravimetric analysis (TGA). It is reported in the literature that perlite dehydration can be associated to the evaporation

of the different forms of water, generally occurring in three temperature ranges: 0-250, 250-500 and 500-800 °C [147]. Based on TGA results, 20-45% of the total water content in perlite is released in the first region, which is attributed to the volatilization of weakly bound molecular water or superficial water adsorbed in the pores (physisorbed water) [157]. In the second region, the sample starts to soften, releasing 45-65% of its total water content corresponding to the molecular water trapped into the inner surfaces or microcracks [158]. The third loss observed above 500°C corresponds to -O–H groups associated with the oxygen atoms through strongly bonded hydrogen [157], together with the burning of carbonaceous constituents adsorbed on the surface of the solid materials remaining or the volatilization of some trace metal oxides.

The TGA results (Figure II-13) shows main a large weight loss between 190 and 650 ˚C for both perlite types. The results presented in Table II-5 show that the raw perlite release 4.41% while the expanded perlite loss only 2.72%. These results are consistent with the literature reporting that water content in the perlite network is between 1.5 and 5.0 wt.%. As seen, the amount of water release in expanded perlite is significantly less than for the raw perlite attributed to water losses occurring in the expansion process. The onset temperature as reported in Table II-2 shows a direct relation between this value and perlite structure. Expanded perlite has an onset temperature at 116.5 °C compared with 228.6 °C for the raw perlite. This difference is attributed to the open structure of expanded perlite as most of the remaining water becomes more accessible to release at lower temperatures [159]. The temperatures corresponding to 3% weight loss are also listed in Table II-2. The T3% of expanded perlite (642.5 °C) is higher than raw perlite (382.0 °C), which can be associated to the release of physisorbed and chemisorbed water content, which is significantly changed after perlite expansion [158].

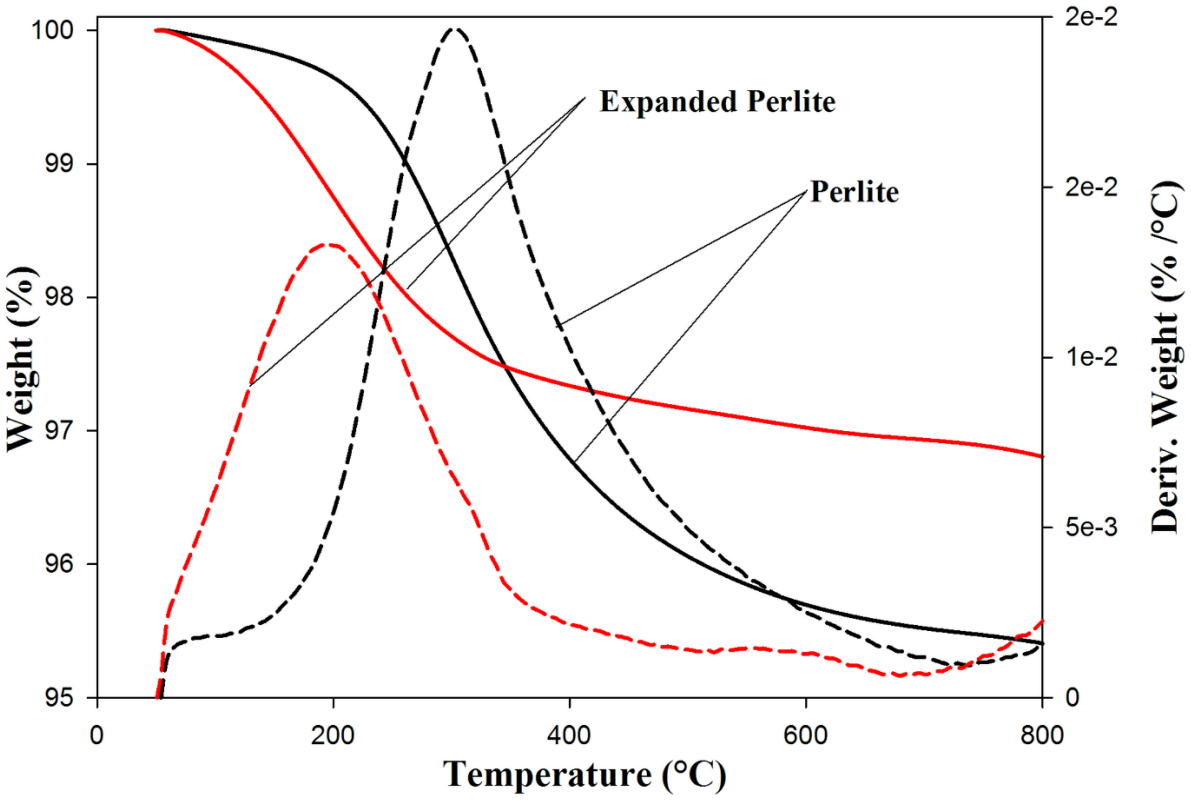

Figure 0-13: TGA and DTG curves of the raw and expanded perlite.

Table 0-5: Thermal parameters determined from TGA curves.

Samples	Raw perlite	Expanded perlite
Tonset (°C)	228.6	116.5
T_{MAX} (°C)	302.1	192.0
Mass loss (%)	4.41	2.72
$T_{3\%}$ (°C)	382.0	642.6

The melting enthalpies (ΔHm), as well as the peak melting (Tm) and crystallizing (Tc) temperatures of PP are listed in Table III-3. It can be seen that the temperatures for the composites were shifted to higher values compared to neat polypropylene; i.e. the melting peak temperature (Tm) increased from 163.3 °C for neat PP to 167.3 °C and 165.5 °C at 15 wt.% of raw and expanded perlite, respectively. This behavior can be related to physical interactions between both perlites and polypropylene molecules such as capillary forces, surface tension, and hydrogen bonding [160]. On the other hand, the crystallization peak temperatures increased from 116.9 °C for neat PP to values around 120 °C for composites at 15 wt.% of raw and expanded perlite indicating that the particles might act as heterogeneous nucleation sites [31]. Finally, the ΔHm of

the composites significantly decreased from 71.5 to 60.9 J/g (raw) and to 41.4 J/g (expanded) leading to a substantial reduction in the degree of crystallinity indicating that the thermal stability of the polypropylene increased with increasing perlite content [148]. The crystallinity (Xc) degree was calculated as:

$$Xc = \frac{\Delta H_m}{\Delta H_{m(crys)}\, w} \times 100 \qquad (1)$$

where ΔH_m is the melting enthalpy of a sample,

$\Delta H_{m(crys)}$ is melting enthalpy of 100% crystalline isotactic PP (138 J/g) [32],

w is mass fraction of the PP in the composites.

As reported in Table II-6, the crystallinity degree decreased from 51.8% for neat PP to 48.0 and 35.0% for raw and expanded perlite, respectively. This decreasing effect is attributed to the nucleation effect of the particles leading to a steric hindrance effect (smaller spherulite sizes and higher crystallites numbers at higher fillers contents) [46].

Table 0-6: DSC results.

Content (wt.%)	Raw perlite				Expanded perlite			
	T_m (°C)	T_c (°C)	ΔH_m (J/g)	Xc	T_m (°C)	T_c (°C)	ΔH_m (J/g)	Xc
0	163.3	118.4	71.5	51.8	163.3	118.4	71.5	51.8
5	168.3	119.2	64.3	49.0	168.5	119.5	73.7	56.2
10	167.4	119.1	60.4	48.6	166.8	119.6	51.5	41.5
15	167.3	119.2	56.3	48.0	165.5	120.1	41.1	35.0

Typical micrographs of the composites fractured surfaces are presented in Figure II-14. The images reveal the spherical shape and typical random distribution of perlite particles. The raw and expanded perlite are characterized by a size of around 11.1 µm and 12.2 µm, respectively. This difference is related to the thermal expansion of expanded perlite. Furthermore, the raw perlite in Figure II-14a seems to have good adhesion with the matrix related to the high number of surface hydroxyl groups forming hydrogen bonding with the high number of hydrogen atoms in polypropylene. On the other hand, poor adhesion between expanded perlite and the polymer is observed in Figure II-14b as particle pull-out occurred. This phenomenon is related to the

decreased amount of surface of the expanded perlite due to the thermal expansion as confirmed by FTIR (Figure II-12) and TGA (Figure II-13).

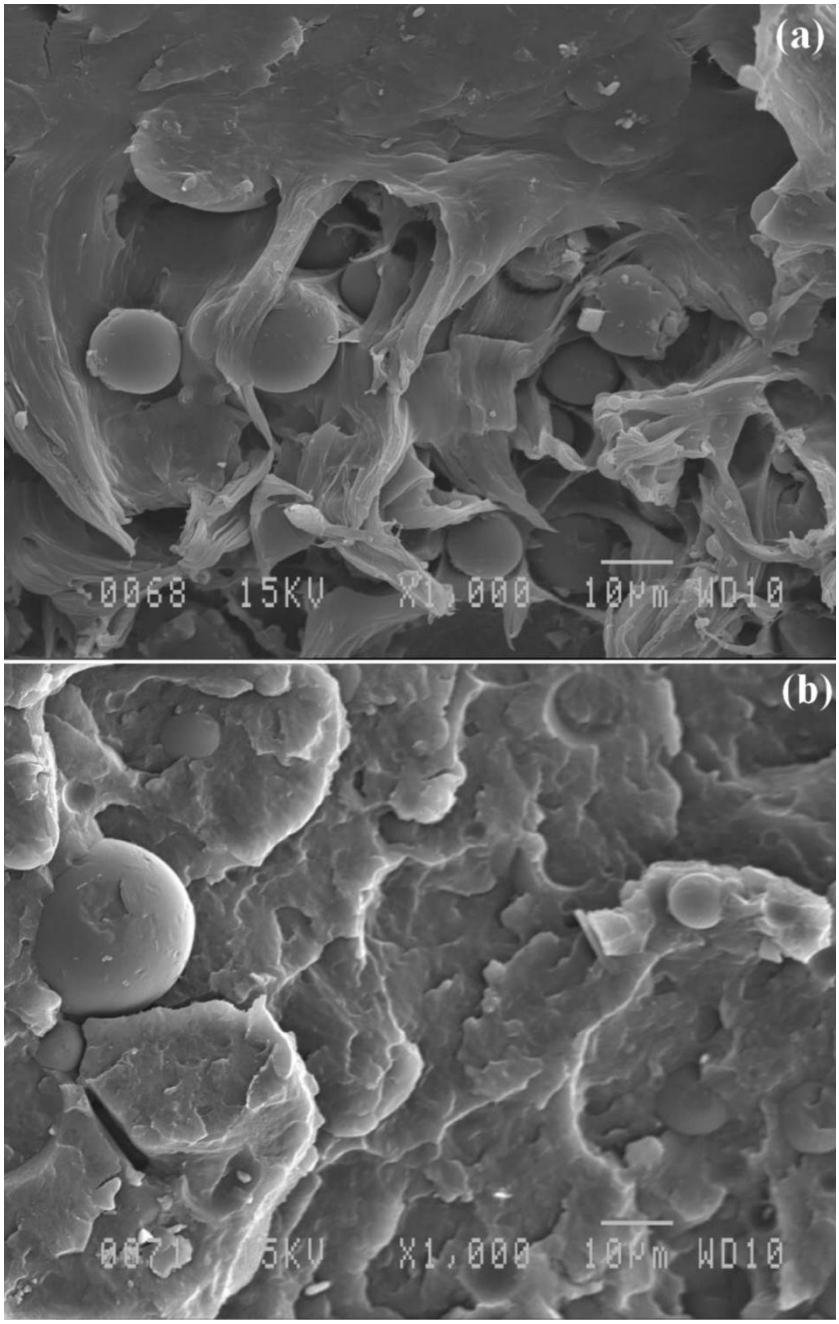

Figure 0-14: SEM micrographs of : (a) raw and (b) expanded perlite composite at 10 wt.%.

Figure II-15 compares the tensile properties of the samples. Figure II-15a shows that Young's modulus increases from 1030 MPa for neat PP up to a maximum of 1456 MPa (41%) at 15 wt. % of raw perlite. On the other hand, the values for expanded perlite (between 601 and 779 MPa) are always lower than the matrix. So raw perlite produces better results compared to expanded perlite composites [163]. As discussed above, these results are associated with a change of the surface

properties (mainly hydroxyl groups number) having an effect on the morphology of the composites, especially interfacial interactions (Figure II-14).

The tensile strength curves of raw and expanded perlite composites are presented in Figure II-15b. It can be seen that for raw perlite, there is only a slight decrease with increasing particle content, less than 24.7% for the raw perlite composites at 20 wt.%. However, the tensile strength for expanded perlite composites is substantially lower (less than 56.9%) at 20 wt.% compared to neat polypropylene. This loss of tensile strength is generally due to poor adhesion between the particles and the matrix as observed by SEM (Figure II-14). As voids around the perlite particles are observed, this substantially decreases the possibility of interfacial stress transfer [163]. Similar results for the strain at yield are reported in Figure II-15c. In this case, expanded perlite produced higher values because of limited interfacial interaction [164].

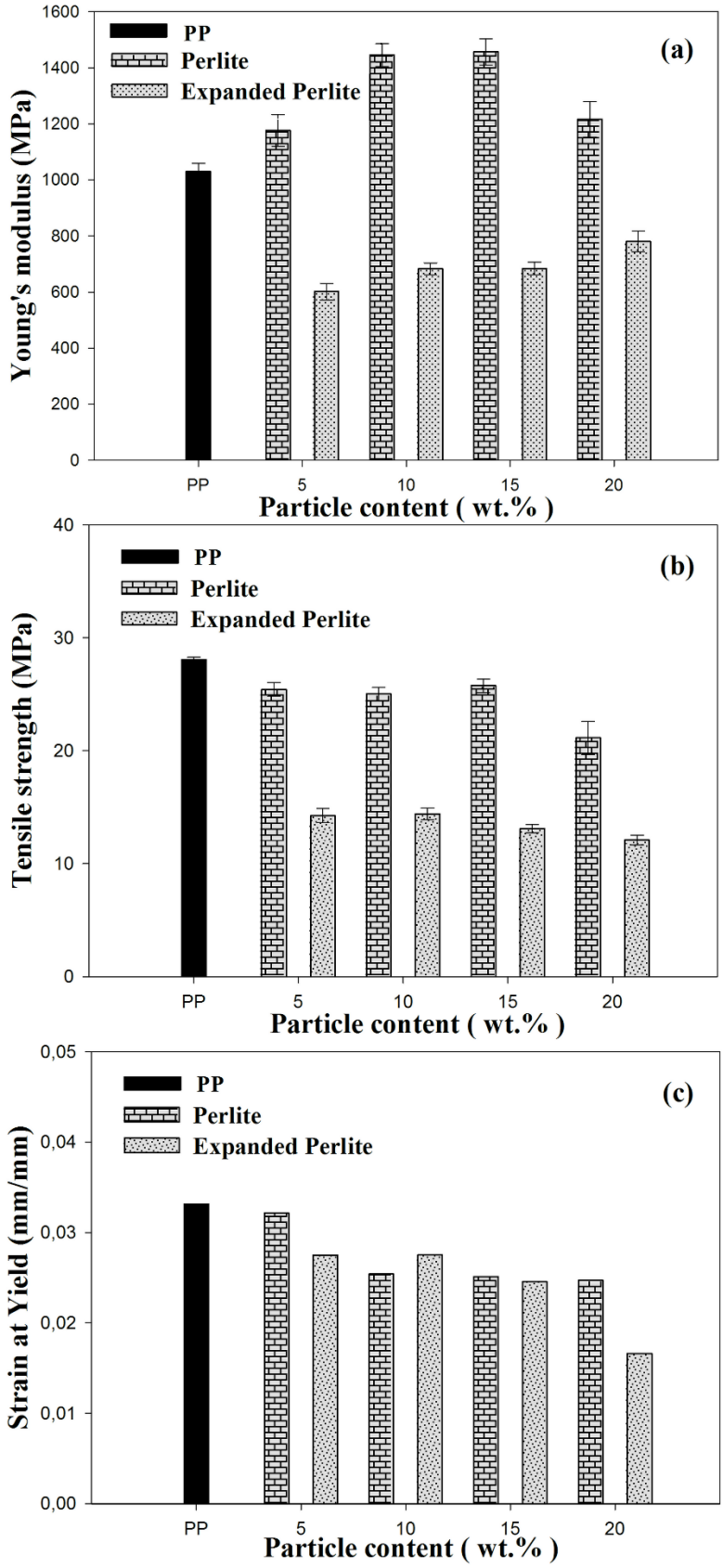

Figure 0-15: (a) Young's modulus, (b) tensile strength and (c) strain at yield as a function of perlite content.

In Figure II-16, the torsion modulus and damping factor of the samples are reported. As expected, the torsion modulus (Figure II-16a) dropped to 15.1 and 13.9 MPa at 5 wt.% of raw and expanded perlite (0.1 Hz), respectively. This behavior is related to the fact that at low particle contents, the perlite acts as a default resulting in a weaker structure. Nevertheless, at higher particle loading, the torsion modulus increases with increasing perlite content, which is associated to a more important response of the rigid particles to the mechanical solicitation. The torsion modulus improvement can be attributed to the presence of the particles to sustain shear stresses and support a part of the load [165]. Figure II-5a also illustrates that the evolution of the torsion modulus is similar over the frequency range studied (0.1 to 40 Hz). It can be concluded that perlite composites behave as elastic solids. Furthermore, the addition of perlite particles increased the viscoelastic properties of PP, especially their elasticity [165]. Figure II-16b shows that the tan δ values are significantly decreased with perlite content. Furthermore, the composites based on expanded perlite show higher tan δ values. It can be concluded that the incorporation of perlite increases the elastic contribution (tan δ = E”/E’) and by doing so decreases the damping factor of the composites [165].

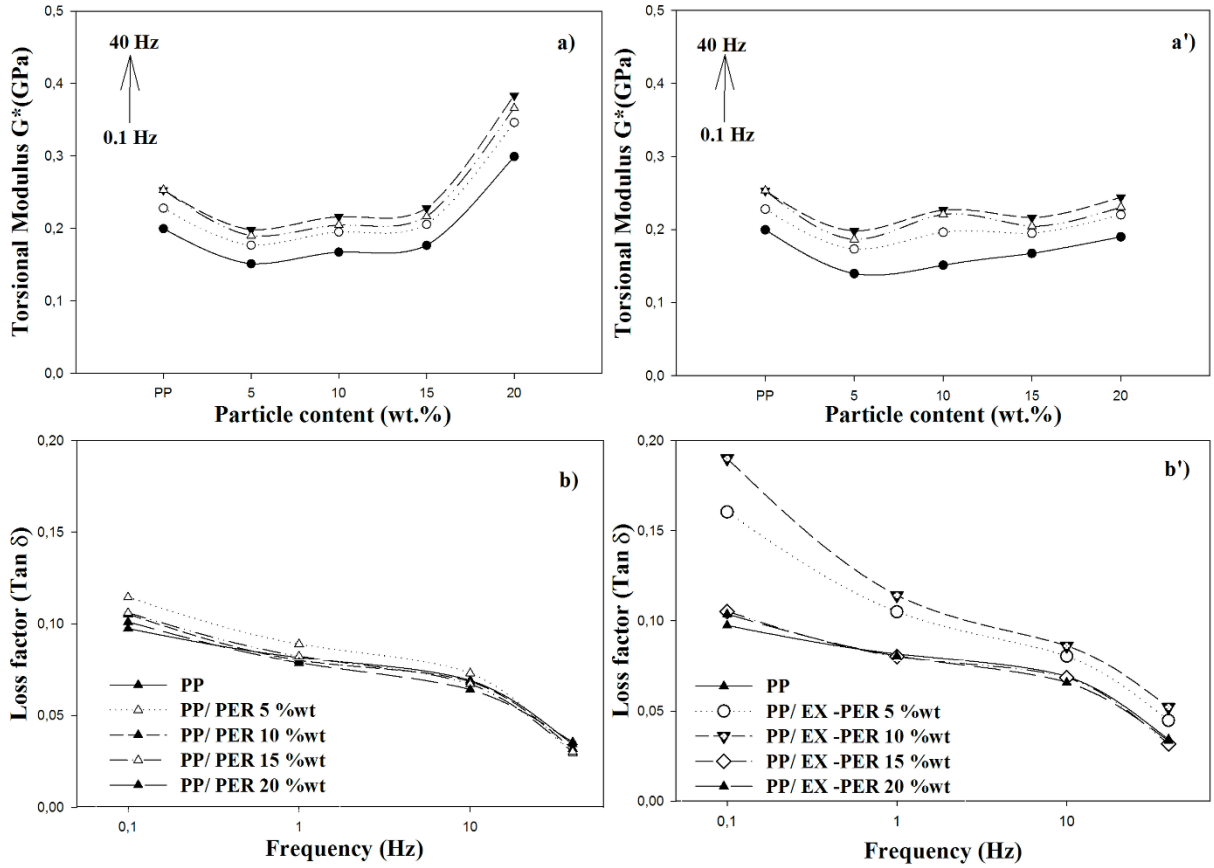

Figure 0-16: Torsion modulus and damping factor of PP composites as a function of particle content: (a, b) raw perlite and (a’, b’) expanded perlite.

Figure II-17 compares the rheological properties (melt state) of the samples. Figure II-17a shows that the incorporation of raw perlite increases the storage modulus of the composites due to the more elastic behavior of the rigid perlite particles. The presence of rigid particle limits polymer chain mobility and changes the molecular dynamics [166]. In Figure II-17, a linear shape of the curves was observed despite a slight reduction at 5 wt.% expanded perlites. This behavior is due, as mentioned above, to the special character of perlite at low amount, which acts as defaults. Furthermore, the raw perlite composites show higher storage modulus than the expanded perlite counterpart. This can be related to the improved dispersion of the raw perlite in the polymer matrix due to the strong hydrogen bonding on the raw perlite particles surface leading to improved elasticity of the PP matrix [159]. The loss modulus of the composites filled with raw and expanded perlite are shown in Figure II-17b and II-17b', respectively. With increasing perlite content, both composite curves show a small but continuous increase in loss modulus, which is more significant with increasing frequency. This behavior can be explained by the strong interactions between the dispersed perlite particles and PP chains, generated by a better compatibility between the polymer and perlite particles [167], as well as good particle dispersion/distribution inside the PP matrix [168]. Moreover, the G' values are higher than G" at higher frequencies for all composites indicating a more solid-like response in the molten state. In fact, there is not sufficient time for the polymer chains to relax leading to a more elastic behavior of the melt at higher frequency [169].

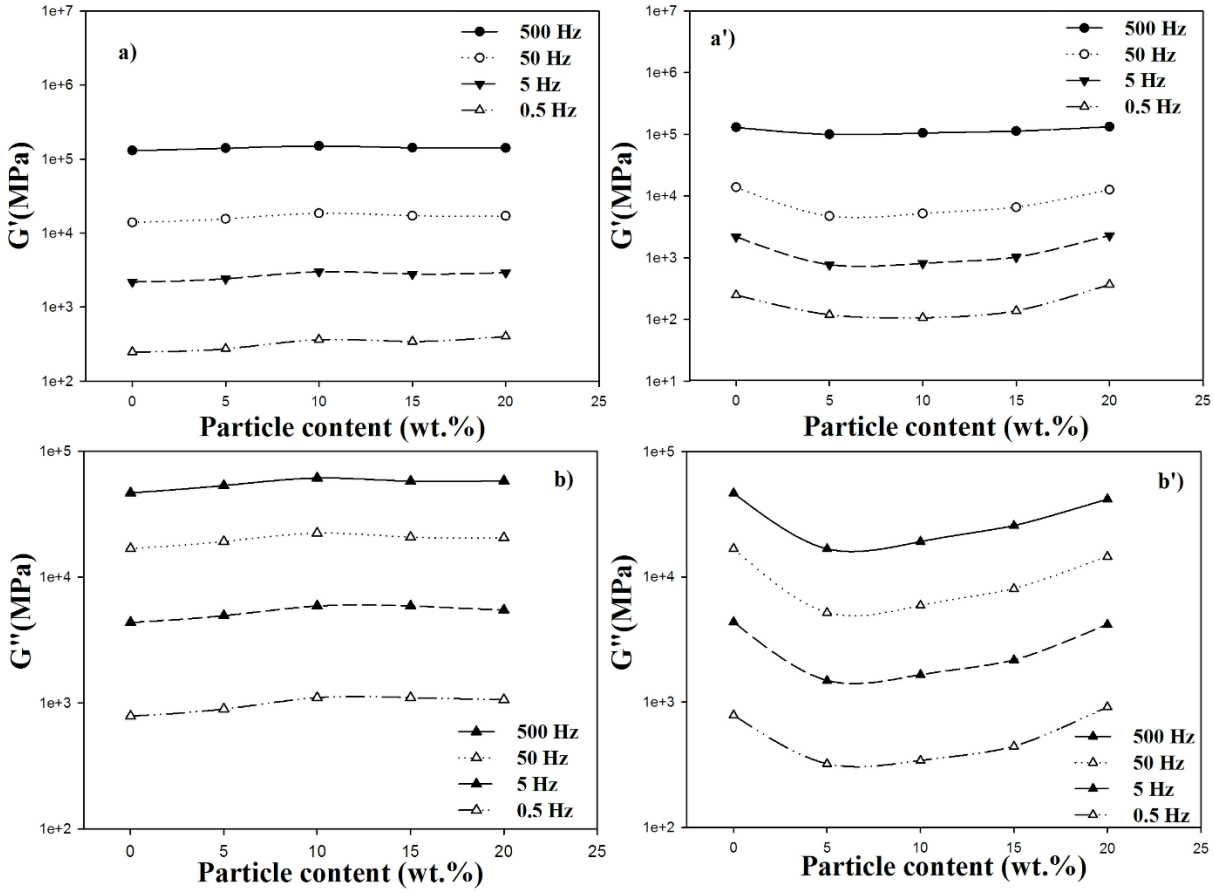

Figure 0-17: Rheological properties of the PP composites as a function of particle content: (a, b) raw perlite and (a', b') expanded perlite.

II.11. Conclusion

Polypropylene composites containing different concentrations (0-20 wt.%) of raw and expanded perlite were prepared by melt blending/molding and characterized using different techniques. The SEM analysis revealed a spherical shape for perlite particles with good dispersion in the matrix. As expected, larger sizes were observed for expanded perlite particles but lower interfacial adhesion with PP was attributed to the decreased number of hydroxyl groups limited hydrogen bonding as determined by FTIR and BET. This change in surface composition had a substantial effect on the mechanical (solid state) and rheological (melt state) properties of the composites. For example, the Young's modulus of raw perlite reinforced composites increased by up to 41% (at 15 wt.%) compared to the neat PP, while the values for expanded perlite reinforced composites dropped to a minimum of 601 MPa at 5 wt.%. On the other hand, it was found that at the same filler content, the rheological properties of both perlite composites show a linear viscoelastic behavior characterized by a transition from a liquid-like to a solid-like behavior at higher frequencies, resulting in a substantial increase in complex viscosity and storage modulus. It can be concluded that the raw perlite composites have much higher mechanical and rheological properties due to the presence of hydroxyl groups on their surface. Finally, based on TGA and mechanical results, the use of raw perlite might be interesting to improve the thermal resistance and the fire retardancy of polymer composites as well as their mechanical properties. More work is now underway to investigate this possibility.

Acknowledgements

This work was supported by Moroccan Foundation for Advanced Science, Innovation and Research (MAScIR), Rabat, Morocco. The authors would like to thank Mehdi Ait Dahi for his fruitful technical support and assistance.

Chapitre III

Effect of clay morphology and surface modification on the thermoplastic nanocomposites' properties: mechanical, thermal, and rheologic properties.

Effect of silane functionalization on properties of polypropylene/clay nanocomposites

Résumé

Des nanocomposites de polypropylène (PP) / argile ont été préparés par mélange à l'état fondu avec différents morphologiques d'argile, tels que la montmorillonite (nano-feuillets), l'halloysite (nanotubes) et la sépiolite (nanofibres). Ces argiles organiquement modifiées par greffage de deux organosilanes, à savoir le 3-aminopropyltriéthoxysilane (APTES) et le vinyltriméthoxysilane (VTMS). Les particules brutes ou modifiées ont été utilisées par la suite comme nanocharges de PP à des concentrations différentes (1-5% en poids). Selon les données expérimentales, les différents types d'argiles ont été modifiées avec succès en utilisant les molécules de silane approuvées par l'amélioration d'élongation à la rupture des nanocomposites en diminuant la taille des nanoparticules d'argile en cas de la montmorillonite, en modifiant leur composition chimique et en augmentant leur espacement interfoliaire. L'efficacité du procédé de silylation en tant que méthode efficace d'améliorer la surface d'adhésion matrice-charge a été démontrée en comparant les propriétés mécaniques des nanocomposites d'argile sans aucune modification. Les propriétés morphologiques et rhéologiques des nanocomposites PP / argile ont également été étudiées en détail. En conclusion, il a été constaté que l'addition des nano-organo-argiles permet d'améliorer les propriétés mécaniques des nanocomposites d'argiles, ce qui permet d'approuver une meilleure adhésion interfaciale entre les organo-argiles et le polypropylène avec une grande dispersion spatiale des particules. Les nanocomposites d'argile greffés PP/organosilane pourraient être utilisés en divers domaines d'application, en particulier l'industrie automobile et l'industrie de la construction.

Mot clé : polypropylène (PP); montmorillonite; halloysite; sépiolite; organosilanes; espacement interfolliculaire.

M. Raji et al. Composites Part B. 2018;146(April):106–15

III.1. Abstract

Polypropylene (PP)/clay nanocomposites were prepared by melt compounding with different grafted clay, such as montmorillonite, halloysite, and sepiolite. These clays organically modified by grafting of two organosilanes namely 3-aminopropyltriethoxysilane (APTES) and vinyltrimethoxysilane (VTMS) were used as nanofillers for PP at different concentration (1-5 wt.%). The physicochemical properties of organosilane-modified clay-type were examined by various structural, thermal and morphological analysis routs. According to experimental data, all clays were successfully intercalated using the silane molecules approved by the decline of the clay nano-particles size, modification of their chemical composition and the increase of their d-spacing. The efficiency of the silylation process as a good way to improve the matrix-fillers interaction was demonstrated by comparing the mechanical characteristics of the clays nanocomposites before and after grafting with organosilanes. Morphological and rheological properties of the PP/clay nanocomposites were also investigated in detail. In conclusion, it was found that the addition of the nano-organoclay allows improving the proprieties of silane-grafted clays nanocomposites, which can endorse better interfacial adhesion between the organoclay and the polypropylene and their great spatial dispersion-distribution. The resulting PP/organosilane-grafted clay nanocomposites could be used by industry, or possible fields of application including automotive and construction industries.

III.2. Introduction

The field of nanotechnology is one of the most popular areas for current international research and development in basically all technical disciplines [64]. This obviously includes polymer-matrix nanocomposite with different reinforcing materials such as clays, talc, mica [2], graphene [3] and specialty phosphate glasses [4-5] at the nanoscale level. Unfortunately, the high price and limited properties of the fully degradable polymer restrict the diversity of the usage. In this respect, an alternative approach has emerged involving the use of natural fillers as one of the most interesting material that can be employed to improve the properties of the final nanocomposite due to its high surface area which enhances hydrophilic polymer–filler interactions [105].

Among the nanofillers used in nanocomposites, clays undoubtedly play a major role. Different kinds of clay reinforcement are currently dominated the polymer industries because they have proven an unavoidable synergistic impact on the overall performance of the nanocomposites [2], due to their nanosized structural and functional properties such as low cost, less weight and low moisture absorption. The combination at the nanometric scale of the expansive surface areas,

anisotropic shape and reactive surfaces of clays with the functional behavior of organic polymers has been pointed out as an attractive way to develop organic–inorganic nanohybrid materials with properties that are inherent to both types of components [106]. Clay minerals used for polymer nanocomposites can be classified into three groups: nano-fibers, nano-scrolls and plate-like structure as shown in figure III-1 [21]. Generally, all these clays structure basically made up of tetrahedrally coordinated silicon atoms fused into an edge-shared octahedral plane of either aluminum hydroxide Al(OH3) or magnesium Mg(OH_3) hydroxide [107]. One example of these groups is plate-like structure belongs to the montmorillonite with ratio of 2:1, created from two tetrahedral sheets sandwiching an octahedral sheet [88]. This structure can undergo a structural rearrangement to give nano-fibrous structure [108]. Sepiolite clay has a rod-like fibrous structure consisting also of stacks of tetrahedral and octahedral oxide layers but with channel openings along the fiber axis. Furthermore, the nano-scrolls structure is specific for halloysite clay, when one octahedral sheet is linked to one tetrahedral sheet with 1:1 ratio [109]. Despite the similarity of the octahedral and tetrahedral sheets in all of these clays, there are some differences in the positions and the number of the interlayer water inside each clays structure as well as their relation to the hydroxyl bonds.

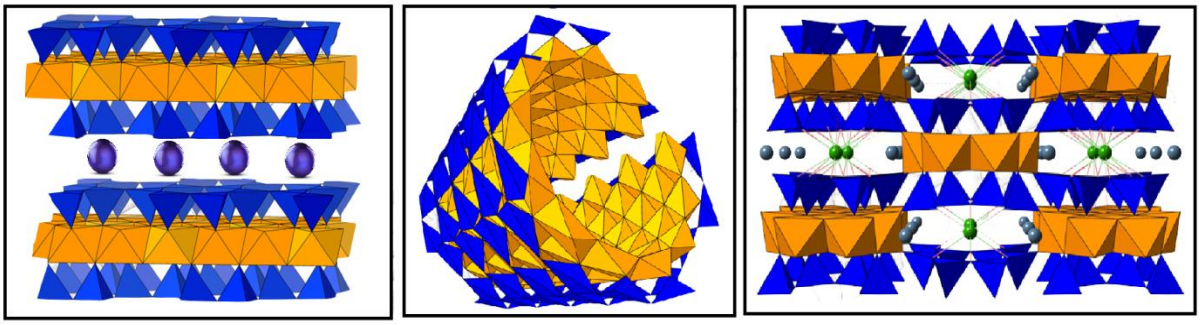

Figure III-1 : Clay minerals structures (plate-like filler, nano-tubes and nano-fibers)

As previously mentioned, the ultimate preparation of the advanced nanocomposites characterized by higher properties is depend on the degree of the compatibility of nanocomposites components and the dispersion/distribution of clay nano-particles into the polymeric matrix. Such an enhancement of the interfacial adhesion can be achieved either by clay and matrix modification with chemical/physical treatments or by use of interfacial additives [110]. A more convenient organiphilization method consists in forming covalent bonds between the polymer and clay. The formation of covalent bonds between polymer and clay is based on the ability of the functional group present in the modification agent of clay, to react with chain end macromolecules. Silane as one of the most coupling agents, is often used to create bonds between polymer and clay surface

due to its ability to react with the hydroxyl group of clay by hydrolysis/condensation and its terminal groups can also react with polymers [111,112]. Additionally, the homogenous dispersion and distribution of clay nano-particles into polymer matrix was reached by using melt compounding. This method is an efficient, cost-effective, quite attractive for polymer processing industries and does not require the use of organic solvents [3].

In the present work, three different clays minerals namely halloysite, montmorillonite and sepiolite were functionalized with two different organosilanes: 3-aminopropyltrimethoxysilane (APTES) and triethoxyvinylsilane (VTMS), After that, the manufacture of silane-grafted polymer nanocomposites were carried out by melt extrusion-injection molding of the polypropylene matrix at various concentrations of organosilanes from 1wt.% to 5wt.% particles content. Several characterization techniques have been used to speculate the effect of each silane-grafted on the structure of clay-type. The aim of this work is to determine the most effectiveness silane functionalization that can give high tensile, torsional and rheological properties of the prepared organoclay-polymer nanocomposites due to their ability to render the clay surface compatible with the polymer matrix [113].

III.3. Experimental

III.3.1. Materials

The polypropylene used in this work was a commercial polymer (trade name is PP5032, extrusion grade with a density of 0.9 g/cm^3 and a melting temperature of 165 °C) supplied by Exxon-Mobil Chemical. Three different commercial clays used as received were: Montmorillonite (MMT-Na) purchased from Southern Clay Products, Sepiolite (SEP) and Halloysite (Hallo), 3-Aminopropyltriethoxysilane (APTES), Vinyltrimethoxysilane (VTMS), Toluene and Acetone are supplied by Sigma–Aldrich.

Table III-1 : Structure and chemical characteristics of silane molecules

Functional group	Chemical name	Structural formula	M (g/mol)	Label
Vinyl	Vinyltrimethoxysilane	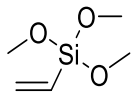	190,31	(VTMS)
Amino	3-Aminopropyltriethoxy silane	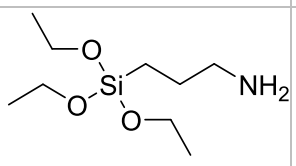	221,37	(APTES)

III.3.2. Silane-functionalized clay

5 g of clay was dispersed in 600 ml of toluene at 25 °C using a mechanical stirrer followed by sonication for at least 30 min. 50 ml of organosilane (3-aminopropyltriethoxysilane and vinyltrimethoxysilane) was added dropwise to the dispersed clay under constant stirring for 24h at 80 °C. Afterward, the suspension was separated and then washed using a mixture of acetone/water for three times by centrifugation at 10.000 rpm and dried at 60 °C under vacuum condition.

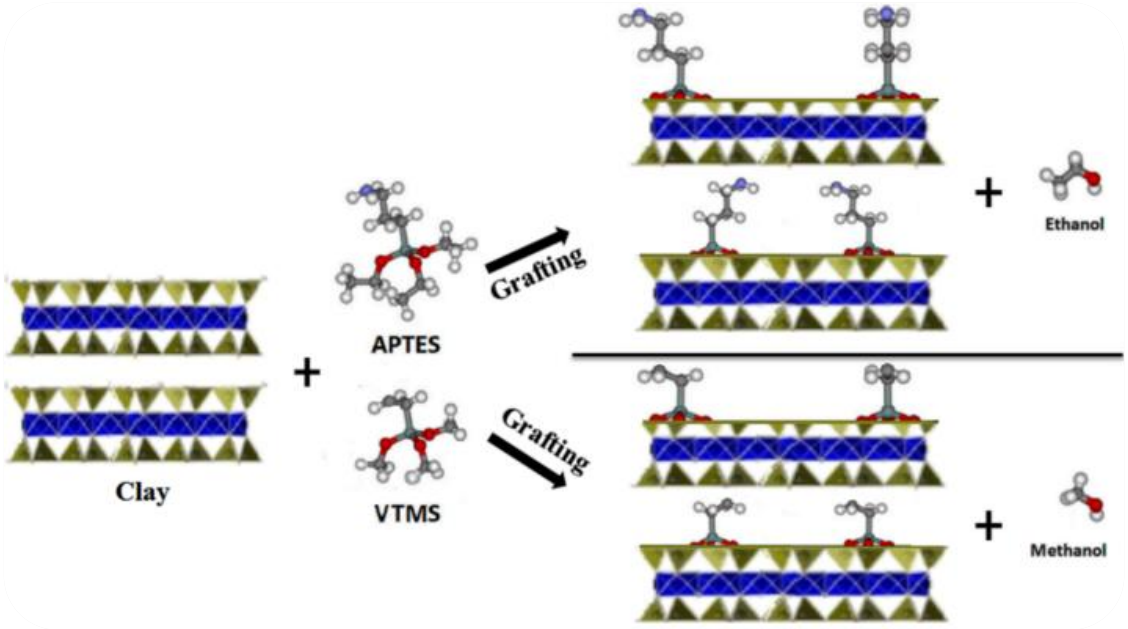

Figure III-2 : Schematic of synthetic procedure for APTES-clay and VTMS-clay

III.3.3. Nanocomposites preparation

PP/silane-grafted clay nanocomposites were prepared via melt extrusion technique using a Leistritz ZSE-18 twin-screw extruder (Leistritz Extrusion technik GmbH, Germany), under the following temperature profile of the extruder barrels, seven zones of the hopper and that of die were 170 °C, 170 °C, 175 °C, 180 °C, 180 °C, 175 °C, 170 °C and 170 °C. The weight fractions of each nano-clay incorporated in polypropylene matrix were ranging from 1 wt.% to 5 wt.% particle content and were obtained using the master batch process (10 wt.% nano-particles). The prepared wire was pelletized in a precision grinder (FRITSCH Pulverisette 19) into pieces of 2-3 mm and molded using the injection molded into an Engel e-Victory injection molding machine with a 40 tons platen capacity. The injection press barrel, nozzle and the mold temperatures were set at 180 °C, 170 °C and 45 °C, respectively.

III.3.4. Characterizations Techniques

III.3.4.1. X-ray diffraction (XRD):

The identification of the crystallographic structure of the clays after and before silylation was performed using the wide-angle X-ray diffraction (WAXD). All data were obtained on a Bruker D8 Discover using the Cu K α radiation (k = 1.54184 nm) and a GADDS detector. The diffraction patterns were analyzed using X'Pert High Score software. The interlayer distances of clay were estimated from the WAXD patterns with Bragg formula [114].

$$2\mathrm{d}\sin\theta = n\lambda \qquad (1)$$

III.3.4.2. Fourier transforms infrared spectroscopy (FTIR):

Fourier transforms infrared spectra (FTIR) of the clay and the functionalized ones were recorded using ABB Bomem FTLA 2000-102 spectrometer (ATR: Specac Golden Gate). The spectra were acquired with a resolution of 4 cm^{-1} and 16 scans.

III.3.4.3. Thermogravimetric analysis (TGA):

The thermal degradation of the clay and the effect of silane functionalization clays were evaluated by thermogravimetric analysis (TGA) using a Q500 from TA Instruments. The representative sample was placed in a platinum pan and heated under air from room temperature up to 800 °C at a heating rate of 10 °C/min. The amount of grafted and intercalated silane molecules has been calculated using the following equation [115].

$$\text{grafted amount } \left({}^{\text{mequiv}}/_{\text{g}}\right) = 10^3 \frac{W_{200-600}}{(100 - W_{200-600})\mathrm{M} \times \mathrm{n} \times 3}$$

Where M (g/mol) is the molecular weight of the grafted silane molecules.

The grafting yield, which corresponds to the percentage of silane molecules which effectively participated in the silylated reaction, the following equation is employed, where [silane] (mequiv/ g) is the silane concentration in feed [116].

$$\text{grafting yield } (\%) = \frac{\text{grafted amount } \times 100}{[\text{silane}]_0} \qquad (1)$$

Where [silane] (mequiv/g) designates the initial silane concentration

III.3.4.4. Dynamic Light Scattering (DLS):

The clay nano-particles were evaluated by dynamic light scattering (DLS) using Zetasizer Nano ZS from Malvern Instruments Ltd to determine the particle size of different kind of clay. All clays were diluted with ultrapure water to minimize the particle-particle interactions.

III.3.4.5. Scanning Electron Microscopy (SEM):

Scanning electron microscopy (SEM) is a proficient instrument to examine the size and the shape of the nano-clays and their dispersion/distribution in the polymer matrix. To obtain clean and accurate fractures, all the composites were cryo fractured in liquid nitrogen.

III.3.4.6. Tensile testing:

Tensile tests of three specimens for each type of nanocomposites were performed according to ISO 527-1:2012 using the universal testing machine INSTRON 8821S (Instron, USA) at a crosshead speed of 5 mm/min using a 5 kN load cell. The Young's modulus, tensile strength, and strain at yield of the nanocomposites were obtained from the stress-strain curves.

III.3.4.7. Torsion testing:

Torsion tests were performed on an ARES-LS Rheometer using the rectangular torsion mode, with the following sample dimension: 5.5 mm width, 58 mm length, and 2 mm thick [117]. The torsion modulus is obtained in oscillatory tests performed at room temperature in sweep frequency mode (0.1-40 Hz) at strain of 0.02.

III.3.4.8. Melt rheology:

Melt rheology tests were performed on a MCR 500 (Physica) rheometer equipped with a CTD600 device. The measurements of each sample (2 mm thick) were analyzed at 190 °C using small amplitude oscillatory shear mode equivalent to 25 mm parallel plate-plate geometry at constant frequency of 0.126 Hz and at a strain of 5 %, for which the materials exhibit a linear viscoelastic behavior as verified by previous strain sweeps.

III.4. Results And Discussion

III.4.1.X-ray diffraction (XRD)

Once the appropriate silane modified clays were prepared, a number of analysis techniques have been performed including XRD, FTIR, TGA analysis. The XRD patterns of raw clays and the silane-grafted by APTES and VTMS molecules are presented in Figure III-3. It is clear that the organo-montmorillonite was successfully functionalized by (APTES), as the basal spacing increased from 1.21 nm corresponding of MMT-Na to 1.9 nm (2θ = 4.6 °) for the MMT-APTES clay. In addition, the MMT-VTMS exhibits a board band at d = 1.31 nm which is close to the band of MMT-Na. These results indicate that there are no significant interlayers or edges grafting of (VTMS) molecule. This observation may endorse that the silylation take place at the surface of the montmorillonite which can be verified by FTIR and TGA results (Figure III-3a).

The diffractogram of the pristine halloysite and silane-functionalized halloysite are shown in Figure III-3b. The XRD pattern of the neat halloysite displays an intense peak at 11.98° with a basal spacing of 0.741 nm for the (001) plane of halloysite. This characteristic peak of halloysite has shifted to lower 2θ value for Hallo-APTES (2θ = 11.46 °, d-spacing of 0.775 nm), and for Hallo-VTMS (2θ = 11.81 °, d-spacing of 0.752 nm). This increase in d-spacing is attributed to the functionalization of halloysite by silane molecules. Figure III-3c illustrates the diffractogram of sepiolite and their functionalized ones, it can be seen that all data are almost identical so no information is delivered by XRD except some change in the intensities of some original peaks in the position range of 20-40 upon silylation. The variations in XRD diffractograms before and after functionalization of clays show that there is a covalent bond formed by the interaction between clays and different organosilanes in the clay galleries generally depending on the chain length of the silane [21].

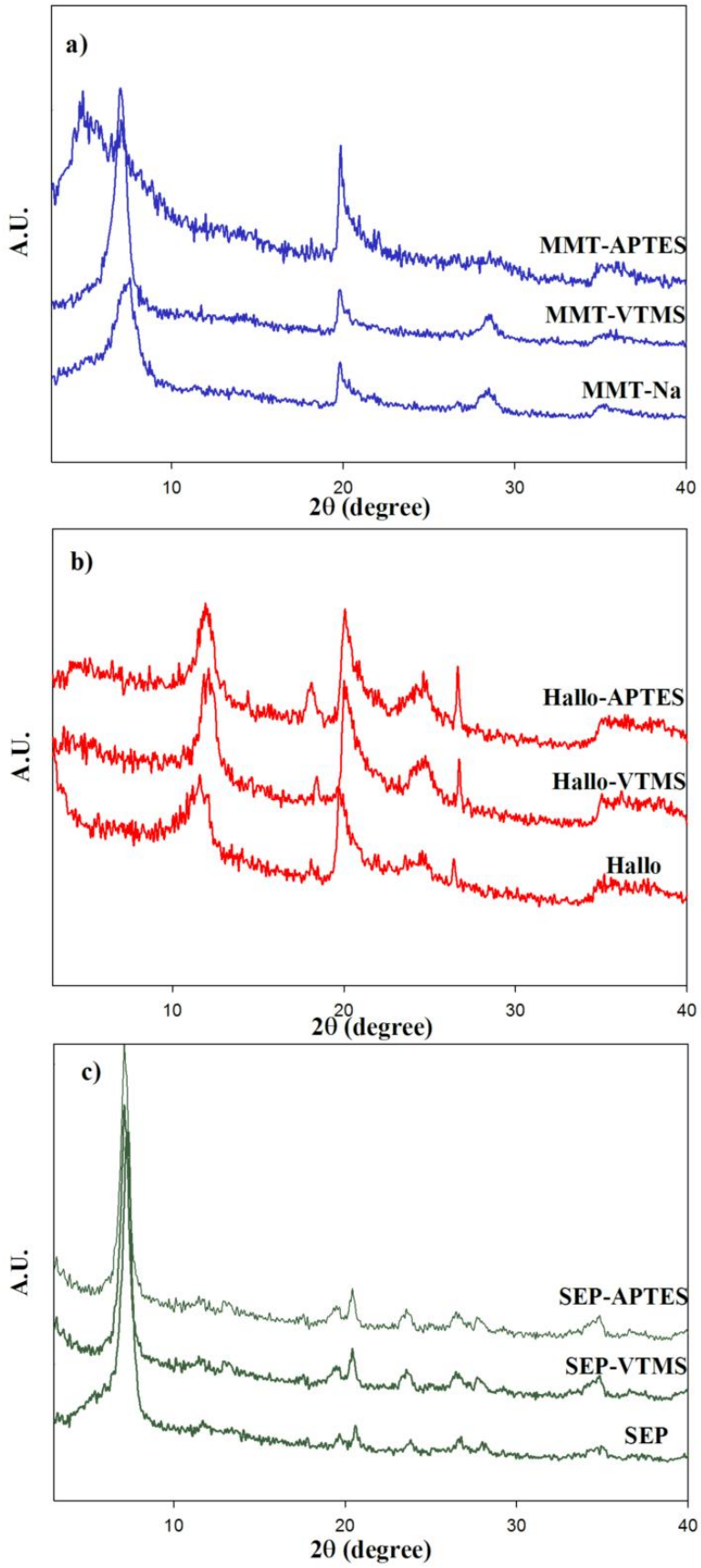

Figure III-3: XRD spectrum of montmorillonite, halloysite, sepiolite, and their silane-functionalized clays

III.4.2.Fourier transforms infrared spectroscopy (FTIR)

The FTIR spectra of raw clays and the functionalized ones by APTES and VTMS silane molecules are shown in Figure III-4. The montmorillonite IR spectrum presented in Figure III-4a shows two important bands around 3623 and 3400 cm^{-1} ascribed to O-H stretching for the silicate and water [2]. Besides, the band in the region of 1646 cm^{-1} is corresponding to the -OH bending mode of the adsorbed water [118]. The characteristic bands of raw clays at 1113 cm^{-1} and 1000 cm^{-1} are assigned to the out-of-plane Si-O stretching mode and to Si-O stretching (in plane) vibration for layered silicates, respectively [119]. Additionally, the bands at 935, 804 and 704 cm^{-1} are attributed to Al–Al–OH, and Al–Mg– OH bending vibrations, respectively [120].

Figure III-4b shows the FTIR spectra of the halloysite, the O–H stretching of inner-surface hydroxyl groups and O–H stretching of inner hydroxyl groups of the halloysite are presented at 3697 and 3623 cm^{-1}, respectively [121]. Although, the absorbed water is indicated by the H–O–H deformation band appears at 1635 cm^{-1}. The band at 1113 cm^{-1} was assigned to the stretching mode of Si-O, while the band at 1032 cm^{-1} was caused by the stretching vibration of Si-O-Si [122]. The O−H bending vibrations of the hydroxyl groups are observed at 910 cm^{-1} and Si-O-Si at 470 cm^{-1} confirm the existence of corresponding groups [123]. The bands attributed to the Al–OH vibrations of the surface hydroxyl groups are observed at 747 and 797 cm^{-1}. Further, the band observed at 538 cm^{-1} was due to the vibration of Al-O-Si [124]. Figure III-4c illustrates the FTIR spectrum of the sepiolite, the characteristic band at 3676 cm^{-1}, is attributed to Mg-OH stretching of hydroxyl groups in octahedral Mg ions located in the interior blocks of natural sepiolite. The coordinated water correspond of O-H stretching band appeared at 3585 cm^{-1} and O–H stretching and deformation of zeolitic water bands observed for sepiolite at 1647 cm^{-1} [125]. The Si-O coordination bands at 1211, 1017, 977 cm^{-1} are all observed as a result of the Si-O vibrations [126]. The bands presented around 800 and 662 cm^{-1} are resulting of the O-H deformations and translations, respectively [127]. The two peaks at 1017 and 435 cm^{-1} represent the stretching and bending of Si-O respectively in the Si-O-Si groups of the tetrahedral [2].

The FTIR spectrum of two silane-grafted clays (sepiolite, halloysite and Montmorillonite) show weaker characteristic signals bands at 2933 cm^{-1} and at 2865 cm^{-1} attributed to aliphatic stretching of C-H groups, respectively [128]. One more band at 1480 cm^{-1} associated to the deformation vibration of CH, normally present in the mono- and the trifunctional silane molecules [116]. Moreover, the clays-APTES exhibit some other FTIR peaks, corresponding to the deformation NH_2 vibration at 1556 cm^{-1} [129]. Additionally, the wide peak of water OH stretch was further

enlarged in the spectra of functionalized clay using APTES molecule, which is attributed to the overlap with the NH_2 stretching vibration. Thus, the presence of silane bands in all functionalized clays spectrum confirm that the OH group on the inner/outer-sphere surface and edge of the clays may react chemically with alkoxysilane Si—OR groups as presented schematically in Figure IV-2.

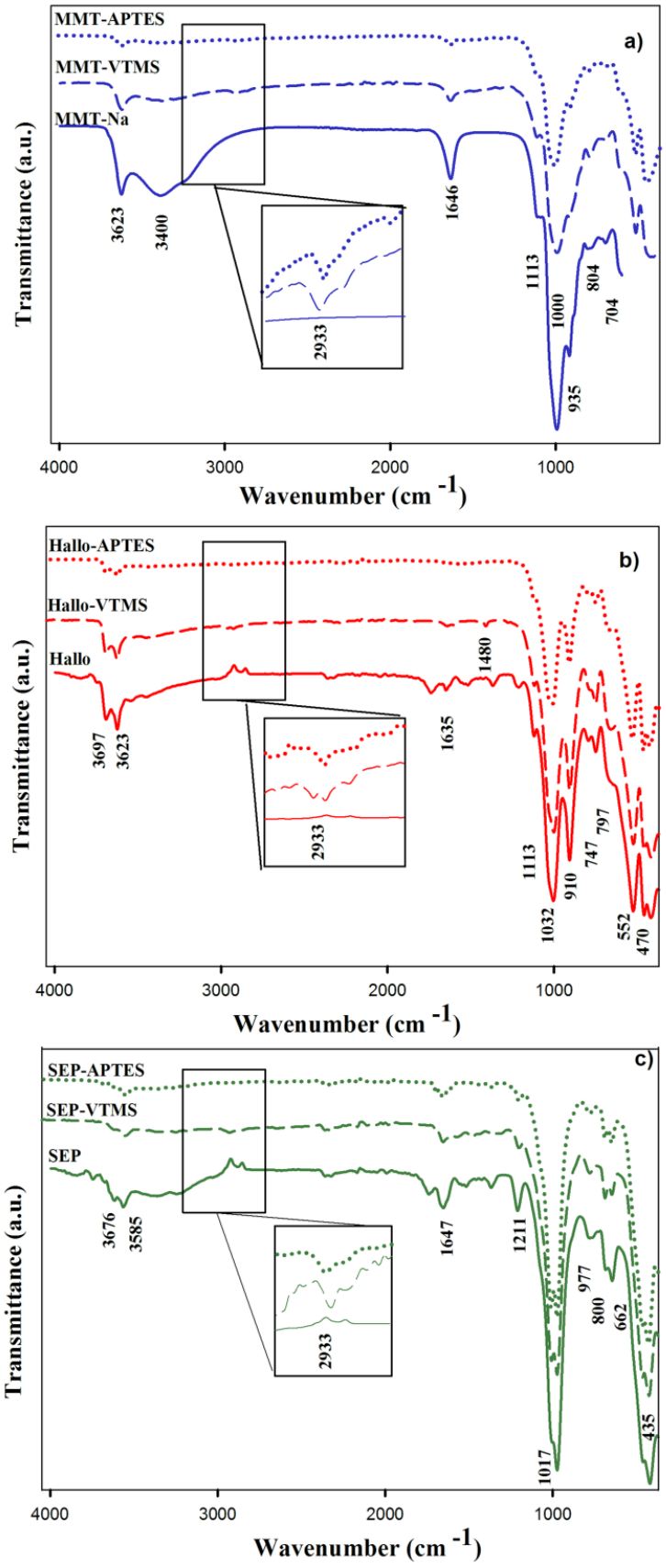

Figure III-4: FTIR spectra of montmorillonite, halloysite, sepiolite, and their functionalized ones

III.4.3.Thermogravimetric analysis (TGA)

The thermogravimetric (TGA) and differential thermogravimetric (DTG) curves of pristine and functionnalized clays by APTES and VTMS molecules are shown in figure III-5. Figure III-5a shows the montmorillonite thermal decomposition and their functionalized ones. Generally, the TGA curve of the montomorillonite displays two-steps degradation behavior associated with the loss of physisorbed water and then a loss of interstitial water presented around 41 °C and 651 °C, respectively. Another step appeared typically for silane functionalized montmorillonite ranging from 233 °C and 295 °C was due to the decomposition of organosilane molecules with a total weight loss varied from 2% for MMT-APTES and 10% for MMT-VTMS. Table III-2 summarizes the grafted amount and the grafting yield results calculated using thermogravimetric, as seen in the table III-2, the grafted amount of each organo-montomorillonite, is about 0.37 for MMT-APTES and 0.53 for MMT-VTMS. The percentage of silane molecules participated in the silylated reaction is about 25.1 for MMT-APTES, and 30.1 for MMT-VTMS [114].

Table III-2: Decomposition steps of silane functionalized montmorillonite

			Sample name		
step	bands	Characteristics	Na-MMT	MMT-APTES	MMT-VTMS
First step	loss of physisorbed water	Tmax°C	41	56	56
		Mass loss %	7	5	7
Second step	decomposition of the intercalated silane	T°C	--	433	287
		Mass loss %	--	2	10
		Grafted amount (mequiv/g)	--	0.1233	0.154
		Grafting yield (%)	--	25.1	30.1
Third step	loss of interstitially water	T°C	651	623	638
		Mass loss %	3	6	5

Figure III-5b presents the halloysite thermal decomposition and their functionalized ones. The decomposition curves of the raw and silane-grafted halloysite can be divided into three steps; The first weight loss is for raw halloysite in the range of 40–140 °C, after functionalization, the step was reduced which indicate an increase in the organophilicity of the halloysite, while the adsorbed water content at the surface was reduced due to the presence of organosilanes. The second step in the range 200–400 °C corresponds to the hydrogen-bonded silane existing in the cross-linking framework in the clay and the decomposition of the oligomerized silane network that was not removed during washing. The hydrogen-bonded silane is much less thermally stable than the covalently bonded silane, and decomposes at a lower temperature, considering the initial silane concentration used, the percentage of the silane molecule in a yield is about 4.73 % for Hallo-APTES, and 6.22% for Hallo-VTMS, whereas the estimated amount of silane-grafted effectively on the halloysite is about 0.087 mequiv/g for Hallo-APTES, and 0.107 mequiv/g for Hallo-VTMS. The last step is between 400–650 °C can be related to the structural dehydroxylation of Al–OH and Si–OH groups and some additional organic decomposition of silane-grafted onto SiOH and AlOH groups on edges or external surface, oligomerized silane, and silane-grafted on AlOH groups at the internal surface of the lumen [109]. Moreover, the higher weight loss shown from functionalized halloysites compared to raw halloysite is consistent with the hydrocarbon chain of the alkyl group from the grafted silane molecules. This also supports the strong chemical interaction of the organosilanes with the Si–O and Al–O groups of halloysite. The remaining materials at 800 °C (85%) are of aluminum oxides and silicon oxides present in halloysite structure [130]. Figure III-5c shows the changes in sepiolite structure with thermal treatment due to its water molecules. The thermal decomposition of neat sepiolite was carried out in four steps. The onset degradation temperature below 250 °C related to the elimination of both zeolitic and adsorbed water in which the sepiolite structure remains unchanged. Coordinated water is lost in two stages: between 250 and 350 °C and between 400 and 550 °C. Therefore, the coordination water loss involves structural changes reduction where a new channel cross-section of the zeolitic is reduced and an irreversible loss of water is produced. In this state, the mineral is called as anhydrous sepiolite. Between 550 °C and 1100 °C, the clay lost all the water molecules and retains their Si-OH groups along its fiber [131]. Above 1100°C, the Si-OH was destroying after total dehydroxylation [83]. From TGA analysis, the organic modified amount was calculated, from the volatilized mass between 125 and 650 °C, it's clear that the percentage of silane molecule grafted on sepiolite is about 3.87% for SEP-APTES, and 6.97 % for SEP-VTMS, whereas a number of intercalated molecules which effectively participated in the silylation reaction is about 0.072 mequiv/g for SEP-APTES, and 0.140 mequiv/g for SEP-VTMS. The TGA curves of both raw and

functionalized sepiolite are similar but an additional decomposition appears around 200–205 °C. This new step close to the decomposition area of zeolitic water corresponds to the degradation of organosilane molecule, which is usually related to silane-grafted on the silicate surface; these results confirm the silylation of sepiolite [131].

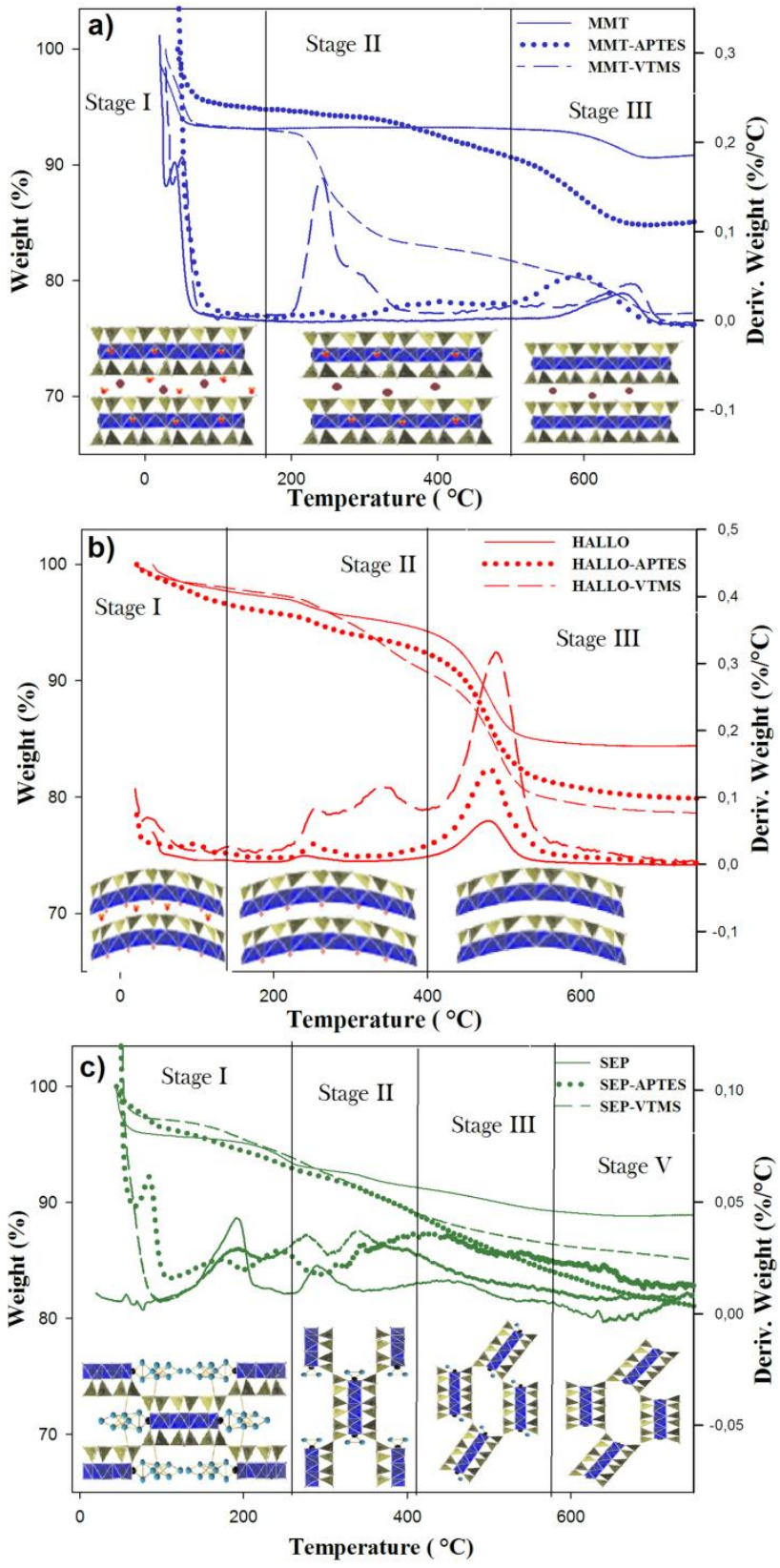

Figure III-5 : TGA curves for the different pure clays and silane functionalized clays used

III.4.4.Scanning electron microscopy (SEM)

The shapes of the all clays (Montmorillonite, halloysite and sepiolite) were studied by Scanning electron microscopy (SEM). A general view using the micrographs of the clays powder can be observed in Figure III-6. Nevertheless, the stronger nanoparticles intermolecular forces, that is a cohesive tension which makes an attempt to the clay particles to aggregate and to form the agglomerates [132]. The figure III-6 show that the montmorillonite possesses a plate-like morphology, halloysite particles are fibers or wires and the individual particles of sepiolite have a needle-like morphology with nanometric sizes.

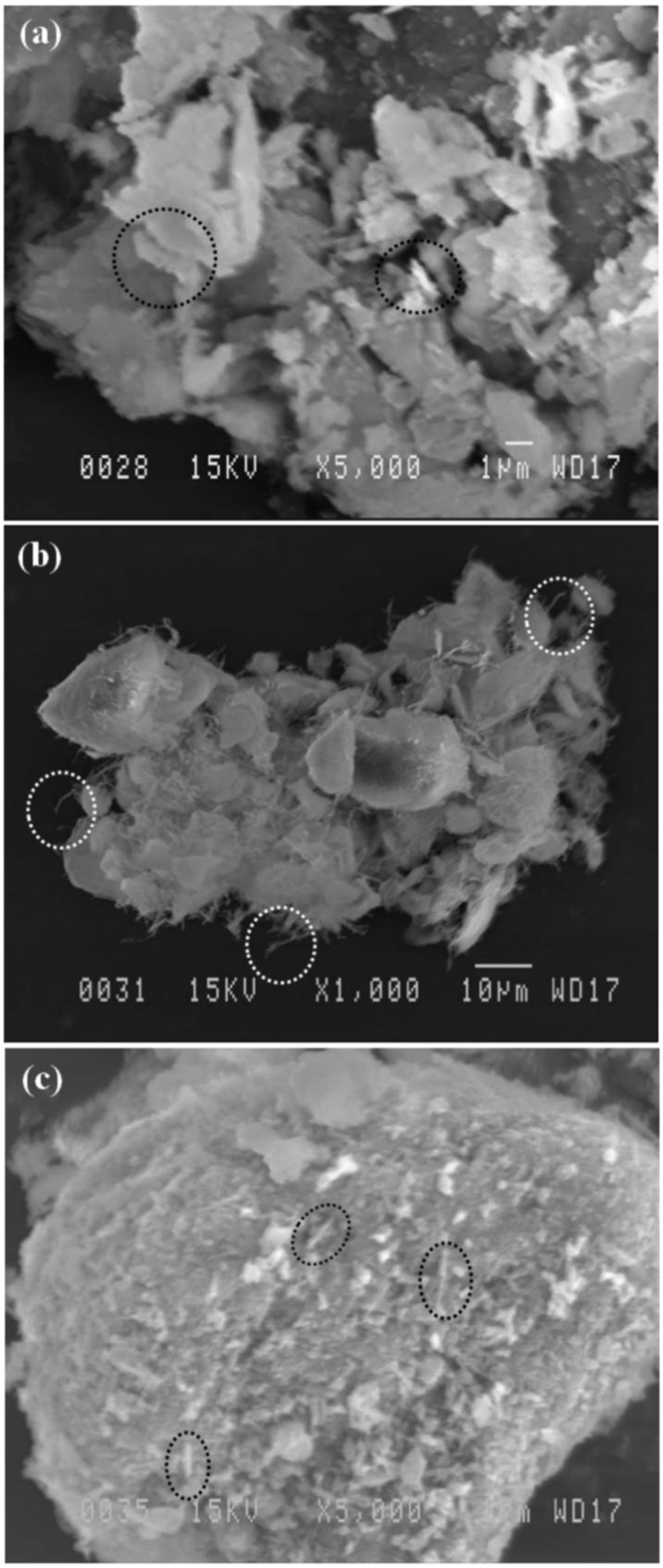

Figure III-6 : SEM photomicrographs of a) montmorillonite, b) halloysite and c) Sepiolite powders

The particle size and dispersion can be observed in figure III-7. These observations can be illustrated by Scanning electron microscopy (SEM) images of the cry fracture surface of the nanocomposites reinforced by the raw and functionalized clays. In general, all micrographs of functionalized clays show that the clays nano-particles are homogeneously dispersed in the PP matrix with a few of agglomerates. In contrast, it is observed on pristine clay nanocomposites micrographs that the particles are aggregates, resulting from the strong particle-particle interaction; the less aggregation and the lack of the voids around the clays nano-particles in the case of functionalized clay nanocomposites indicate that the use of silane functionalization can improve the interfacial adhesion between the clays nano-particles and PP polymer matrix [133]. Indeed, the use of melt compounding process to manufacture the nanocomposites is evident and enabled better nano-particles clay distribution [134]. On the other hand, the size of 50 particles can be measured to get an average nanoparticles size summarized as follow in table III-3. The particles sizes of all clays were decreased as compared to pristine ones, attributed to the change of the clay structure by silylation. The sizes of each clay particles measured by SEM are near to that measured by zetasizer, which means that they are no obvious agglomeration except for the montmorillonite, it seems that pristine montmorillonite dispersion in polymer matrix was not good and raw particles were aggregated.

Table III-3: the average particles size of raw and modified clay nanocomposites from SEM analysis

Clay/Nanocomposites		Particles size (nm)
Montmorillonite	Neat	230*
	Pristine	1084,41
	APTES	134,21
	VTMS	248,50
Halloysite	Neat	159*
	Pristine	341,36
	APTES	98,22
	VTMS	257,16
Sepiolite	Neat	150*
	Pristine	305,73
	APTES	142,46
	VTMS	146,37
***measured by zetasizer**		

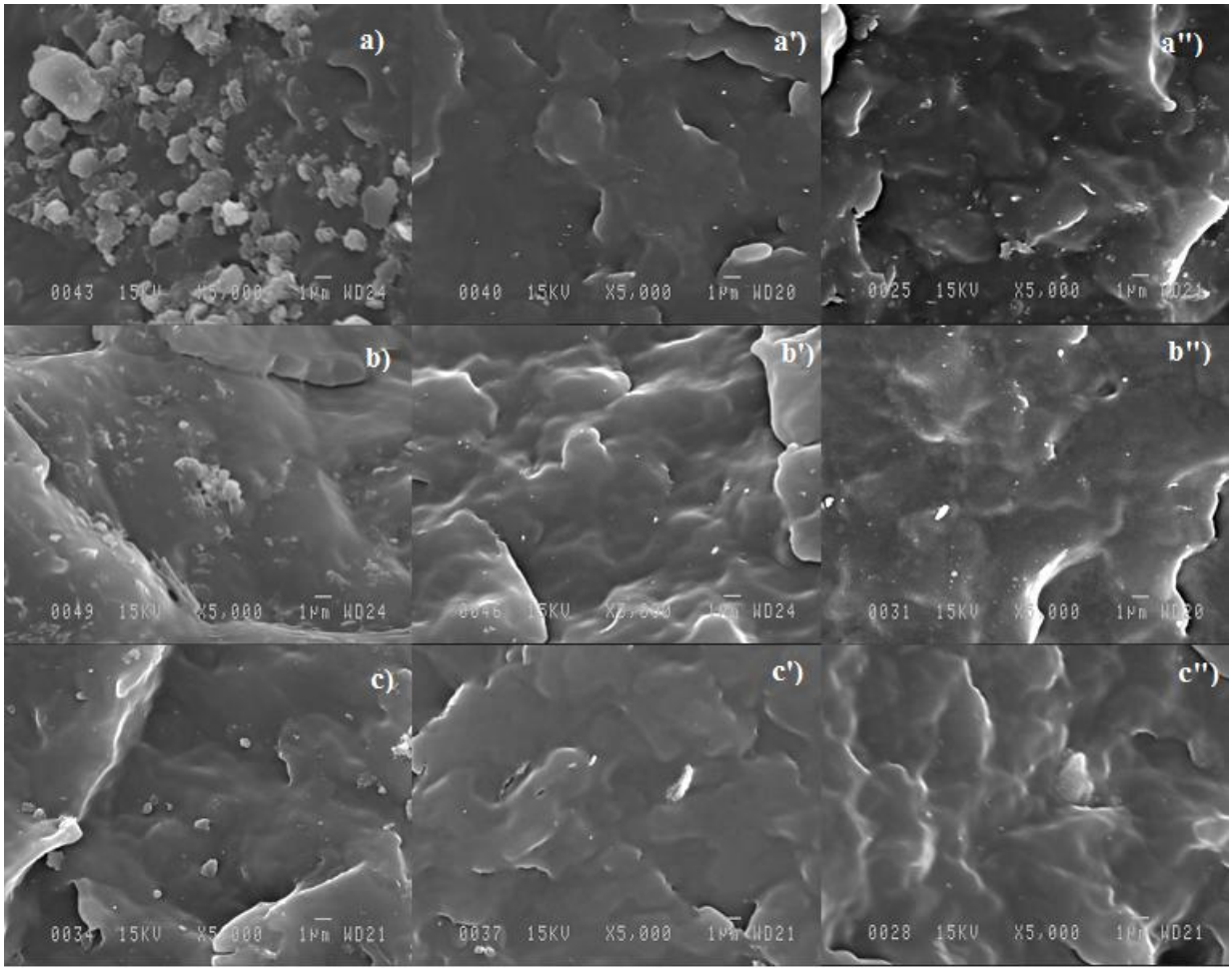

Figure III-7 : SEM micrographs of : a) halloysite; b) Montmorillonite; c) sepiolite; a') halloysite-APTES; b') MMT-APTES; c') sepiolite-APTES, a") and halloysite-VTMS; b") Montmorillonite-VTMS; c") sepiolite-VTMS.

III.4.5.Tensile testing

Figure III-8 shows the Young's modulus and the tensile strength of the pristine clays and functionalized ones. As seen in figure III-8. Young's modulus values of all clay composites significantly increase with increasing clay content and are better after silylation treatment. It also notes that the clays-APTES prove higher Young's modulus values due to better clay-polymer interaction which owing by the highest grafted at yield molecules silane calculated by TGA analyses. The Young's modulus values in the case of pristine clays are improved from 1034 MPa of PP to an optimum 2657.9 MPa, 2716.8 MPa and 2956.5 MPa at 5 wt.% for montmorillonites, halloysite and sepiolite, respectively. This significant improvement in the mechanical properties of clay nanocomposites can be attributed to high aspect ratio of clays and strong interaction between the hydroxyl groups of clays and the polymer matrix which restricted the mobility of polymer chains, their degree of freedom and enhance the adhesion between the composite

components by the formation of a strong linkage between the organic and the inorganic phase [135]. Moreover, the difference between Young's modulus values of all clay composites depend on clay particles size which is one of the factors that can contribute to the good compatibility of clays in melt compounding. The comparison of the tensile strength of the pristine clays and the functionalized ones are presented in Figure III-8. Remarkable enhancements of tensile strength values have been observed by the incorporation of montmorillonite, halloysite and sepiolite from 28.06 for neat polymer until a maximum at 5 wt.% up to 33.56 MPa, 30.91 MPa and 33.56 MPa, respectively. As a result, the functionalization of clays improve significantly the tensile strength values compared to pure clay nanocomposites due to better dispersion of the clay particles with high aspect ratio and high intrinsic stiffness, as well as the strong interaction between nano-clay particles and polymer matrix [88] approved by the exfoliation of the modified clay along the extrusion.

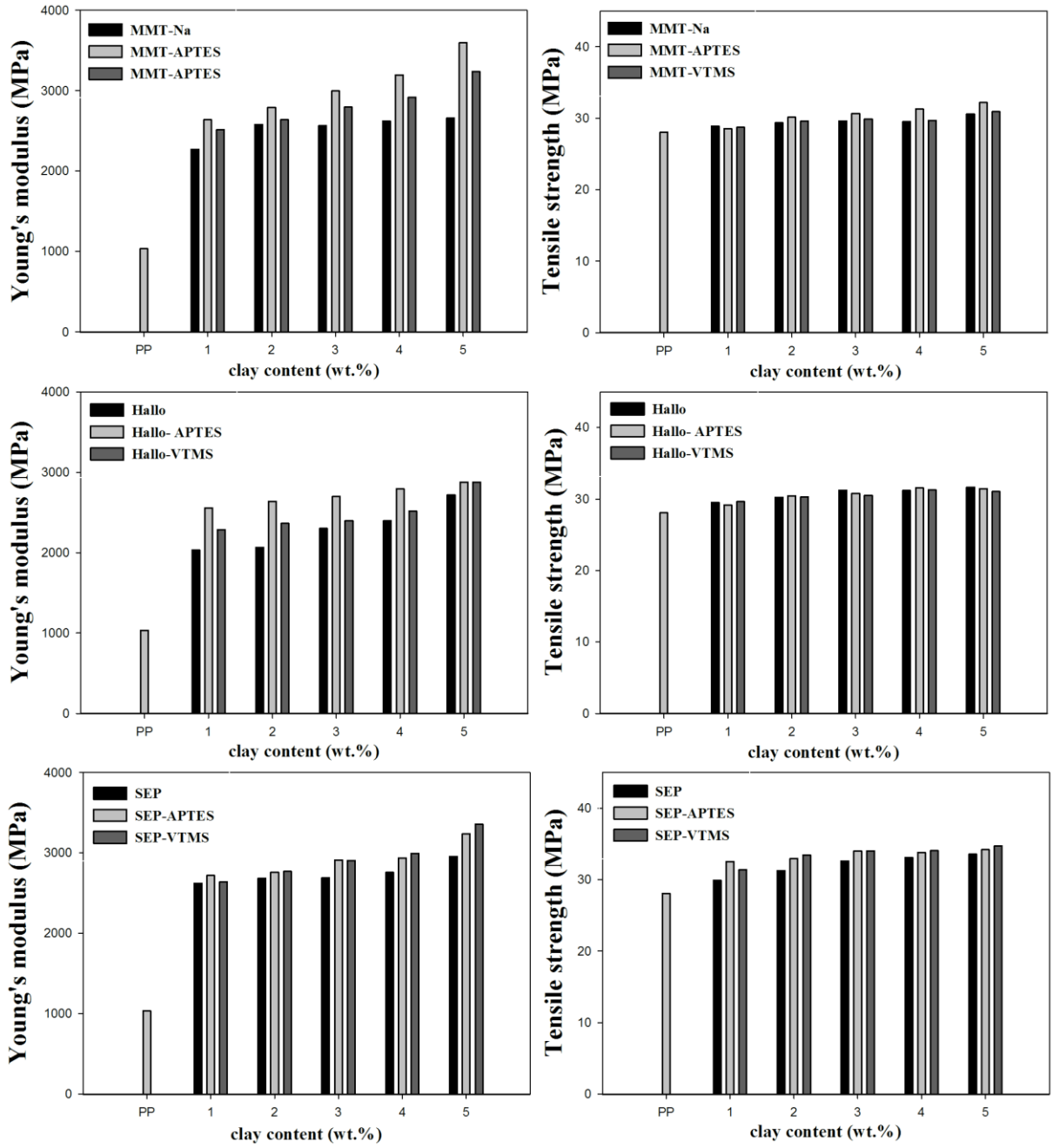

Figure III-8 : Young's Modulus and tensile strength of clay nanoparticles and their functionalized ones

III.4.6.Torsional testing

Figure III-9 shows the effects of the clay content and their functionalization on the nanocomposite's response to shear stress. For all nanocomposites, an increased in torsional modulus (G*) values with the clay loading has been noticed. It can be also seen that the functionalization of clays significant effect the torsional properties relative to the pristine clays. It clearly illustrates that the torsional modulus values markedly varied from 0.1 Hz to 10 Hz, leading to conclude that the nanocomposites response as a function of frequency is like an elastic solid

[136]. Figure III-9 present the evolution of loss factor (tan δ) of the pristine clay nanocomposites and their functionalized ones versus clay loading at two different frequencies. The tan δ of all the nanocomposites approached a constant value with the increase of clay content and showing a remarkable decrease with increasing frequency from 0.1 to 10 Hz. This evolution as function of clay content and frequencies is due to the elastic character of the clay particles, which prevails over a viscous behavior at high frequency [3].

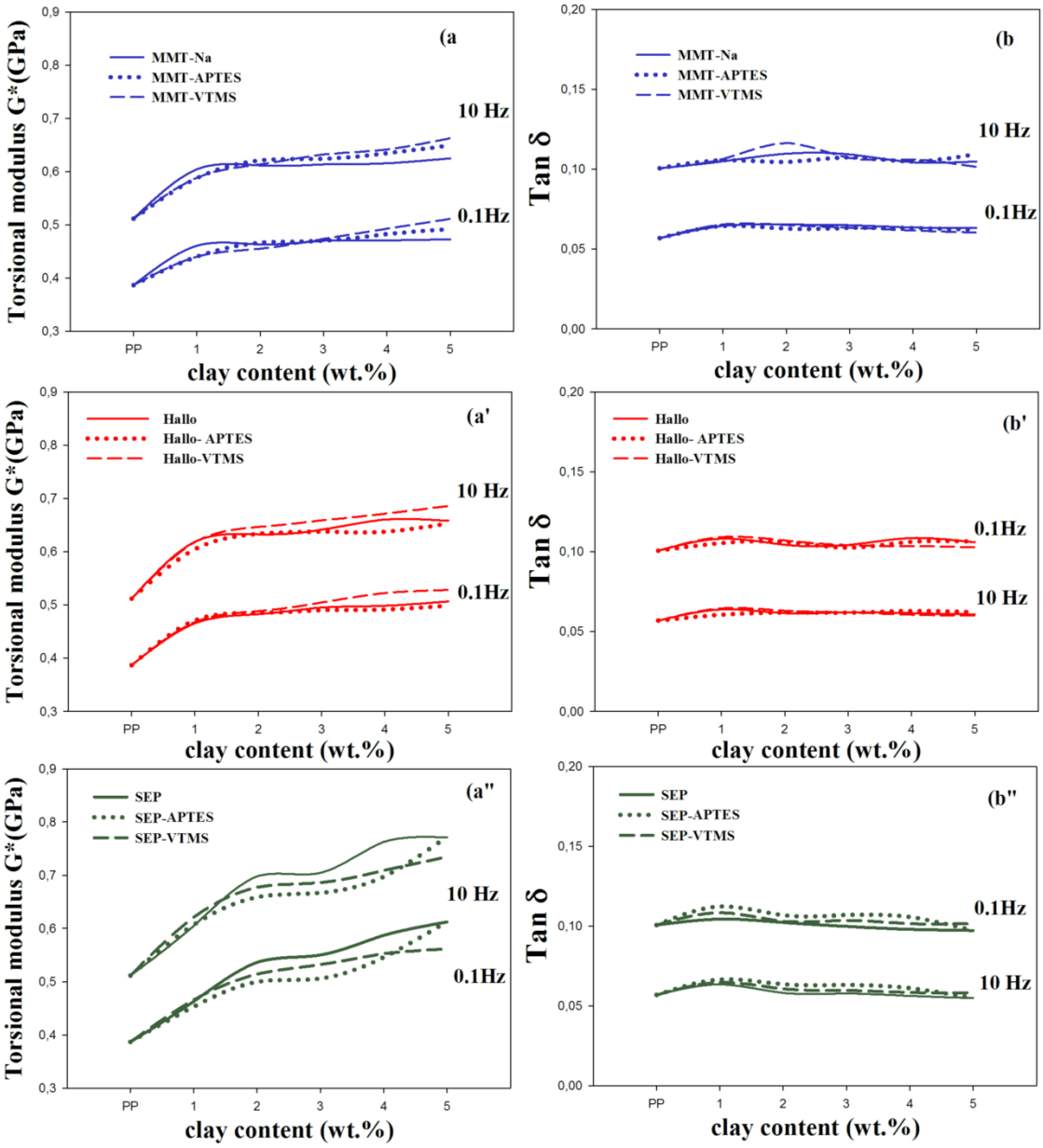

Figure III-9 : the torsion modulus and tan δ of PP composites made with the raw and silane-grafted clays at different frequencies

III.4.7.Melt rheology

The rheological properties of the pristine clays and functionalized clay nanocomposites were investigated in the melt state at constant a frequency of 0.126 Hz. Figure III-10 shows the complex viscosity against the clays content of virgin PP nanocomposites made with the pristine and functionalized clays. It is evident that the results show an increase in complex viscosity with halloysite loading, with a higher values presented for all functionalized clays due to the nanoscale dispersion of functionalized clay obtained by the exfoliation process using the melt extrusion and to a better interaction between nanoclay particles and the macromolecular chains of polymer matrix [137]. However, for the both fillers montmorillonites and sepiolite, the complex viscosity decrease with the increase of pristine montmorillonite or sepiolite loading which may be due to the presence of agglomerates or to highest particles size. Figures III-10 show the crossover point (G' = G'') as a function of clay content. The crossover point decreases by the incorporation of nano-clay particles indicating that the elastic behavior prevails over the viscous character due to the elastic character of nano-clays particles [6]. Nevertheless, in the case of functionalized clay nanocomposites, the crossover point present higher crossover points values than pristine ones which means that the viscous behavior prevails over the elastic behavior as compared to raw clay nanocomposites [138], this reduction in nanocomposites rigidity can be explained by the presence of the silane molecules grafted on clays nano-particles and possibly will give better interaction between nano-clays particles and polymer matrix.

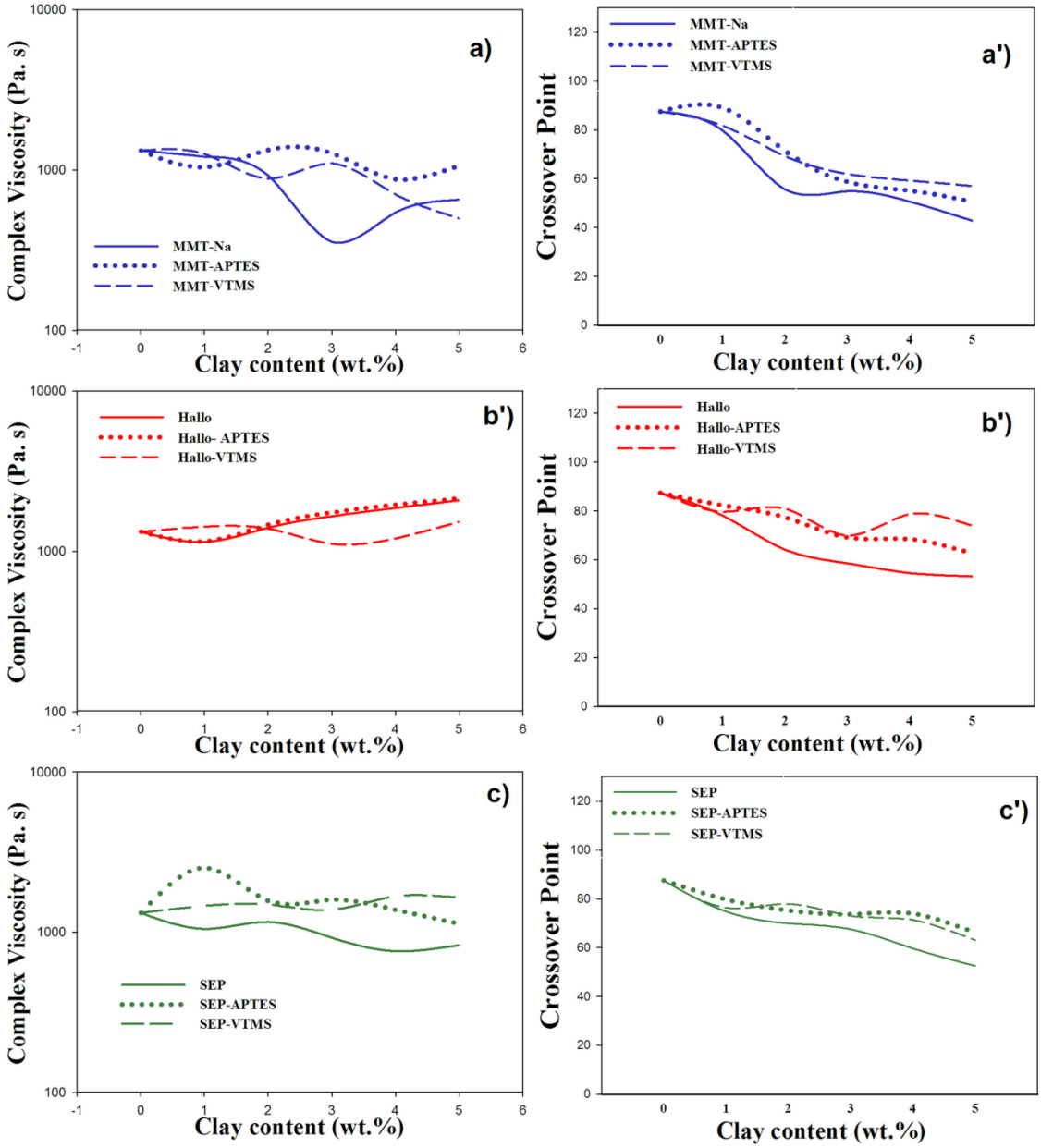

Figure III-10 : Rheological properties of pristine and functionalized clay as function of clay content: a), b), c) complex viscosity, a'), b'), c') crossover point.

III.5. Conclusion

Nanocomposites based on PP and modified clay, have been prepared by melt compounding using a variety of clay minerals. The use of different kinds of clays highlights the main parameters, which influenced the general behavior of the obtained nanocomposites. These clays have been modified with two organosilanes promoted covalent bonds between polymer and clay by reactive extrusion favoring strong interactions between clay and PP matrix. A series of tests have been performed to characterize the successful grafting of silane onto clay. It has been found that the functionalization technique makes possible the covalent bonding between the hydroxyl groups of clay minerals and polymer matrix confirmed by the enhancement of mechanical properties. Thus, for pristine clays, Young's modulus of PP increase from 1034 MPa to an optimum 2657.9, 2716.8 and 2956.5 MPa at 5wt.% for MMT, Hallo and SEP corresponding to a percentage gain of 157, 162, 186%, respectively, However, in the case of functionalized-clays nanocomposites, the Young's modulus of PP were higher than of the neat clays nanocomposites at the same clay concentration, These results prove that the silylation of clays were a valuable method to enhance interfacial adhesion between clay and PP matrix.

Acknowledgements

This work was supported by Moroccan Foundation for Advanced Science, Innovation and Research (MAScIR), Rabat, Morocco. The authors would like to thank Mehdi Ait Dahi for his fruitful technical support and assistance.

Chapitre IV

Effect of clay-intercalation process on the thermoplastic nanocomposites' properties: mechanical, thermal, and optical properties.

Effects of bleaching and functionalization of kaolinite on the mechanical and thermal properties of polyamide 6 nanocomposites

Résumé

Les nanocomposites de polyamide 6 (PA6) / kaolinite ont été préparés par mélange à l'état fondu. La kaolinite a été blanchie par une réaction solvothermale en utilisant l'acide oxalique, puis le produit blanchi a été intercalée par une réaction de déplacement car la kaolinite c'est une argile non-gonflante en utilisant du diméthylsulfoxyde (DMSO) une molécule polaire de petite taille, puis du méthanol (MeOH) par une méthode de déplacement. Ainsi, la kaolinite blanchie a été intercalée par les molécules CTAB et TEOS. La poudre de kaolinite et tous les échantillons préparés avec un taux de kaolinite fixe (8 wt. %), ont été caractérisés par diffraction des rayons X (DRX), spectroscopie infrarouge à transformation de Fourier (FTIR), analyse thermique, microscopie électronique à balayage (MEB) et test de traction. On a également observé l'influence du processus de blanchiment de la kaolinite et des méthodes d'intercalation sur l'indice de blancheur des composites, dans laquelle l'indice de blancheur des composites fonctionnalisés en kaolinite était augmenté jusqu'à 10,65% par rapport au PA6 net, respectivement. Les résultats thermiques ont révélé que l'intercalation et la fonctionnalisation affectent grandement la stabilité thermique du polymère vierge. D'autre part, l'intercalation de la kaolinite améliore la dispersion / distribution et l'adhérence interfaciale des nanoparticules de kaolinite, ce qui permet d'améliorer de façon remarquable les propriétés des nanocomposites représentés par des valeurs de module de Young élevées allant jusqu'à une croissance maximale de 80,6% par l'ajout des nanoparticules de kaolinite fonctionnalisées.

Mots clés : polyamide 6 ; diméthylsulfoxyde; kaolinite; blanchiment; méthodes d'intercalation.

M. Raji et al. RSC advances. 2020 ;10(febuary) :4916–4926

IV.1.Abstract

The polyamide 6 nanocomposites (PA6)/kaolinite were synthesized by melt compounding. First kaolinite was bleached by a solvothermal reaction using oxalic acid as a leaching agent and then the bleached product was modified using dimethylsulfoxide (DMSO) and subsequently methanol (MeOH) via a displacement method. Thus, CTAB and TEOS molecules were intercalated into kaolinite nano-platelets. Seven types of nanocomposites were synthesized using an eight-weight percentage of pristine, bleached and intercalated kaolinite. The kaolinite powder and the nanocomposites specimens were characterized by X-ray diffraction (XRD), Fourier transformation infrared spectroscopy (FTIR), thermal analysis, scanning electronic microscopy (SEM), whiteness index and tensile test. The influence of bleaching process of kaolinite and the intercalation methods on nanocomposites whiteness index was also observed, in which the whiteness index of the functionalized kaolinite nanocomposites was enhanced by up until 10.65% when compared to the neat PA6, respectively. The thermal results revealed that the intercalation and functionalization effect greatly the thermal stability of the virgin polymer. On the other hand, the intercalation of kaolinite enhances dispersion/distribution, improve the interfacial adhesion, and increase the aspect ratio of kaolinite nanoparticles affords remarkable nanocomposites property enhancements represented by high Young's modulus values that go until a maximum percentage's growth of 80.6% for silane-grafted kaolinite nanoparticles.

IV.2. Introduction

Polyamide 6 (PA6) is an important semi-crystalline polyamide commonly used in numerous applications as automotive components, sports equipment, electric/electronic, packaging, textiles, power tool housings, gears and so on due to its higher impact toughness, high crystalline melting point, good resistance to solvents, high strength, ease processing, high wear resistance and superior elongation at break [139]. However, some intrinsic disadvantages such as reduced tensile strength and lower flexural modulus restrict its field of applications [140]. Since the first results obtained by Toyota Research in 1993s on the dispersion of nano-layered clay (montmorillonite) in a polyamide 6 matrix have continued attracting much attention worldwide research in the field of nanocomposites consisting of a PA6 and clay platelet reinforcement to enhance the overall nanocomposites properties [141]. The originality of this work is the synthesis of the nanocomposites for the first time with functionalized bleached kaolinite through solvothermal reaction followed by displacement method with excellent thermo-mechanical properties.

Kaolin is a rock term contains clay mineral group and also is an industrial mineral commodity, generally includes kaolinite, halloysite, dickite, and nacrite [142]. Amongst all those four clay types, a most important is kaolinite because it is well-known for their good properties, including notably high whiteness or near white, too soft, fine in particle size, lath-shaped and platy particles, low in surface area and chemically inert [143]. These properties make it a versatile industrial mineral, it finds great applications as a coating and filler pigment for paper, as a filler for paint, rubber, insecticide, formulation of medicine, cosmetics, etc. it has also drawn the attention of researchers in the fields of clay polymer nanocomposites [144].

Kaolinitic clay is dioctahedral with a chemical formula ($Al_2O_3.2SiO_2.2H_2O$) consisting of two kinds of layered aluminosilicate clay 1:1 [145]. One is made of a gibbsite-type structure where each aluminum cations inhabits the center of an octahedron with six oxygen atoms and hydroxyl groups in the vertices, these units are covalently linked to the other layered, formed by silica-type structure, where each silicon atom occupying the center of a tetrahedron with oxygen atoms in the summits [146]. The kaolin has multilayer walls with positively charged alumina faces Al–OH functional groups on the inner surface and with negatively charged edges Si–OH functional groups on the outer surface [147]. These characteristics make kaolin a great absorbent for both cationic and anionic molecules aimed at their chemical modifying. Generally, in order to lessening the cohesion forces of kaolinite stacks, due to the reduction of the number of –OH groups toward change the hydrophilic surface of kaolin layers into organophilic ones, allowing the polymer macromolecules to intercalate into kaolin layers and form stable homogeneous structure [148].

As previously mentioned, pure kaolinite is white in color, nonetheless the presence of small quantities of impurities may be sufficient enough to impart color to the ores [149]. Particularly for examples as the oxides, hydroxides and hydrated oxides of ferric iron such as hematite (red), maghemite (reddish brown), goethite brownish (yellow), lepidocrocite (orange), ferrihydrite (brownish red) [149–158]. The presence of these impurities affecting negatively their thermal and optical properties and it is one of parameters that determine the quality of kaolinite [153]. For this reason it’s necessary to remove or decrease the content of these impurities in the pristine by adopting numerous physical and chemical treatments like sieving, magnetic separation, froth flotation, selective flocculation, biological and chemical leaching with various chemicals like oxalic and other organic acids [31]. Amongst those, the oxalic acid is a reagent of choice and a most effective leachant because of its excellent dissolving attack on iron oxides, which led to subsequent removal relatively easy [158,159].

The exfoliation of kaolinite in a polymer matrix leads to nanocomposites with enhanced properties compared to those of the starting inorganic and/or organic materials such as increased strength, Young's modulus, and heat resistance, decreased gas permeability and flammability [160]. In general, the morphology and size of kaolinite particles are important indexes for its viscosity, plasticity, surface area and porosity volume of the kaolinite, which not only provides good reactivity towards polymer matrix but also implies more homogeneous mixing during processing [160–162]. Lattice expansion of kaolinite was used to achieve weakening of the interlayer van der Waals interactions and a network of hydrogen bonds between the kaolin layers which may seem difficult by organic molecules directly [163]. For this reason, there are only a few varieties of small and highly polar organic micro-molecules, which can be used as a precursor for the synthesis, via solvothermal reactions, for example, dimethylsulfoxide (DMSO), N-methylformamide (NMF), urea (U), aniline, hydrazine and potassium acetate [164,165]. Amongst, only the DMSO organic solvent that have the ability to be intercalated directly because of its high dipole moments [29-39]. Thus, the methanol (MeOH) is one of polar guest species [175,176], which can be used as a second expansion step permitting insertion, and is an effective intermediate of large-sized, non-reactive molecules by displacement intercalation methods [42-44].

In this work, the expansible kaolin was intercalated with cetyltrimethylammonium bromide (cationic surfactant) and functionalized triethoxy(octyl)silane to transforms the hydrophilic-kaolin to organophilic and consequently to achieve better compatibility with non-polar matrices in the composites because the dispersion/distribution of fillers. Furthermore, the stronger interfacial interactions between the PA6 matrix and fillers lead to a higher level of properties.

IV.3. Material and Methods

IV.3.1. Material

The materials utilized were polyamide 6, was obtained from Ultramid O-BASF the chemical company, (density: 1.13 g/mL and melting temperature: 220°C). Natural yellow kaolin (density: 1.8 g/cm^3) typically forms by hydrothermal alteration of alkali granite of Oulmes, located in the center of the Moroccan Meseta, contained Kaolinite as the principal mineral and small quantities of quartz and illite. Other secondary minerals phases found in this yellow kaolin are iron oxides (goethite and/or hematite) make its whiteness index around of 33.1% [180]. The cetyltrimethyl ammonium bromide (CTAB), and triethoxy(octyl)silane (TEOS), dimethylsulfoxide DMSO, oxalic acid, sodium hydroxide NaOH, and methanol (MeOH) used in this study were purchased from Sigma-Aldrich.

IV.3.2. Methods

IV.3.2.1. Purification of kaolin

Kaolinite purification was done in our laboratory according to the dispersion–decantation method [3]. A 10 g kaolinite was suspended in 500 mL of water for 24 h. The suspension was filtered through a 100 mm sieve and dried at 110°C for 24 h. Then, the material was crushed and sieved at 1 mm. Purified kaolinite is abbreviated as "KR"

IV.3.2.2. Bleaching process of kaolin

The oxalate leaching tests were carried out in a round bottomed flask of 1 l with mechanical stirring in a heating mantle. A typical experiment proceeded as follows; the oxalate leaching solution was prepared by dissolving 1.8M of oxalic acid in 400 mL of distilled water. The pH value of the solution was adjusted to 4 with sodium hydroxide NaOH. Then, the sample of KR weighing 40 g was added in 400 ml of leaching solution at 90°C for 2h under high-intensity stirring. A Thermo Scientific Sorvall WX Floor Ultracentrifuge was used for solid-liquid separation of the bleached kaolinite sample (KB) at 10,000 rpm for 20 min. The general dissolution reaction is shown in Equation 1:

$$Fe_3O_4 + 8HC_2O_4^- \rightarrow 2Fe^{III}(C_2O_4)_3^{3-} + Fe^{II}(C_2O_4)_2^{2-} + 4H_2O \quad (1)$$

IV.3.2.3. Preparation of DMSO intercalated kaolinite

To prepare the dimethylsulfoxide DMSO intercalated kaolinite, labeled KD was accomplished as follows: 180 mL of DMSO was dispersed well in distilled water with a volume ratio of 6:1. Then, Kaolinite (30.0 g) was poured into the solution. The suspension was maintained under magnetic stirring for 12 h at 150 °C and thus allowed to stir for 12 h at room temperature. Subsequently, A Thermo Scientific Sorvall WX Floor Ultracentrifuge was used for solid-liquid separation of the sample at 10000 rpm for 20 min and washed 3 times by using isopropanol to remove the excess DMSO. The product was dried at 60 °C for 24 h and then ground into powder for further use.

IV.3.2.4. Preparation of MeOH intercalated kaolinite

The methoxy-modified Kaolinite (KM) intercalation as the precursor was prepared by adding 10g of KD into a closed container that contained 40 mL methanol (MeOH). The suspension was stirred continuously at room temperature for 7 days. The solid in the mixture was successfully separated

via centrifugation and dried at 60 °C for further use. The MeOH intercalated Kaolin was denoted KM

IV.3.2.5. Functionalization of intercalated kaolinite

Chemical functionalization of the intercalated kaolinite was carried out in MeOH. Kaolinite (10g) was first suspended at 25 °C through sonication for 30min. Then, 10mL of organic molecules (cetyltrimethyl ammonium bromide (CTAB) and triethoxy(octyl)silane (TEOS)) were added into the solution successively, and the reaction mixture was mechanically stirred for 24h at 80°C in temperature. Afterward, the solid was separated and washed using the mixture of acetone/water for 3 times by centrifugation at 10000 rpm and dried at 60°C under vacuum condition. The two products will be labeled as KC (cetyltrimethyl ammonium bromide), KS (triethoxy(octyl)silane).

IV.3.2.6. Preparation of PA6/kaolinite nano-composites

The PA6 nanocomposites at 8wt. % of kaolinite fillers loading were prepared in the molten state using a twin-screw micro-extruder (Thermo Scientific Haake Minilab Model II) at 220°C with a screw speed of 80 rpm. The samples were then pelletized into granules of about of 2–3 mm in length via (Thermo Fisher, UK). All the specimens were molded using a CARVER compression molding press into rectangle molds (100 x 70 x 1 mm3) with a clamping force 15 tons and the platen heated to 220°C as required in ASTM D4703 procedure C to prepare the nanocomposites [181]. All process steps are summarized in figure IV-1.

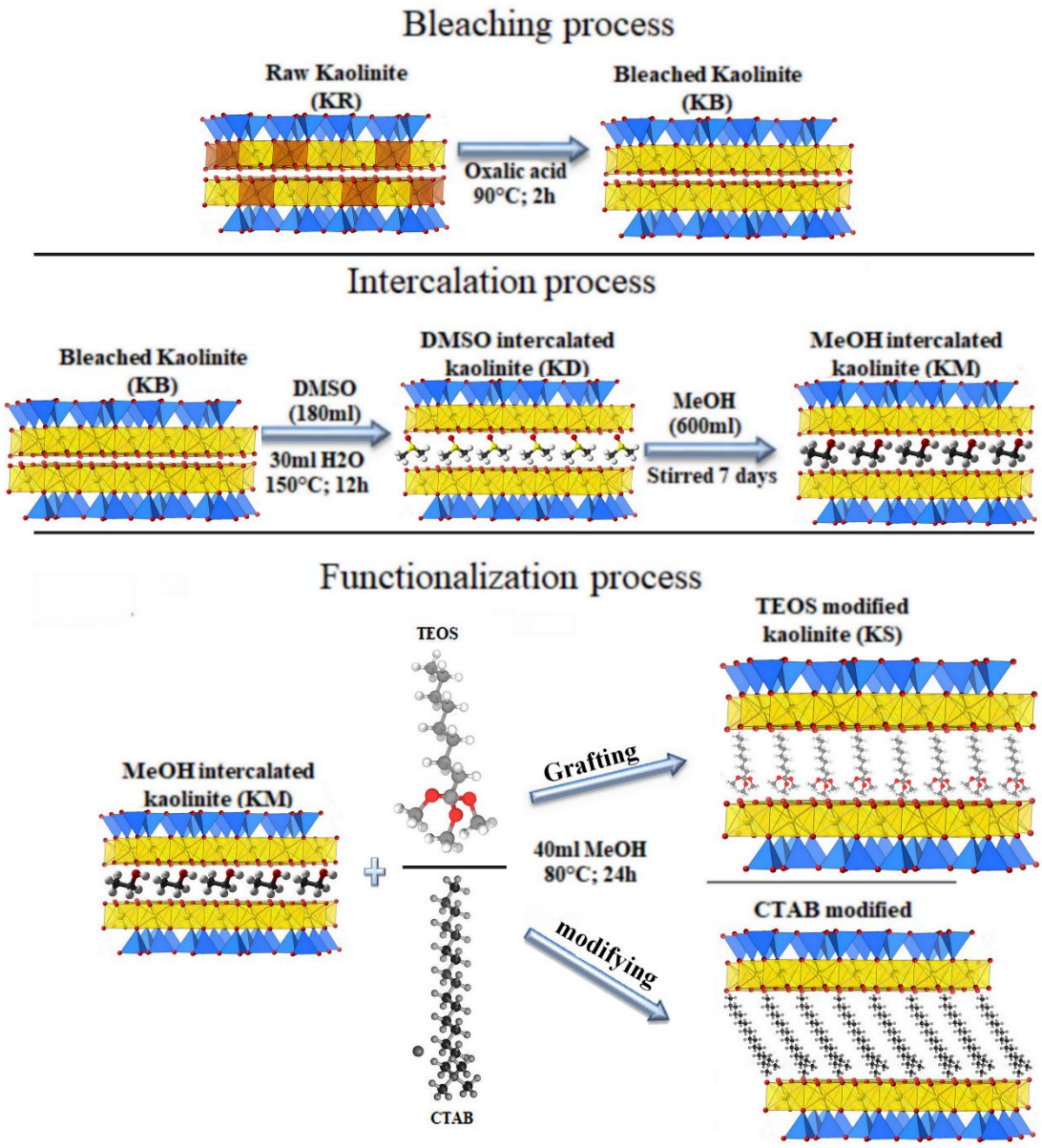

Figure IV-1 : Schematic of the chemical treatments of kaolinite nanoparticles.

IV.4. Characterization

IV.4.1. X-Ray Diffraction (XRD)

X-ray diffraction (XRD) was used to confirm the intercalation of kaolinite clay. The data were recorded on a Bruker D8 Discover using the CuKa radiation (1.54184 nm) and a GADDS detector. The samples were consolidated in an aluminum holder and scanned at 45 kW from 0.5–908 of 2h. The diffraction patterns were analyzed using the X'Pert High Score software. The interlayer distances of kaolinite were estimated from the WAXD patterns with Bragg formula (equation 2) [114].

$$2d \sin\theta = n\lambda \quad (2)$$

The intercalation ratio used to evaluate the degree of intercalation reaction and defined as the rate of diffraction peak intensities that can reflect the change of interlayer spacing before and after intercalation of kaolinite, calculated from the equation 3 [182].

$$\mathrm{I}_R = I_I/(I_K + I_I) \quad (3)$$

Where I_K and I_I are the intensities of (001) diffractions of kaolinite and intercalated kaolinite, respectively.

IV.4.2. Fourier transforms infrared spectra (FTIR)

Fourier transforms infrared spectra (FTIR) of the pristine kaolinite powder, bleached, treated and the functionalized ones were obtained using an ABB Bomem FTLA 2000-102 spectrometer (ATR: Specac Golden Gate) via an accumulation of 16 scans with a resolution of 4 cm^{-1}.

IV.4.3. Thermogravimetric analysis (TGA)

The thermal degradation of the kaolinite powder, bleached, treated and the functionalized ones were evaluated by thermal gravimetric analyses (TGA) recorded on a Q5000 (TA instruments). Samples of about 30 mg were placed in platinum pans and heated under air from 50 °C up to 850°C at a heating rate of 10°C/min.

IV.4.4. Differential Scanning Calorimetry (DSC)

The measurements of glass transition temperature of the pristine kaolinite nanocomposites, bleached, treated and the functionalized ones were carried out using a Q100 from TA Instruments. Throughout the DSC work, each sample (5mg) of the polymer sample prepared by extrusion methods were encapsulated in aluminum pans and placed in the holder to be heated, cooled, and heated repeatedly from 25°C to 250°C at a heating rate of 10°C/min. In order to calculate the value of the crystallinity index (Xc) [3], the following equation was used:

$$X_c(\%) = \frac{\Delta H_m}{(1-\omega)\Delta H_m^0} \times 100 \quad (4)$$

ΔH_m: Measured heating enthalpy

ΔH_m^0: Theoretical value of melting enthalpy at 100% crystalline of PA6 (191 J/g)

(1-ω) is the weight fraction of polymer in the nanocomposites

IV.4.5. Scanning electron microscopy (SEM)

To characterize the size and the morphology of the kaolinite particles, scanning electron microscopy (SEM) was performed on a JEOL JSM 840A scanning electron microscope at 15 kV.

IV.4.6. Whiteness index

The color of the kaolin powders and their bleached, treated and the functionalized ones was undertaken using a Spectrophotometer CM-700d/600d-Konica Minolta according to Practices ASTM E 313-10 [183]. The samples as with thick plaques (2mm) and flattened surface were placed under the specimen measuring port.

IV.4.7. Tensile testing

Tensile tests for five specimens of each type of nanocomposites were performed according to ISO 527-1:2012 [184]. The tests were performed on a universal testing machine Tinius Olsen H10KT at a crosshead speed of 5 mm/min using a five kN load cell. Tensile properties such as Young's modulus, tensile strength, and strain at yield of the composites were obtained from the stress–strain curves.

IV.5. Results and discussions

IV.5.1. X-Ray Diffraction (XRD)

The X-ray diffractograms patterns of intercalated kaolinite compared to that of pristine and bleached kaolinite can be shown in figure IV-2. The XRD patterns of KR and KB are nearly identical, demonstrating that very little or no structural modification of the kaolinite arisen during the bleaching process, and that no crystalline secondary material was formed [157]. The untreated and treated kaolinite display two peaks characteristic of muscovite at 2θ = 8.74 and 2θ = 17.64 corresponding to d=10.11 Å and d=5.03 Å, respectively [185]. Another peak at 2θ = 19.74 corresponding to d= 4.5 Å is attributed to illite clay as an associated clay mineral [3]. Finally, it can be observed that only the muscovite and illite minerals are detected by XRD as ancillary mineral present with a minor amount in all kaolinite samples, which come from primary kaolin deposits; iron oxides such as magnetite (Fe_3O_4), hematite (Fe_2O_3), titanium oxide-ferrous

(Fe_2TiO_4), and greigite (Fe_3S_4) were not detectable because their concentration in the kaolin is relatively low. Iron minerals are the main metal impurity in kaolinite samples.

On the other hand, the 001 reflections of pristine and bleached samples display a broadband in the region around of 2θ = 12.28 corresponding to the interlayer spacing of 10.05 Å, which is assigned to the diffraction peaks (001) of kaolinite as the dominant mineralogical phase [186]. However, the kaolinite treated by DMSO (KD) exhibits two reflections (001) and (002) corresponding to diffraction values of d_{001}=11.37 Å and d_{002}=5.7 Å, respectively. The intercalation ratio (or degree of reaction) of the modified kaolinite reached by DMSO to around 98.85%. This value confirms that the oxygen of the S=O group in DMSO is triply hydrogen bonded with the inner-surface hydroxyls of the gibbsite sheet of the kaolin layer, and one methyl group of DMSO is keyed into the ditrigonal hole in the tetrahedral sheet with the other S–C bond nearly parallel to the sheet [187]. When pre-intercalate kaolinite was intercalated with MeOH as an attempt made recently to replace the precursor (DMSO), the basal reflection in a dry state shows a d001 value (11.37 Å) nearly identical to that of DMSO intercalated kaolinite with an intercalation ratio of 85%. The reason may be due to the fact that the methoxy-modified inner surface resulted from the grafting of methanol molecules at the initial aluminol (AlOH) of the Al–O octahedron through the condensation to AlOMe groups between the hydroxyl groups of the two moieties, escaping the free methanol molecules from the interlayer space during a drying process [175]. In the XRD pattern plotted in figure IV-2, the KC and KS samples clearly identified (002) reflections at 2θ = 9.42 and 2θ = 8.92, corresponding to d002 values of 9.4 Å and 9.91 Å, respectively. These d-spacing increments indicate the successful intercalation of CTAB and TEOS molecules, generating a breaking of the hydrogen bonding between adjacent kaolinite layers space, representing an interalamellar expansion (obtained by subtracting the kaolinite c-spacing) of Δd_{002} (KC) = 0.58 nm Δd_{002} (KS) = 0.63 nm. That generally results in significant changes to the kaolinite surface properties.

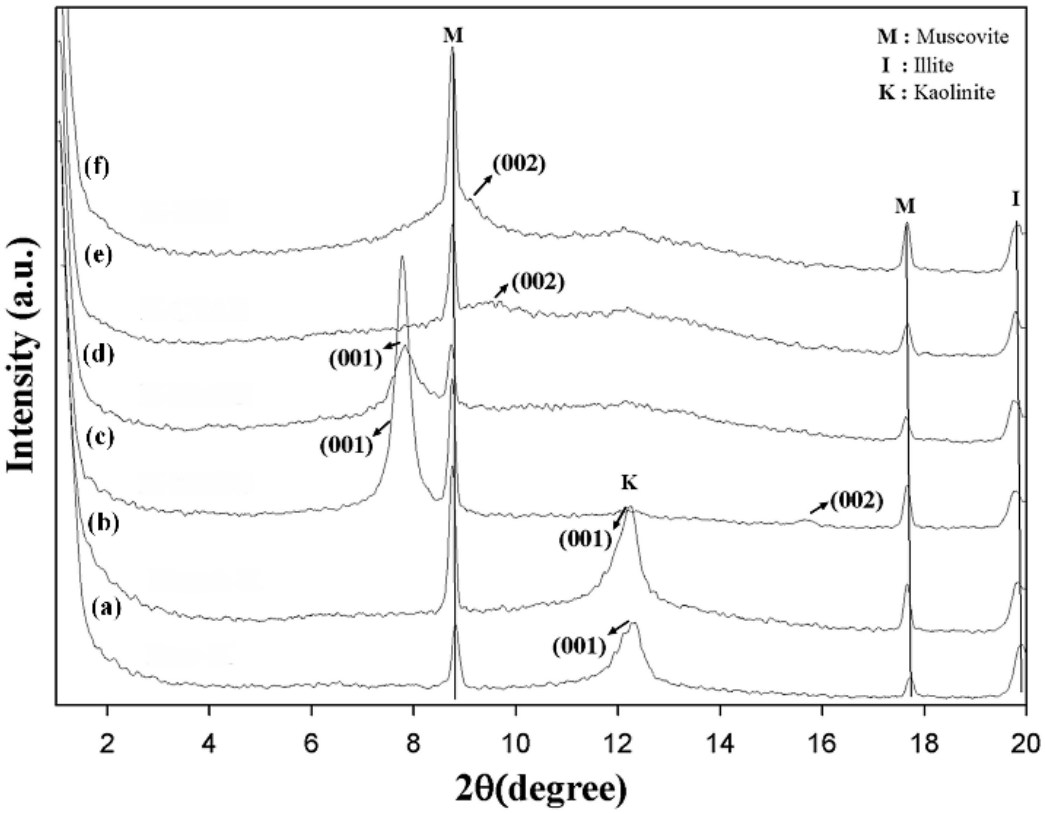

Figure IV-2 : Low-angle XRD patterns of: (a) KR, (b) KB, (c) KD, (d) KM, (e) KC and (f) KS.

Table IV-1 : Angle 2θ, and basal spacing (d_{001}, d_{002}) of the intercalated kaolinite in relation to pristine kaolinite.

Sample	$2\theta_1$(degree)	d_{001} (Å)	$2\theta_2$(degree)	d_{002} (Å)
KR	12.18	7.26	24.85[175]	3.6[175]
KB	12.24	7.23	24.85[157]	3.6[157]
KD	7.76	11.39	15.48	5.7
KM	7.77	11.37	20.64[175]	4.3[175]
KS	-	19.82	8.92	9.91
KC	-	18.8	9.42	9.4

IV.5.2. Structural characteristics (FTIR)

The FTIR spectra of intercalated kaolinite compared to that of pristine and bleached kaolinite are shown in Figure IV-3. For raw and bleached kaolinite, the transmittance bands at 3694, 3621 cm^{-1} are ascribed to the stretches of inner-surface hydroxyls groups and to the vibrations of inner hydroxyl groups lying between the tetrahedral and octahedral sheets, respectively [175].

Moreover, an additional weak band at 1619 cm^{-1} is due to O−H bending vibration of water molecules [172]. In the 1200 cm^{-1} and 700 cm^{-1} region, main functional groups assigned to characteristic band of Si-O and Al-OH [2]. Primarily, the strong transmittance bands at 1113 cm^{-1} and 1016 cm^{-1} are mostly related to out-of-plain Si-O stretching and in-plane Si-O stretching vibrations, respectively [166]. While the sharp band at around 987 cm^{-1} and the weak shoulder at 901 cm^{-1} are due to the Al-OH bending vibrations of kaolinite [188]. There is another typical band at 931 cm^{-1} corresponding of the interalamellar aluminol group in the kaolinite layers [129].

After intercalation with DMSO, the stretching vibration of inner hydroxyls groups has not been affected, but there is one new band at 3654 cm^{-1} has appeared which was assigned to the formation of hydrogen bonds to the interalamellar hydroxyls groups of the kaolinite (S=O-OH) [187]. Another two observed bands at 3528 cm^{-1} and 3490 cm^{-1} results from the hydrogen bonding of the DSMO molecules with the inner-surface hydroxyl groups of the kaolinite layers [176]. An apparition of new bands corresponds to the vibrations of methyl groups in DMSO molecules: asymmetric C-H stretching (3017 cm^{-1}), symmetric C-H stretching (2934 cm^{-1}), asymmetric C-H deformation (1407 cm^{-1}) and symmetric C-H deformation (1388 cm^{-1}) of DMSO methyl group [169]. That reflected the existence of the DMSO molecules in KD specimen. Then, after methanol-grafting, the all appeared bands were weakened, that decrease in intensity of bands were attributed to the deintercalation of KD and the intercalation of kaolinite with MeOH [189].

KM was further used as the precursor to intercalate with TEOS and CTAB. Figure (IV-3,e) (IV-3,f) show the infrared spectrum of KS and KC, respectively. The bands characteristic of inter- and intra-lamellar hydroxyl groups have no obvious changes, however, the appeared band at 3654 cm^{-1} attributed to the formation of inter-lamellar hydroxyl groups in the case of KD and KM samples was disappeared, thereby confirming functionalization of the kaolinite mineral with either by TEOS or CTAB. In addition to the increase in the intensities of the bands at 3017 cm^{-1} and 2934 cm^{-1} correspond to the antisymmetric and symmetric stretching vibrations of methyl groups (C-H3) generating by intercalation of KR with the surfactant [148], there is another band at 2850 cm^{-1} assigned to the stretching vibration of methylene groups ($C-H_2$) [148]. However, the typical band for the inter-lamellar Al-OH group at 931 cm^{-1} was disappeared for KS, which confirming the participation of the aluminol group in a covalent bond with the OH groups of the both TEOS molecules [129],[190]. The presence of two additional appeared bands for KC at 2955 cm^{-1} and 1460 cm^{-1} arises from the C-N group and N-H groups of the organic modifier, verifying the intercalation of surfactant molecules between the silicates, respectively [148].

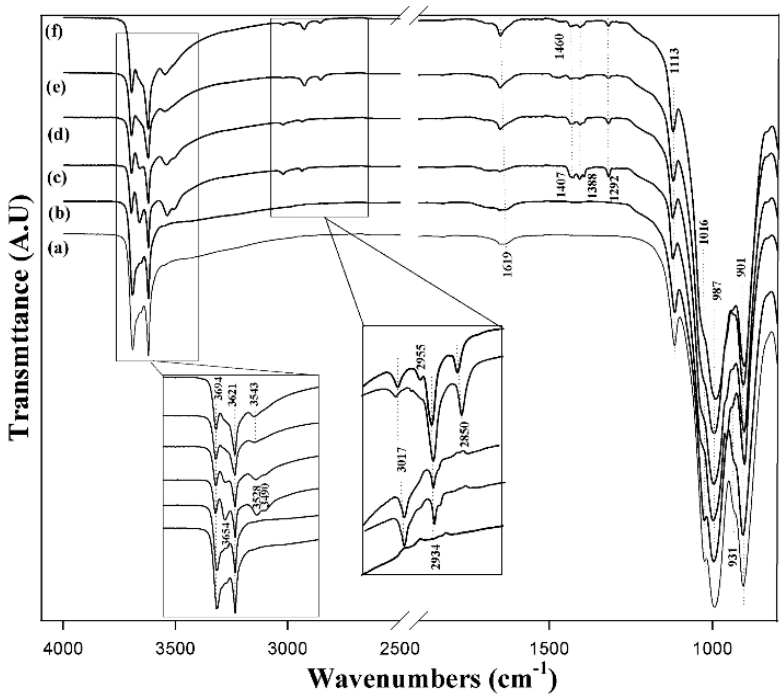

Figure IV-3 : FTIR spectra of: (a) KR, (b) KB, (c) KD, (d) KM, (e) KC and (f) KS.

IV.5.3. Thermogravimetric analysis (TGA)

Thermal gravimetric analysis (TGA) was mainly used to compare the effect of organic molecules on intercalated kaolinite with the pristine and bleached kaolinite. Figure IV-4 shows the mass loss (TG) and derivative mass loss (DTG) curves of KR, KB and its intercalation compounds. As seen in the TG curve of KR sample and bleached one, there were two steps, for which the first took place around 56 °C for raw and bleached kaolinite samples, with mass loss less than of 1.2% was corresponds to the departure of physisorbed water [164]. The second step related to the dehydroxylation of kaolinite [151], causing by the transformation of kaolinite $Al_2Si_2O_5(OH)_4$ to metakaolinite $Al_2Si_2O_7$ that generally started at 450 °C and terminated at 600 °C, represent the mass losses of 11.4 % and 10.4 % corresponding to raw KR and KB samples [82]. On the other hand, KD curve present three major mass losses, the ones centering at 178.5°C corresponding of 13.68% loss masses resulted from the elimination of DMSO molecules [173] and the second one presented in the same range (450–600 °C) of peek of the dehydroxylation of kaolinite with a decrease in width of the DTG peak [187]. There was also a very minor mass loss at about 57 °C, attributed to adsorbed water introduced during the DMSO intercalation [164]. The KM sample display also a less obvious DTG peak that starting between 60 and 200 °C and contributed to a mass loss of 8.8%, which ascribed to the degradation of water, MeOH and methoxy groups in between Kaolinite layers [160]. Moreover, the last step one around 460°C probably caused by two

simultaneous thermal phenomena: the loss of the grafted methoxy groups, and the dehydroxylation of kaolinite [160].

The TG pattern of CTAB and TEOS functionalized kaolinite are mainly characterized by five major mass losses, the first step associated with the loss of externally-adsorbed water presented around 56 °C [130]. Thus, the second stage was due to the decomposition of non-intercalated CTAB and TEOS molecules are occurred around 186 °C accounting for 3.8% and 4.9% of the total masses, respectively [179]. The third stage with a total weight loss of 1.58% for CTAB intercalated kaolinite at around of 255°C and with a total weight loss of 0.5% for TEOS intercalated kaolinite at around of 278°C , was related to the partial thermally decompose of organic moieties that were grafted on the external surface of the nano-platelets kaolinite. The decomposition temperature of the TEOS intercalated kaolinite is higher than the decomposition temperature of the CTAB intercalated kaolinite, indicating that hydrogen-bonded molecules (CTAB) are less thermally stable than the covalently bonded molecules (TEOS) [141]. The weight losses of 10.2% around of 474°C for KC and of 11.5 % around of 467°C are associated with the dehydroxylation of the aluminosilicate lattice for kaolinite and the complete decomposition functionalized molecules grafted onto SiOH and AlOH groups on the internal surface of kaolinite [129]. Finally, weight losses of 1.6% for KC and 1.4% for KS at around 556°C are assigned to the evaporation and decomposition of oligomerized molecules and the residual organic and inorganic moieties (CTAB, TEOS) [2]. For all kaolinite types, the remaining materials at 800°C are of aluminum oxides and silicon oxides present in kaolinite structure [191].

Table IV-2 : Data derived from thermal curves (TGA and DTG) of the intercalated kaolinite as compared to pristine kaolinite.

Steps	Characteristics	samples					
		KR	KB	KD	KM	KS	KC
(1)	T_{max} (°C)	57	56	57	59	57	56
	Mass loss (%)	1.21	1.24	0.1	0.21	0.16	0.15
(2)	T_{max} (°C)	-	-	178.52	180.1	186.4	181.08
	Mass loss (%)			13.68	8.85	4.96	3.85
(3)	T_{max} (°C)	-	-	-	-	279.2	255.72
	Mass loss (%)	-	-	-	-	0.5	1.58
(4)	T_{max} (°C)	474.26	472.59	475.03	468.95	477.2	464.92
	Mass loss (%)	11.44	10.4	8.46	9.77	11.52	10.2
(5)	T_{max} (°C)	-	-	-	-	555.87	555.68
	Mass loss (%)	-	-	-	-	1.39	1.61
Residual contents (%)		87.35	88.36	77.76	81.35	81.50	82.61

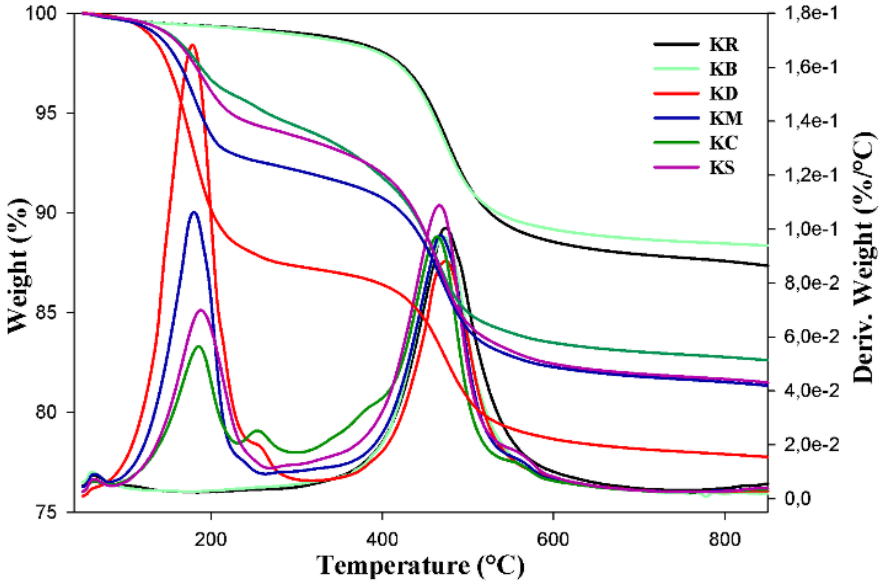

Figure IV-4 : Thermogravimetric curves of KR, KB, KD, KM, KC and KS.

IV.5.4. Differential Scanning Calorimetry (DSC)

Differential scanning calorimetry (DSC) was used to investigate the impact of the kaolinite nanoparticles and their chemical functionalization on the melting temperature (Tm), crystallization temperature (Tc), specific enthalpy of melting (ΔHm), and the degree of crystallinity (Xc). Figure

IV-5 presents the DSC curves of the neat PA6 and PA6 composites with pristine, bleached and intercalated kaolinite, likewise, their melting thermographs parameters are summarized in Table V-3. It is noted that the neat PA6 present only one endothermic peak at approximately a melting temperature (Tm_1) of 225.51°C, which is ascribed to the melting of α crystals and characterized by a melting enthalpy (ΔHm) of 56.33 J/g [192]. On the other hand, the incorporation of kaolinite nanoparticles preferentially leads to appear another endothermic peak around 211˚C corresponding to γ crystals and defined as Tm_2 [192]. These γ crystals always show lower melting temperature compared to the more stable α crystals [192]. This transformation from α to thermodynamically γ structures is generating by the capability of the amide groups along the PA6 polymer chain to form an intrachain hydrogen bonds with the OH ions in the basal plane of the kaolinite and become aligned along the a-axis crystallographic direction [193]. As listed in Table IV-3, it can be seen that there is a minor change in the Tm_2 of neat PA6 and PA6 nanocomposites with pristine, bleached and intercalated kaolinite; a maximal shift from 225.51 °C for the neat PA6 to 223.42 °C for the PA6/KS nanocomposite [194]. Probably the kaolinite nanoparticles did not act as a nucleating agent that generally favored the formation of crystal nuclei. This result can also be evidenced by the temperature of crystallization (Tc) values were around 190°C of the nanocomposites in relation to the pure PA6 polymer [194]. In general, it can be observed that the crystallinity degree (Xc) of the nanocomposites increased as compared to the neat PA6 polymer. This can be attributed to the interaction of the kaolinite nanoparticles with the phase of the PA6 that restricted the mobility of the polymer chains hindering the crystallization process [195]. Finally, melt enthalpy (ΔHm) of the PA6 nanocomposites significantly decreased with the incorporation of kaolinite nanoparticles, which indicates that the thermal stability of the polymer matrix improved with the addition of kaolinite nanoparticles [12].

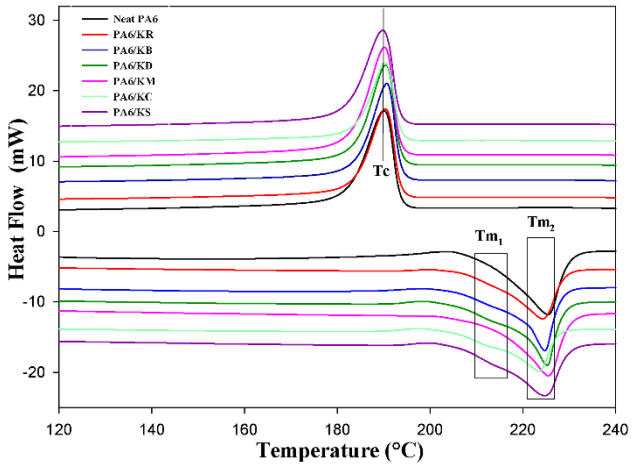

Figure IV-5 : DSC curves of the nanocomposites polymer compounds of PA6 : neat PA6, KR, KB, KD, KM, KC and KS

Table IV-3 : DSC results for the nanocomposites polymer compounds of PA6

samples	Tm_1 (°C)	Tm_2 (°C)	Tc (°C)	ΔHm (J/g)	*X*c (%)
PA6	-	225.51	190.03	56.33	29.49
PA6/KR	210.93	224.15	190.41	55.62	31.65
PA6/KB	210.91	224.71	190.61	53.21	30.28
PA6/ KD	211.37	225.31	190.44	55.39	31.52
PA6/ KM	211.36	225.5	190.17	55.46	31.56
PA6/ KS	210.51	223.42	190.38	54.58	31.06
PA6/ KC	211.84	224.74	189.81	54.23	30.86

IV.5.5. Scanning electron microscpy (SEM)

A general view using the micrographs of the kaolinite powder can be observed in figure IV-6. The stronger particles intermolecular forces, that is a cohesive tension which makes an attempt to the kaolin particles to aggregate and to form the agglomerates [132]. It can be seen from the figure V-6 that the kaolinite mineral possesses a pseudo-hexagonal shaped plate-like particles with a widely irregular shape, rough surface, and different particle sizes (smaller than 12.5 µm).

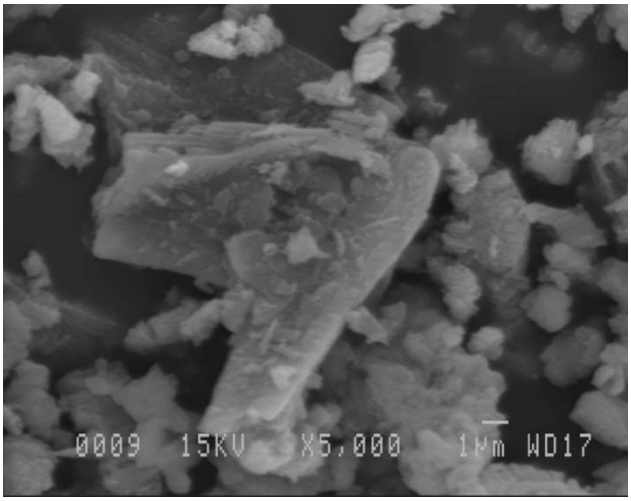

Figure IV-6 : SEM photomicrograph of raw kaolinite powder.

IV.5.6. Whiteness indices

In order to study the possibility of bleaching kaolinite powders via chemical processing, the CIE Whiteness Index value was measured [183]. The whiteness index (WI) of kaolinite powders and their nanocomposites specimens are shown in figure IV-5. In the figure (IV-5; a), it can be seen that the whiteness index of kaolin was improved through firstly the bleaching treatment and then by the chemical intercalation. Precisely, the use of leaching agent exhibited a significant increase in whiteness index of kaolinite powder from 33.09%, yielding a value of 46.97%. Confirming that the oxalate solution have been employed to dissolve the iron oxides compounds as a coloring impurities [154]. From figure (V-5; a), it was observed that the pre-intercalation of kaolinite by DMSO can increase the whiteness index of kaolinite to a value of 58.70 %, this is due to the interlayer distance of kaolinite expanding carried out provide an improve in the brightness and opacity those depend on increases of the specific surface area of kaolin particles [196]. However KM sample shows a slight decrease in whiteness index value to 56.16 % ascribed to the reduction of the basal spacing value of dried sample that is generating by the escape of methanol molecules from the interlayer space of kaolinite during the drying process, which is in agreement with the XRD results treated before [197]. In the case of the both intercalated kaolinite (KC and KS), their whiteness indices have increased to 57.02 % and 57.26 %, respectively. This increment may be attributed to the higher interlayer distances generating by the great intercalation of the molecules in the interlayer space of kaolinite [196–198].

Figure (IV-5; b) shows the whiteness index values of raw and intercalated kaolinite nanocomposites. The whiteness index of the nanocomposite remarkably decreases by the incorporation of raw kaolinite in PA6 polymer matrix from a value of 19.04 % to 2.17%, which is

can be explained by the opaque white to the yellow color of raw kaolinite particles [199] and their refractive property due to their higher particles size [196]. However, with decreasing particles size of kaolinite by the intercalation, more the nanocomposites will tend to diffract the incident light and presenting a higher whiteness index [200]. This effect is likely due to a combination of the color of the intercalated kaolinite particles, greater surface curvature and roughness, as well as their good dispersion-distribution of the kaolinite particles into the polymer matrix that consequently altered the light-scattering properties, resulting in a whiter appearance [199]. In the case of KS, the whiteness index present the highest value (29.69%) caused by the condensation of the silane-coupling agents to hydrophobic/hydrophilic silica particles during compounding process in the presence of high temperature, these silica particles are white in nature [105,201].

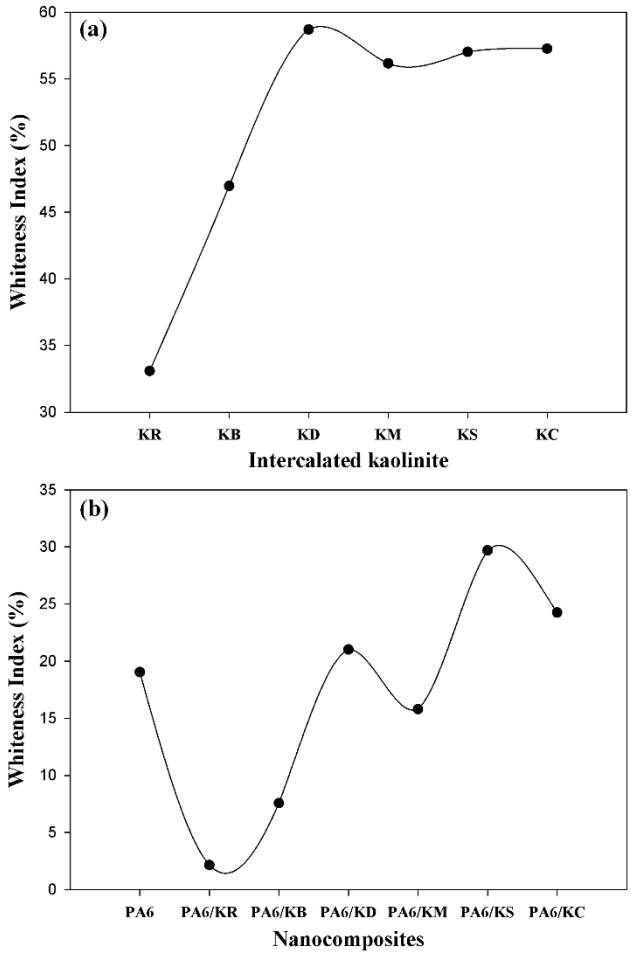

Figure IV-7 : Whiteness indices of kaolinite samples after different modifications process: (a) kaolinite powders and (b) the nanocomposites polymer compounds of PA6-Kaolinite.

IV.5.7. Tensile testing

Figures IV-8 shows the effect of kaolinite nanoparticles and their exfoliation process on Young's modulus, tensile strength, and strain at yield results of the nanocomposites polymer compounds of PA6-Kaolinite. The obtained results (figure IV-8; a) show that Young's modulus values were increased by the incorporation of 8 wt.% kaolinite particles content from 1200 MPa for neat PA6 to 1316 MPa, and 1354 MPa for raw and bleached kaolinite particles, respectively. Giving respectively an increase of 9.7% and 12.8% that is attributed to higher kaolinite particles rigidity compared to the matrix [157],[37]. On the other hand, the nanocomposites containing kaolinite nanoparticles that were intercalated by DMSO or MeOH molecules showed the higher Young's modulus values than those containing unmodified kaolinite particles representing an improvement of 23.9%, 21.9%, respectively. This improvement in Young's modulus values can be attributed to a large aspect ratio and high intrinsic mechanical characteristics as well as the good dispersion/distribution homogeneity of kaolinite nano-platelets into a polymer matrix that is generating by the exfoliation of both DMSO or MeOH intercalated kaolinite samples during the compounding process [202]. Likewise, the Young's modulus of nanocomposites polymer compounds of PA6-Kaolinite increases also to 2167 MPa and 2010 MPa for 8wt. % addition of KS and KC nanoparticles content corresponding to the percentage's growth of 80.6% and 67.5%, respectively. This spectacular enhancement of Young's modulus can't be only ascribed to a large aspect ratio and the homogeneous distribution of both KC and KS nanoparticles [161]. But also to the strong interfacial interaction between kaolinite nanoparticles and PA6 chains via forming hydrogen bonding (CTAB) [203] or covalent bonding (TEOS) [204] between hydroxyl groups of the nano-platelets kaolinite and polyamide-6 polymer known to induce better compatibility [2] and high adhesion of kaolinite nanoparticles with hydrophobic PA6 polymer [205–207].

Figures IV-8;a depicts also the data of the tensile strength for the nanocomposites polymer compounds of PA6-Kaolinite. As seen in this figure, a slight improvements of tensile strength values have been observed by the incorporation of 8 wt.% kaolinite particles content from 42.23 MPa for neat PA6 polymer up to 43.64 MPa, and 44.57 MPa for raw and bleached kaolinite particles loading, respectively. This increment is related to the physical anchoring between the kaolinite particles and the PA6 polymer chains that lead to transfer the stress from the matrix to the kaolinite particles interface [70,30]. Nevertheless, in the case of the nanocomposites containing kaolinite nanoparticles that were intercalated by DMSO or MeOH molecules, the tensile strength showed a remarkable increase up to 44.84 MPa and 44.1MPa for 8wt.% addition of KD and KM nanoparticles content, respectively. This enhancement occurs due to the improved quality of

distribution in size and dispersion of DMSO or MeOH intercalated kaolinite nano-platelets within the PA6 polymer matrix generating by the delamination or exfoliation of kaolinite nanoparticles during the melt compounding nanocomposites preparation [141]. Finally, the use of functionalized nano-platelets kaolinite enables an enhancement of the tensile strength properties of nanocomposites polymer compounds of PA6-Kaolinite due to the more efficient at transferring the load from the PA6 matrix to nano-platelets kaolinite [2]. By analyzing the results in figure V-8, it is possible to observe that the values of the tensile strength of the PA6 nanocomposites are more increased by the use of KS (45.85 MPa) and KC (45.47 MPa) as nanoparticles loading. In fact, the exfoliation process can play an important role in the reduction of the kaolinite nanoparticles size and improve the filler dispersion/distribution into the polymer matrix. As well as to enhance the interfacial adhesion and the compatibility between the components, that are the main causes to get the high tensile strength properties engendering in our study either by the use of surfactant (CTAB) and more by the use silane molecules (TEOS) [203,208].

The extracted percentage of the strain at yield for the nanocomposite's polymer compounds of PA6-Kaolinite are plotted in figure (IV-8, b). The incorporation of both raw and bleached kaolinite particles in ductile polymer matrix exhibit a remarkable decrease in the strain at yield values due to the dropping the plastic energy in the composites by the addition kaolinite as rigid particles [9,25,209]. Adding the kaolinite particles in the polymer composites achieved a less deformability of the materials because of stress concentration engendering by the presence of decohesion between the kaolinite particles and polymer matrix accelerating the composite break [4]. In the case of the addition of the kaolinite particles at nanoscale sizer to the produced nanocomposites, the effect of KD and KM nanoparticles is less pronounced on the strain at yield values because of their high surface area and their interaction with the polymer matrix that are favorable to stress transfer as compared KR and KB particles. This can be allowed to conclude that the exfoliation of kaolinite particles in the ductile matrix can lead to masks the stiffness of the kaolinite particles and the large aspect ratio of nanoparticles [141]. It is also observed on figure (IV-8;b) that the strain at yield values of the nanocomposites reinforced by KS or KC nanoparticles has improved because the functionalization of the nanoparticles may enhance the interaction between hydroxyl groups of the nano-platelets kaolinite and polyamide-6 chains via forming hydrogen bonding or covalent bonding, which impedes a good stress transfer [2].

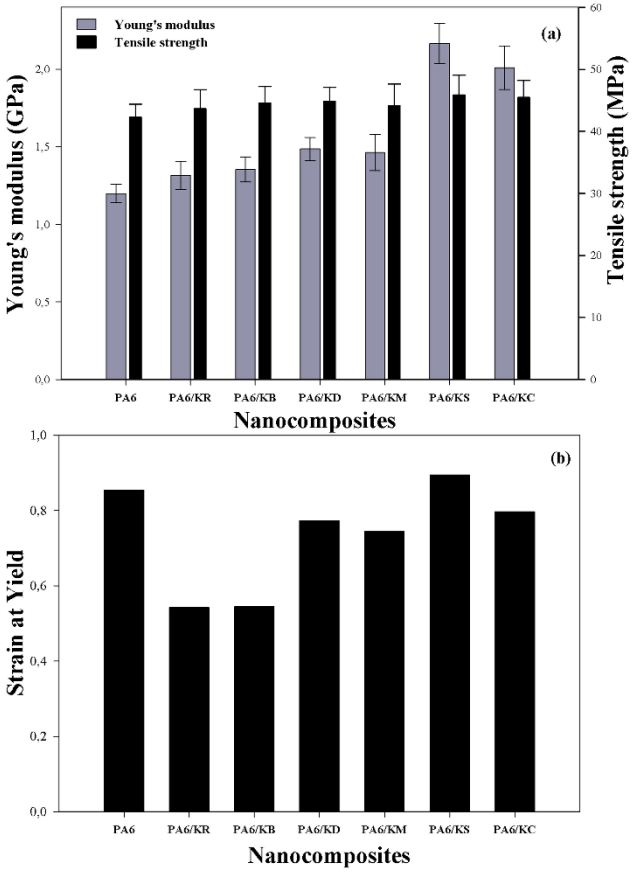

Figure IV-8: Tensile properties of the nanocomposites polymer compounds of PA6-Kaolinite

IV.6. Conclusion

Oulmes kaolin rock mainly contains kaolinite as a major mineral with small quantities of the muscovite and illite as well as the iron oxides as the major impurity. In this work, the iron dissolution from kaolin mineral was occurred via solvothermal reaction in aqueous oxalic acid as leaching agent with the consequent greet whitening results of the kaolinite proved by high whiteness index. The use of displacement method to intercalate the kaolinite particles was examined by various physicochemical techniques, including FTIR, XRD, and TGA. Thus, suggesting the formation of new chemical bonding between the hydroxyl groups of kaolinite nanoparticles and chemical groups of the used intercalated molecules. The great exfoliation and lessening of the kaolinite nanoparticles size were confirmed by high whiteness index of the nanocomposites. Finally, the addition of the pristine and intercalated kaolinite was shown to increase thermal stability and mechanical properties, but the functionalization of kaolinite nanoparticles was more improved both behaviors due to the greet interfacial adhesion, high aspect ratio and random dispersion/distribution of kaolinite particles into the polymer matrix.

Acknowledgements

This work was supported by Moroccan Foundation for Advanced Science, Innovation and Research (MAScIR), Rabat, Morocco. The authors would like to thank Mehdi Ait Dahi for his fruitful technical support and assistance.

CONCLUSION GENERALE et FUTURE PERSPECTIVE

CONCLUSION GENERALE et FUTURE PERSPECTIVE

Les recherches effectuées, durant les années de thèse, ont permis de contribuer à la compréhension physique et chimique des matériaux composites. L'objectif de ce travail est la production de nouveaux composites polymères de hautes performances structurales, thermiques et mécaniques par l'utilisation d'une roche très abondante au Maroc comme un renfort naturel. Pour ce faire, une analyse fine des relations structure/morphologie/propriétés a été réalisée pour des composites à base de plusieurs types de matrice thermoplastiques avec des aluminosilicates de structure chimique cristalline ou amorphe.

L'état de l'art existant sur les composites thermoplastiques à base de charge naturel a permis d'appréhender les problématiques principales liées à l'élaboration de nouveaux composites avec des propriétés thermiques et mécanique élevé. Ces propriétés sont souvent associées à plusieurs éléments comme la structure chimique des constituants, leur fraction volumique, leur arrangement spatial, mais les deux paramètres déterminants dans l'amélioration des propriétés finales du matériau ; à savoir la bonne adhésion entre la charge et le polymère ainsi que le bon état de dispersion-distribution des charges. Par ailleurs, les différentes classes des composites et ses différentes techniques d'élaboration : la voie fondue, la voie solvant et la polymérisation in situ ont été étudiées. L'accent a également mis sur la structure des argiles, leurs propriétés et les différentes classes argiles-polymères structures.

Compte tenu des propriétés structurales des aluminosilicates (illite, perlite) et leurs disponibilités en bonne quantité au Maroc, nous avons utilisé l'illite et la perlite comme renforts pour deux matrices polymères différents (HDPE et PP), nous ont orienté spécifiquement vers:

- Les composites à base d'illite (aluminosilicate de structure cristalline) à différents taux de charge (0-40 % en masse) avec une matrice thermoplastique de type polyéthylène haute densité et un ajout de compatibilisant de type (SEBS-g-MA)

- Les composites à base de types de structure de perlite (aluminosilicate de structure non-cristalline ou amorphe) ; la perlite brute et la perlite expansée a différents taux de charge (0-20 % en masse) avec une matrice thermoplastique de type polypropylène.

Nous avons démontré que toutes les propriétés des composites semblent être conditionnées par la taille des entités dispersées, la qualité de la dispersion des charges, ainsi que par l'affinité entre le polymère et les charges. Toutefois, les propriétés des composites à base de perlite expansée se sont

révélées mauvaises, car le broyage masque l'effet d'expansion. A contrario dans le cas des composites à base de la perlite brute.

En partant de cette sélection, les particules d'argiles possèdent une très grande énergie de surface et se trouvent naturellement agrégées ce qui ne facilite pas sa dispersion élémentaire au sein de matrices polymères. Donc, il est souvent indispensable de modifier leur surface afin de favoriser leur dispersion dans une matrice polymérique peu polaire, ainsi que les interactions entre les particules d'argiles polymère, sont des paramètres prépondérants pour l'amélioration des propriétés du composite final. L'étude des nanocomposites d'argile à différents forme (sepiolite, halloysite et montmorillonite) a permis d'établir plusieurs conclusions. D'abord, les différentes études montrent l'efficacité de l'ajout des particules d'argiles pour favoriser la cristallisation du polymère et améliorer la stabilité thermique, ainsi que l'utilité d'un traitement de surface par l'utilisation deux types de silane pour contribuer à l'amélioration de l'état de dispersion des particules d'argiles dans la matrice polymère et à la qualité de l'interface des particules d'argiles /polymère, et par conséquence à l'amélioration des propriétés mécanique.

Deux paramètres sont essentiels pour l'amélioration des propriétés des nanocomposites avec des charges argileuses de taille nanométrique : les valeurs importantes du rapport surface/volume des particules d'argile induisant une augmentation considérable des possibilités d'interactions entre l'argile et la matrice polymère. Deuxième facteur prépondérant est la diminution des distances interparticulaires jusqu'à atteindre l'échelle des dimensions des chaînes polymériques. Basée sur la même méthodologie, l'étude des nanocomposites à base de polyamide 6 (PA6) et de la kaolinite blanchies et intercalées comme étant une argile non gonflante a permis de démontrer l'effet positif et original du de l'intercalation des feuillets de la kaolinite. Ceci prouve l'intérêt de l'intercalation pour aboutir à la création d'interfaces fortes entre les particules et la matrice ainsi que l'obtention d'une dispersion fine et homogène des particules dans la matrice polymère et de l'impact de ces paramètres sur les propriétés globales des nanocomposites. Les travaux ont permis la possibilité d'intercaler des types d'argiles gonflantes ou pas et de minimiser ses tailles de particules à l'échelle nanométriques ce qui leur rendre les meilleurs renforts pour des matrices thermoplastiques, présentant des propriétés exploitables, et susceptibles d'élargir leurs domaines d'application. Ce travail ouvre d'autres horizons, qui pourraient être approfondis comme l'étude de la possibilité d'intercalation du n'importe quel type d'argile pour but de minimiser la taille de ses particules et de fabriques des nanocomposites à hautes caractéristiques et l'utilisation d'autre type de matrice ; thermoplastique ou thermodurcissable. Et finaliser ce travail par l'étude de la durabilité de ce type des composites.

GLOBAL CONCLUSION and FUTUR PERSPECTIVE

GLOBAL CONCLUSION and FUTUR PERSPECTIVE

Research carried out during the thesis has contributed to the physical and chemical understanding of composite materials preparation and properties. The objective of this work is the manufacturing of new polymer composites with high structural, thermal and mechanical performances by the use of an abundant rock in Morocco as a natural reinforcement, precisely the illite; perlite and kaolinite. The study was conducted concerned on the samples prepared by extrusion and injected process based on thermoplastic polymers with and without compatibility agent or with and without modifications. The clay was purified by filtering followed by drying, grinding and sieving. The mineral clay as a hydrophilic in nature is rendered hydrophobic and therefore organophilic by cationic exchange in the case of swelling clays or by organic solvent. Structural and morphological characterization techniques such as FTIR, XRD, and SEM have been used to identify the class of clay and the success of the purification process. The thermal, mechanical, rheological and structural properties of the polymeric matrix are greatly improved by the addition of crystalline or amorphous structural clay. Thus, the clay plays a role of a nucleating agent, which promotes crystallization at a high temperature for all composites. Remarkable enhancement in mechanical properties by the incorporation of clays, unlike the elongation at the maximum stress of thermoplastics for which the addition of clay tends to reduce them. It should be noted, that the chemical modifications played an important role in the improvement of the interfacial adhesion between the clay particles and the polymer matrix. The melt rheology results has given us an idea about the viscoelastic behaviors of composites during implementation and the favorability of their conditions of preparation. The work has made it possible to intercalate all types of clays (swelling or not) to minimize its particle sizes at the nanoscale, which makes them a good reinforcement for thermoplastic matrices, presenting exploitable properties, and likely to expand their fields of application.

This work opens other horizons, which could be deepened as the study of the possibility of intercalation of any type of clay in order to minimize the size of its particles and manufacturing of nanocomposites at nanoscales with high characteristics and the use of other types of the matrix; thermoplastic or thermosetting. Moreover, finalize this work by studying the durability of this type of composites.

REFERENCES

[1] Essabir H, Raji M, Essassi EM, Rodrigue D, Bouhfid R, Qaiss A el kacem. Morphological, thermal, mechanical, electrical and magnetic properties of ABS/PA6/SBR blends with Fe3O4 nano-particles. Journal of Materials Science: Materials in Electronics ,. 2017;28(22):17120–17130.

[2] Raji M, El M, Mekhzoum M, Qaiss A el K, Bouhfid R. Nanoclay Modification and Functionalization for Nanocomposites Development: Effect on the Structural, Morphological, Mechanical and Rheological Properties. In: Nanoclay Reinforced Polymer Composites ,. 2016. p. 1–34.

[3] Raji M, Essabir H, Essassi EM, Rodrigue D, Bouhfid R, Qaiss A el K. Morphological, Thermal, Mechanical, and Rheological Properties of High Density Polyethylene Reinforced With Illite Clay. Polymers and Polymer Composites. 2016;16(2):101–13.

[4] Sana A, Laaziz A, Raji M, Hilali E, Essabir H, Rodrigue D, et al. Bio-composites based on polylactic acid and argan nut shell : Production and properties. International Journal of Biological Macromolecules ,. 2017;104:30–42.

[5] Abdellaoui H, Bensalah H, Raji M, Rodrigue D, Bouhfid R. Laminated Epoxy Biocomposites Based on Clay and Jute Fibers. Journal of Bionic Engineering ,. 2017;14(2):379–89.

[6] El Mechtali FZ, Essabir H, Nekhlaoui S, Bensalah MO, Jawaid M, Bouhfid R, et al. Mechanical and Thermal Properties of Polypropylene Reinforced with Almond Shells Particles: Impact of Chemical Treatments. Journal of Bionic Engineering. 2015;12(3):483–94.

[7] Essabir H, Nekhlaoui S, Bensalah MO, Rodrigue D, Bouhfid R, Qaiss AEK. Phosphogypsum Waste Used as Reinforcing Fillers in Polypropylene Based Composites: Structural, Mechanical and Thermal Properties. Journal of Polymers and the Environment ,. 2016;

[8] Essabir H, Boujmal R, Bensalah MO, Rodrigue D, Bouhfid R, Qaiss AEK. Mechanical and thermal properties of hybrid composites: Oil-palm fiber/clay reinforced high density polyethylene. Mechanics of Materials ,. 2016;98:36–43.

[9] Raji M, Essabir H, Bouhfid R, Qaiss A el kacem. Impact of Chemical Treatment and the Manufacturing Process on Mechanical, Thermal, and Rheological Properties of Natural Fibers-Based Composites. In: Handbook of Composites from Renewable Materials ,. Hoboken, NJ, USA: John Wiley & Sons, Inc.; 2017 [cited 2017 Oct 19]. p. 225–52.

[10] Boujmal R, Kakou CA, Nekhlaoui S, Essabir H, Bensalah M-O, Rodrigue D, et al. Alfa fibers/clay hybrid composites based on polypropylene. Journal of Thermoplastic Composite Materials ,. 2017 Sep 7 [cited 2017 Nov 27];https://do.

[11] Essabir H, Raji M, Bouhfid R, Qaiss A el K. Nanoclay and Natural Fibers Based Hybrid Composites: Mechanical, Morphological, Thermal and Rheological Properties. In: Nanoclay Reinforced Polymer Composites ,. 2016. p. 29–49.

[12] Bensalah H, Gueraoui K, Essabir H, Rodrigue D, Bouhfid R, Qaiss AEK. Mechanical, thermal, and rheological properties of polypropylene hybrid composites based clay and graphite. Journal of Composite Materials ,. 2017;DOI: 10.11:1–14.

[13] Prasad A, Fotou G, Li S. The effect of polymer hardness, pore size, and porosity on the performance of thermoplastic polyurethane-based chemical mechanical polishing pads. Journal of Materials Research ,. 2013;28(17):2380–93.

[14] Hutchinson JM. Physical aging of polymers. Progress in Polymer Science. 1995;20(4):703–60.

[15] Esposito Corcione C, Prinari P, Cannoletta D, Mensitieri G, Maffezzoli a. Synthesis and characterization of clay-nanocomposite solvent-based polyurethane adhesives. International Journal of Adhesion and Adhesives. 2008;28(3):91–100.

[16] Issa B, Obaidat IM, Albiss BA, Haik Y. Magnetic nanoparticles: Surface effects and properties related to biomedicine applications. International Journal of Molecular Sciences. 2013;14(11):21266–305.

[17] Universiti S, Universiti Z. Stiffness Prediction of Hybrid Kenaf / Glass Fiber Reinforced Polypropylene Composites using Rule of Mixtures (ROM) and Rule of Hybrid Mixtures (RoHM) Stiffness Prediction of Hybrid Kenaf / Glass Fiber Reinforced Polypropylene Composites using Rule of. 2013;(NOVEMBER).

[18] G. Gamona B, Evona P, L. Rigala B. Twin-screw extrusion impact on natural fibre morphology and material properties in poly(lactic acid) based biocomposites. Industrial Crops and Products. 2013;46:173–85.

[19] Babrekar H a., Kulkarni N V., Jog JP, Mathe VL, Bhoraskar S V. Influence of filler size and morphology in controlling the thermal emissivity of aluminium/polymer composites for space applications. Materials Science and Engineering B: Solid-State Materials for Advanced Technology,. 2010;168(1):40–4.

[20] Wang B. Dispersion of Cellulose Nanofibers in Biopolymer Based Dispersion of Cellulose Nanofibers in Biopolymer Based Nanocomposites. 2008;157.

[21] Šupová M, Martynková GS, Barabaszová K. Effect of Nanofillers Dispersion in Polymer Matrices: A Review. Science of Advanced Materials,. 2011;3(1):1–25.

[22] Geethamma VG, Joseph R, Thomas S. Short Coir Fiber-Reinforced Natural-Rubber Composites - Effects of Fiber Length, Orientation, and Alkali Treatment. Journal of Applied Polymer Science. 1995;55(4):583–94.

[23] Rohini R, Katti P, Bose S. Tailoring the interface in graphene/thermoset polymer composites: A critical review. Polymer (United Kingdom),. 2015;70:A17–34. Available from: http://dx.doi.org/10.1016/j.polymer.2015.06.016

[24] Raji M, NekhlaouiIz S, Hassani EEA El, Essassi EM, Rodrigue D, Rachid Bouhfid, et al. Utilization of volcanic amorphous aluminosilicate rocks (perlite) as alternative materials in lightweight composites. Composites Part B: Engineering. 2019;

[25] Raji M, Essabir H, Rodrigue D, Bouhfid R, Abou el kacem Qaiss. Influence of Graphene Oxide and Graphene Nanosheet on the Properties of Polyvinylidene Fluoride Nanocomposites. Polymers and Polymer Composites. 2017;

[26] Essabir H, Raji M, Laaziz S., Rodrigue D, Bouhfid R, Abou el kacem Qaiss, Thermo-mechanical performances of polypropylene biocomposites based on untreated, treated and compatibilized spent coffee grounds. Composites Part B. 2018;146(April):106–15.

[27] Essabir H, Raji M, Bouh R. Recent Advances in Nanoclay/Natural Fibers Hybrid Composites. In: Nanoclay Reinforced Polymer Composites,. 2016. p. 29–49.

[28] Nekhlaoui S, Essabir H, Bensalah MO, Fassi-Fehri O, Qaiss a., Bouhfid R. Fracture study of the composite using essential work of fracture method: PP–SEBS–g–MA/E1 clay. Materials & Design ,. 2014 Jan ;53:741–8.

[29] Bhat G, Hegde RR, Kamath MG, Deshpande B. Nanoclay Reinforced Fibers and Nonwovens. Journal of Engineered Fibers and Fabrics. 2008;3(3):22–34.

[30] Essabir H, Raji M, Bouh R. Nanoclay and Natural Fibers Based Hybrid Composites: Mechanical, Morphological, Thermal and Rheological Properties. In: Nanoclay Reinforced Polymer Composites ,. 2016. p. 29–49.

[31] Zari N, Raji M, Mghari H El, Bouhfid R. Nanoclay and polymer-based nanocomposites: Materials for energy efficiency. In: Polymer-based Nanocomposites for Energy and Environmental Applications Published Woodhead. 2018. p. 75–103.

[32] Majeed K, Jawaid M, Hassan A, Abu Bakar A, Abdul Khalil HPS, Salema A a., et al. Potential materials for food packaging from nanoclay/natural fibres filled hybrid composites. Materials & Design ,. 2013 Apr [cited 2014 Aug 4];46:391–410.

[33] Kord B, Kiakojouri S. Effect of nanoclay dispersion on physical and mechanical properties of wood flour/polypropylene/glass fibre hybrid composites. BioResources. 2011;6(2):1741–51.

[34] Widya T, Macosko C. Nanoclay Modified Rigid Polyurethane Foam. Journal of Macromolecular Science, Part B: Physics ,. 2005;44(6):897–908.

[35] Mohan TP, Kanny K. Water barrier properties of nanoclay filled sisal fibre reinforced epoxy composites. Composites Part A: Applied Science and Manufacturing ,. 2011;42(4):385–93. Available from: http://dx.doi.org/10.1016/j.compositesa.2010.12.010

[36] Haq M, Burgueño R, Mohanty AK, Misra M. Hybrid bio-based composites from blends of unsaturated polyester and soybean oil reinforced with nanoclay and natural fibers. Composites Science and Technology ,. 2008;68(15–16):3344–51.

[37] Results IM, References DC. Polypropylene/Polystyrene blends reinforced with hybrid Inorganic fillers: Effect of modified kaolin nanoclays and short glass fibers. In: modification of polypropylene/polystyrene blend using nanoclay and sisal cellulose nanofiber. p. 129–215.

[38] Ashik KP, Sharma RS. A Review on Mechanical Properties of Natural Fiber Reinforced Hybrid Polymer Composites. Journal of Minerals and Materials Characterization and Engineering. 2015;3(September):420–6.

[39] Zuhri MYM, Sapuan SM, Ismail N. Oil Palm Fibre Reinforced Polymer Composites: A Review. Progress in Rubber Plastics and Recycling Technology. 2009;25(4):233–46.

[40] Beyou E, Akbar S, Chaumont P, Cassagnau P. Polymer nanocomposites containing functionalised multiwalled carbon nanoTubes: a particular attention to polyolefin based materials. Syntheses and Applications of Carbon Nanotubes and Their Composites ,. 2013;77–115. Available from: 115

[41] Ku H, Wang H, Pattarachaiyakoop N, Trada M. A review on the tensile properties of natural fiber reinforced polymer composites. Composites Part B: Engineering. 2011;42(4):856–73.

[42] Haque Z, Yadav S, Kumar S. Mechanical Behaviour of COIR / GLASS Fiber Reinforced EPOXY Based Composites. 2016;568–72.

[43] Dragan K. Ageing of composites in the rotorcraft industry. Ageing of Composites ,. 2008;311–25.

[44] Bledzki A. Composites reinforced with cellulose based fibres. In: Progress in Polymer Science ,. 1999. p. 221–74.

[45] Tejado A, Pen C, Labidi J, Echeverria JM, Mondragon I. Physico-chemical characterization of lignins from different sources for use in phenol – formaldehyde resin synthesis. Bioresource technology. 2007;98:1655–63.

[46] Jose JP, Malhotra SK, Thomas S, Joseph K, Goda K, Sreekala MS. Advances in polymer composites: Macro- and microcomposites – state of the art, new challenges, and opportunities. In: Polymer Composites First Edition Edited by Sabu Thomas, Kuruvilla Joseph, Sant Kumar Malhotra, Koichi Goda, and Meyyarappallil Sadasivan Sreekala. 2012. p. 1–16.

[47] Thakur VK, Thakur MK, Michael R. Kessler. Handbook of Composites from Renewable Materials "Volume 1 Structure and Chemistry." 2017. 575 p.

[48] Hussain F, Hojjati M, Okamoto M, Gorga RE. Review article: Polymer-matrix Nanocomposites, Processing, Manufacturing, and Application: An Overview. Journal of Composite Materials. 2006;40(17):1511–75.

[49] Yu L, Dean K, Li L. Polymer blends and composites from renewable resources. Progress in Polymer Science (Oxford). 2006;31(6):576–602.

[50] Dahlen C, Springer GS. Delamination Growth in Composites under Cyclic Loads. Journal of Composite Materials ,. 1994 May 27;28(8):732–81.

[51] Mohammed L, Ansari MNM, Pua G, Jawaid M, Islam MS. A Review on Natural Fiber Reinforced Polymer Composite and Its Applications. International Journal of Polymer Science ,. 2015;2015:1–15.

[52] Xia Z, Li L. Advances in Ceramic Matrix Composites. 2014;1–709.

[53] Surappa MK. Aluminium matrix composites: Challenges and opportunities. Sadhana. 2003;28(1–2):319–34.

[54] Cox J, Luong D, Shunmugasamy V, Gupta N, Strbik O, Cho K. Dynamic and Thermal Properties of Aluminum Alloy A356/Silicon Carbide Hollow Particle Syntactic Foams. Metals ,. 2014;4(4):530–48.

[55] Composites P, Properties M, Performance T. 4 - Polymer-Matrix Composites: Mechanical Properties and Thermal Performance ,. Second Edi. Carbon Composites. Elsevier Inc.; 2017. 218-255 p.

[56] Verma D, Gope PC, Shandilya a., Gupta a., Maheshwari MK. Coir fibre reinforcement and application in polymer composites: A review. Journal of Materials and Environmental Science. 2013;4(2):263–76.

[57] Abdellaoui H, Bouhfid R, Qaiss A el K. Clay, Natural Fibers and Thermoset Resin Based Hybrid Composites: Preparation, Characterization and Mechanical Properties. In: Nanoclay Reinforced Polymer Composites ,. 2016. p. 225–46

[58] Taj S, Munawar MA, Khan S. Natural Fiber-Reinforced Polymer Composites:review. In: Proc Pakistan Acad Sci ,. 2007. p. 129–44.

[59] Essabir H, Bensalah MO, Rodrigue D, Bouhfid R, Qaiss AEK. Biocomposites based on Argan nut shell and a polymer matrix: Effect of filler content and coupling agent. Carbohydrate Polymers ,. 2016;143:70–83.

[60] Chen T, Liu W, Qiu R. Mechanical Properties and Water Absorption of Hemp Fibers-Reinforced Unsaturated Polyester Composites: Effect of Fiber Surface Treatment with a Heterofunctionl Monomer. BioResources. 2013;8(2):2780–91.

[61] Essabir H, Elkhaoulani A, Benmoussa K, Bouhfid R, Arrakhiz FZ, Qaiss A. Dynamic mechanical thermal behavior analysis of doum fibers reinforced polypropylene composites. Materials & Design ,. 2013 Oct;51:780–8.

[62] Li, Z., Zhang, Y., and Zhou X. Short fiber reinforced geopolymer composites manufactured by extrusion. Journal of Materials in Civil Engineering. 2005;17(6):624–31.

[63] Curvelo a. a S, De Carvalho a. JF, Agnelli J a M. Thermoplastic starch-cellulosic fibers composites: Preliminary results. Carbohydrate Polymers. 2001;45(2):183–8.

[64] Paul DR, Robeson LM. Polymer nanotechnology: Nanocomposites. Polymer. 2008;49(15):3187–204.

[65] Elsevier F, Mech JNF, Engineering P. Talc-thermoplastic compounds: particle orientation in flow and rheological properties. 1996;62.

[66] Song SH, Park KH, Kim BH, Choi YW, Jun GH, Lee DJ, et al. Enhanced thermal conductivity of epoxy-graphene composites by using non-oxidized graphene flakes with non-covalent functionalization. Advanced Materials. 2013;25(5):732–7.

[67] Ghasemi I, Kord B. Long-term Water Absorption Behaviour of Polypropylene/Wood Flour/Organoclay Hybrid Nanocomposite. Iranian Polymer Journal. 2009;18(9):683–91.

[68] Jacob M, Thomas S, Varughese KT. Mechanical properties of sisal/oil palm hybrid fiber reinforced natural rubber composites. Composites Science and Technology. 2004;64(7–8):955–65.

[69] Zhang J, Chaisombat K, He S, Wang CH. Hybrid composite laminates reinforced with glass/carbon woven fabrics for lightweight load bearing structures. Materials and Design ,. 2012;36(July 2016):75–80.

[70] Essabir H, Bensalah MO, Rodrigue D, Bouhfid R, Qaiss A. Structural, mechanical and thermal properties of bio-based hybrid composites from waste coir residues: Fibers and shell particles. Mechanics of Materials. 2016;93:134–144.

[71] Thwe MM, Liao K. Durability of bamboo-glass fiber reinforced polymer matrix hybrid composites. Composites Science and Technology. 2003;63(3–4):375–87.

[72] Abdul Khalil HPS, Jawaid M, Abur Bakar a. Woven Hybrid composites: water absorption and thicjness swelling behaviours. BioResources ,. 2011;6(2):1043–52.

[73] Thakur VK, Thakur MK, Pappu A. Hybrid Polymer Composite Materials Properties and Characterisation. 2017. 420 p.

[74] Lebaron PC, Wang Z, Pinnavaia TJ. Polymer-layered silicate nanocomposites: An overview. Applied Clay Science. 1999;15(1–2):11–29.

[75] Manjunatha G, George R, Hiremath I. Functionalized Graphene for Epoxy Composites with Improved Mechanical Properties. 2016;6:41–6.

[76] Chen B, Evans JRG, Greenwell HC, Boulet P, Coveney P V, Bowden AA, et al. A critical appraisal of polymer-clay nanocomposites www.rsc.org/csr | Chemical Society Reviews A critical appraisal of polymer – clay nanocomposites. 2008;(April).

[77] Chen BK, Shih CC, Chen AF. Ductile PLA nanocomposites with improved thermal stability. Composites Part A: Applied Science and Manufacturing ,. 2012;43(12):2289–95.

[78] Kodjie SL, Li L, Li B, Cai W, Li CY, Keating M. Morphology and Crystallization Behavior of HDPE / CNT Nanocomposite. 2006;(August 2005):231–45.

[79] Bouhfid R, Essabir H, Qaiss A el kacem. GRAPHENE-BASED NANOCOMPOSITES:MECHANICAL, THERMAL, ELECTRICAL, AND RHEOLOGICAL

PROPERTIES. In: Rheology and Processing of Polymer Nanocomposites, First Edition Edited by Sabu Thomas, ReneMuller, and Jiji Abraham by JohnWiley & Sons, Inc. 2016. p. 405–30.

[80] Leszczy a, Njuguna J, Pielichowski K, Banerjee JR. Polymer / montmorillonite nanocomposites with improved thermal Part II : Thermal stability of montmorillonite nanocomposites based on different polymeric matrixes. 2007;454(1):1–22.

[81] Essabir H, Raji M, Essassi EM, Rodrigue D, Bouhfid R, Qaiss A el kacem. Morphological, thermal, mechanical, electrical and magnetic properties of ABS/PA6/SBR blends with Fe3O4 nano-particles. Journal of Materials Science: Materials in Electronics ,. 2017;

[82] Letaief S, Liu Y, Detellier C. Single Kaolinite Nanometer Layers Prepared by an In Situ Polymerization À Exfoliation Process in the Presence of Ionic Liquids. Langmuir. 2011;27:15248–54.

[83] Núñez K, Gallego R, Pastor JM, Merino JC. The structure of sepiolite as support of metallocene co-catalyst during in situ polymerization of polyolefin (nano)composites. Applied Clay Science ,. 2014 Nov :101:73–81.

[84] Kuilla T, Bhadra S, Yao DH, Kim NH, Bose S, Lee JH. Recent advances in graphene based polymer composites. Progress in Polymer Science. 2010;35(11):1350–75.

[85] Hansen E, Nilsson NH, Lithner D, Lassen C. Hazardous substances in plastic materials. Hazardous substances in plastic materials ,. 2013;148.

[86] Saba N, Tahir P, Jawaid M. A Review on Potentiality of Nano Filler/Natural Fiber Filled Polymer Hybrid Composites. polymers. 2014;6:2247–73.

[87] Scott auerbach M, Carrado kathleen a., Dutta prabir k. HANDBOOK OF LAYERED MATERIALS. 2004.

[88] Zeng QH, Yu AB, Lu GQ, Paul DR. Clay-based polymer nanocomposites: research and commercial development. Journal of nanoscience and nanotechnology. 2005;5:1574–92.

[89] Lowe DJ. Natural Rubber / Organoclay Nanocomposites. 2012;(April).

[90] Shen W, He HP, Zhu JX, Yuan P, Ma YH, Liang XL. Preparation and characterization of 3-aminopropyltriethoxysilane grafted montmorillonite and acid-activated montmorillonite. Chinese Science Bulletin. 2009;54(2):265–71.

[91] Mineralogia P. Spectroscopic characterization of a sepiolite-based Maya Blue pigment. Periodico Di Mineralogia. 2010;21–37.

[92] Lavikainen L. The structure and surfaces of 2 :1 phyllosilicate clay minerals. In 2016.

[93] Yang H, Peng Z, Zhou Y, Zhao F, Zhang J, Cao X, et al. Preparation and performances of a novel intelligent humidity control composite material. 2011;43:386–92.

[94] Bergaya F, Lagaly G. General Introduction : Clays , Clay Minerals , and Clay Science. In: Handbook of Clay Science ,. 2nd ed. Elsevier Ltd.; 2013. p. 1–19.

[95] Gacitua EW, Ballerini AA, Jinwen Z. Polymer Nanocomposites : Synthetic And Natural Fillers. Maderas Ciencia y tecnología. 2005;7(3):159–78.

[96] Wang G-T, Liu H-Y, Yu Z-Z, Mai Y-W. Evaluation of Methods for Stiffness Predictions of Polymer/Clay Nanocomposites. Journal of Reinforced Plastics and Composites. 2009;28(13):1625–49.

[97] Pavlidou S, Papaspyrides CD. A review on polymer–layered silicate nanocomposites. Progress in Polymer Science. 2008;33:1119–98.

[98] Pillai LR, Thavamani P. Effect of DOP as Dispersion Medium on MMT- nano Clay in NBR Polymer Matrix. 2014;29–32.

[99] Ding H, Wang Y, Liang Y, Qin F. Preparation and Characterization of Cetyl Trimethylammonium Intercalated Sericite. 2014;2014:1–9.

[100] Tang LC, Wan YJ, Yan D, Pei YB, Zhao L, Li YB, et al. The effect of graphene dispersion on the mechanical properties of graphene/epoxy composites. Carbon ,. 2013;60:16–27.

[101] Arrakhiz FZ, El Achaby M, Malha M, Bensalah MO, Fassi-Fehri O, Bouhfid R, et al. Mechanical and thermal properties of natural fibers reinforced polymer composites: Doum/low density polyethylene. Materials & Design ,. 2013 Jan;43:200–5.

[102] Huang D, Mu B, Wang A. Preparation and properties of chitosan/poly (vinyl alcohol) nanocomposite films reinforced with rod-like sepiolite. Materials Letters ,. 2012 Nov;86:69–72.

[103] Nicole M Stark LMM. Surface chemistry changes of weathered HDPE/wood-flour composites studied by XPS and FTIR spectroscopy. Polymer Degradation and Stability. 2004;86:1–9.

[104] Karsli NG, Yesil S, Aytac A. Composites : Part B Effect of hybrid carbon nanotube / short glass fiber reinforcement on the properties of polypropylene composites. Composites: Part B ,. 2014;63:154–60.

[105] Ehsan Mohammadpour MA. Modeling the tensile stress-strain response of carbon nanotube/polypropylene nanocomposites using nonlinear representative volume element. Materials and Design. 2014;1(1).

[106] Thakur VK, Kessler MR. Self-Healing Polymer Nanocomposite Materials : A Review Self-healing polymer nanocomposite materials : A review. Polymer ,. 2018;(February).

[107] Arrakhiz FZ, El Achaby M, Kakou a. C, Vaudreuil S, Benmoussa K, Bouhfid R, et al. Mechanical properties of high density polyethylene reinforced with chemically modified coir fibers: Impact of chemical treatments. Materials & Design ,. 2012 May [cited 2014 Jul 11];37:379–83.

[108] Thakur VK, Thakur MK, Raghavan P, Kessler MR. Progress in green polymer composites from lignin for multifunctional applications: A review. ACS Sustainable Chemistry and Engineering. 2014;2(5).

[109] Nowaczyk G, Głowinkowski S, Jurga S. Rheological and NMR studies of polyethylene/calcium carbonate composites. Solid state nuclear magnetic resonance ,. 2004 Jan :25(1–3):194–9.

[110] Thakur V, Vennerberg D, Kessler M. Green aqueous surface modification of polypropyl- ene for novel polymer nanocomposites. ACS Appl Mater. 2014;6:9349.

[111] Elkhaoulani A, Arrakhiz FZ, Benmoussa K, Bouhfid R, Qaiss A. Mechanical and thermal properties of polymer composite based on natural fibers: Moroccan hemp fibers/polypropylene. Materials & Design ,. 2013 Aug;49:203–8.

[112] Musil V, Jurkin T, Konjice S. Structuring of polypropylene matrix in composites. Polymer. 2009;30(4):183–92.

[113] Nekhlaoui S, Essabir H, Kunal D, Sonakshi M, Bensalah MO, Bouhfid R, et al. Comparative Study for the Talc and Two Kinds of Moroccan Clay as Reinforcements in Polypropylene-SEBS-g-MA Matrix. Polymer Composites. 2014;10(1–10).

[114] Hakur VK, Yan J, Lin M-F, Zhi C, Golberg D, Bando Y, et al. T Novel polymer nanocomposites from bioinspired green aqueous functionalization of BNNTs. Polym Chem. 2012;3:962.

[115] Gao F. Clay / polymer composites : the story. Materials Today. 2004;7(November):50–5.

[116] Liu J, Liu W, Wang J. Influence of interfacial adhesion strength on formability of AA5052/polyethylene/AA5052 sandwich sheet LIU. Transactions of Nonferrous Metals Society of China ,. 2012 Dec;22:s395–401.

[117] Lertwimolnun W, Vergnes B. Influence de la dispersion sur le comportement rhéologique de nanocomposites polypropylène/argile. Rhéologie ,. 2004 Nov 1 ;5:27–35.

[118] Fu S, Feng X, Lauke B, Mai Y. Effects of particle size , particle / matrix interface adhesion and particle loading on mechanical properties of particulate – polymer composites. Composites: Part B. 2008;39:933–61.

[119] Chen H, Zeng D, Xiao X, Zheng M, Ke C, Li Y. Influence of organic modification on the structure and properties of polyurethane/sepiolite nanocomposites. Materials Science and Engineering: A ,. 2011 Jan;528(3):1656–61.

[120] Oliveira M, Machado A V. Preparation of polymer-based nanocomposites by different routes. In: Nanocomposites: Synthesis, Characterization and Applications ,. NOVA Publishers; 2013. p. 1–22.

[121] Kojima Y, Usuki A, Kawasumi M, Okada A, Kurauchi T, Kamigaito O. Synthesis of nylon 6–clay hybrid by montmorillonite intercalated with ε-caprolactam. Journal of Polymer Science Part A: Polymer Chemistry ,. 1993 Mar 30;31(4):983–6.

[122] Shubhra QT, Alam A, Quaiyyum M. Mechanical properties of polypropylene composites: A review. Journal of Thermoplastic Composite Materials ,. 2011 Dec 12 :26(3):362–91

[123] El Achaby M, Ennajih H, Arrakhiz FZ, El Kadib a., Bouhfid R, Essassi E, et al. Modification of montmorillonite by novel geminal benzimidazolium surfactant and its use for the preparation of polymer organoclay nanocomposites. Composites Part B: Engineering ,. 2013 Aug :;51:310–7.

[124] de Paiva LB, Morales AR, Valenzuela Díaz FR. Organoclays: Properties, preparation and applications. Applied Clay Science ,. 2008 Dec :42(1–2):8–24.

[125] Singla P, Mehta R, Upadhyay SN. Clay Modification by the Use of Organic Cations. Green and Sustainable Chemistry. 2012;2:21–5.

[126] Calderon JU, Lennox B, Kamal MR. Thermally stable phosphonium-montmorillonite organoclays. Applied Clay Science ,. 2008 Jun :;40(1–4):90–8.

[127] Essabir H, Achaby ME, Hilali EM, Bouhfid R, Qaiss A. Morphological, Structural, Thermal and Tensile Properties of High Density Polyethylene Composites Reinforced with Treated Argan Nut Shell Particles. Journal of Bionic Engineering ,. 2015;12(1):129–41.

[128] Arrakhiz FZ, Benmoussa K, Bouhfid R, Qaiss A. Pine cone fiber/clay hybrid composite: Mechanical and thermal properties. Materials & Design ,. 2013 Sep;50:376–81.

[129] ISO 527-1:2012. Plastics-determination of tensile properties -Part 1: General principles.

[130] ASTM D 4092 – 01. Standard Terminology for Plastics: Dynamic Mechanical Properties. ASTM Int ,. 2013;1–4.

[131] Bidsorkhi HC, Soheilmoghaddam M, Pour RH, Adelnia H, Mohamad Z. Mechanical, thermal and flammability properties of ethylene-vinyl acetate (EVA)/sepiolite nanocomposites. Polymer Testing ,. 2014 Aug;37:117–22.

[132] Lanson B, Beaufort D, Berger G, Bauer a, Cassagnnère a, Meunier a. Authigenic kaolin and illitic minerals during burial diagenesis of sandstones: a review. Clay minerals ,. 2002;37(1):1–22.

[133] Kakou CA, Arrakhiz FZ, Trokourey A, Bouhfid R, Qaiss A, Rodrigue D. Influence of coupling agent content on the properties of high density polyethylene composites reinforced with oil palm fibers. Materials & Design ,. 2014 Jun ;63:641–649.

[134] Jeong E, Lim JW, Seo KW, Lee YS. Effects of physicochemical treatments of illite on the thermo-mechanical properties and thermal stability of illite/epoxy composites. Journal of Industrial and Engineering Chemistry ,. 2011;17(1):77–82.

[135] Alkan M, Hopa Ç, Yilmaz Z, Güler H. The effect of alkali concentration and solid/liquid ratio on the hydrothermal synthesis of zeolite NaA from natural kaolinite. Microporous and Mesoporous Materials ,. 2005 Nov ;86(1–3):176–84.

[136] Wang Y, Xu D, Tsui KY. Discrete Element Modeling of Contact Creep and Aging in Sand. 2008;(September):1407–11.

[137] M.FLANIGEN EDITH , A.KHATAMI HASSAN SH "American CS. Molecular Sieve Zeolites-I ,. Flanigen EM, Sand LB, editors. WASHINGTON, D. C.: AMERICAN CHEMICAL SOCIETY; 1974 . 201-229 p. (Advances in Chemistry; vol. 101).

[138] Navrátilová Z, Wojtowicz P, Vaculíková L, Šugárková V. Sorption of alkylammonium cations on montmorillonite. Acta Geodyn Geomater. 2007;4(3):59–65.

[139] Lambert JF, Millman WS, Fripiat JJ. Revisiting kaolinite dehydroxylation: a silicon-29 and aluminum-27 MAS NMR study. Journal of the American Chemical Society ,. 1989 May;111(10):3517–22.

[140] Saikia NJ, Bharali DJ, Sengupta P, Bordoloi D, Goswamee RL, Saikia PC, et al. Characterization, beneficiation and utilization of a kaolinite clay from Assam, India. Applied Clay Science ,. 2003 Nov;24(1–2):93–103.

[141] Katti K, Katti D. Effect Of Clay-Water Interactions On Swelling In Montmorillonite Clay. Civil Engineering. 1997;9:1–9.

[142] Frost RAYL, Vassallo AM. The Dehydroxylation Of The Kaolinite Clay Mineralsusing Infrared Emission Spectroscopy. Clays and Clay Minerals. 1996;44(5):635–51.

[143] O'Gorman J V., Walker PL. Thermal behaviour of mineral fractions separated from selected American coals. Vol. 52, Fuel. 1973. p. 71–9.

[144] Bagdassarov N, Ritter F, Yanev Y. Kinetics of perlites degassing : TG and DSC analysis. Glastech Ber Glass Sci, Techno. 1999;72(9):277–90.

[145] Arrakhiz, F.Z, El Achaby M, Benmoussa K, Bouhfid R, Essassi EM, Qaiss A. Evaluation of mechanical and thermal properties of Pine cone fibers reinforced compatibilized polypropylene. Materials & Design ,. 2012 Sep;40:528–35.

[146] Amendola E, Scamardella AM, Callegaro G, Lavorgna M, Piscitelli F, Romeo V. Epoxy Nanocomposites Based on Silylated Montmorillonite : Effect of the Coupling Agents Structure on the Mechanical Properties. Macromolecules. 2012;6:33–6.

[147] Essabir H, Nekhlaoui S, Malha M, Bensalah MO, Arrakhiz FZ, Qaiss A, et al. Bio-composites based on polypropylene reinforced with Almond Shells particles: Mechanical and thermal properties. Materials & Design ,. 2013 Oct;51:225–30.

[148] Soheilmoghaddam M, Wahit MU, Yussuf AA, Al-Saleh M a., Whye WT. Characterization of bio regenerated cellulose/sepiolite nanocomposite films prepared via ionic liquid. Polymer Testing ,. 2014 Feb;33:121–30.

[149] Prateek, Thakur VK, Gupta RK. Recent Progress on Ferroelectric Polymer-Based Nanocomposites for High Energy Density Capacitors: Synthesis, Dielectric Properties, and Future Aspects. Chem Rev. 2016;116:4260–317.

[150] Elkhaoulani A, Arrakhiz FZ, Benmoussaa K, Bouhfida R, Qaiss A. Mechanical and thermal properties of polymer composite based on natural fibers: Moroccan hemp fibers/polypropylene. Materials and Design. 2013;49:203–208.

[151] da Silva WP, e Silva CMDPS, da Silva LD, Lins M a. a. Comparison between models with constant and variable diffusivity to describe water absorption by composite materials. Materialwissenschaft und Werkstofftechnik ,. 2012;43(10):825–31.

[152] Khazaei J. Water Absorption Characteristics OF THREE WOOD VARIETIES. Agronomical research in Moldavia. 2008;23(2):5–16.

[153] Saba N, Jawaid M, Hakeem KR, Paridah MT, Khalina A, Alothman OY. Potential of bioenergy production from industrial kenaf (Hibiscus cannabinus L.) based on Malaysian perspective. Renewable and Sustainable Energy Reviews ,. 2015;42:446–59.

[154] Barkoula NM, Alcock B, Cabrera NO, Peijs T. Fatigue properties of highly oriented polypropylene tapes and all-polypropylene composites. Polymers and Polymer Composites. 2008;16(2):101–13.

[155] Abdellaoui H, Bensalah H, Raji M, Rodrigue D, Bouhfid R, Qaiss A el kacem. Laminated Epoxy Biocomposites Based on Clay and Jute Fibers. Journal of Bionic Engineering. 2017;14(2):379–89.

[156] Sarifuddin N, Ismail H, Ahmad Z. The Effect of Kenaf Core Fibre Loading on Properties of Low Density Polyethylene / Thermoplastic Sago Starch / Kenaf Core Fiber Composites. 2013;24(2):97–115.

[157] Nyström B. Natural Fiber Composites : A Review. Engineering ,. 2007;15(March):281–5.

[158] AKIN-OKTEM C, TINCER T. Preparation and Characterization of Perlite-Filled High- Density Polyethylenes . II . Thermal and Flow Properties. Journal of Applied Polymer Science. 1995;55:1093–9.

[159] Tekin N, Kadinci E, Demirbaş Ö, Alkan M, Kara a., Doğan M. Surface properties of poly(vinylimidazole)-adsorbed expanded perlite. Microporous and Mesoporous Materials. 2006;93(1–3):125–33.

[160] Ritter F. Kinetics of perlites degassing : TG and DSC Paper Original. Glass Science and Technology. 2016;72(August):277–90.

[161] Sari A, Karaipekli A, Alkan C. Preparation, characterization and thermal properties of lauric acid/expanded perlite as novel form-stable composite phase change material. Chemical Engineering Journal. 2009;155(3):899–904.

[162] Singh M, Garg M. Perlite-based building materials - a review of current applications. Construction & Building materials. 1991;5(2):75–81.

[163] Senff L, Hotza D, Labrincha J a. Effect of lightweight aggregates addition on the rheological properties and the hardened state of mortars. Applied Rheology. 2011;21(1):13668–8.

[164] Phosawat W, Chareonpanich M, Sudasna-na-Ayudthya P. Production of Zeolite Y from Perlite. online: http://kucon.lib.ku.ac.th/.

[165] ASTM International. Standard Practice for Compression Molding Thermoplastic Materials into Test Specimens, Plaques , or Sheets 1. 2013;1–13.

[166] Joo Y, Sim JH, Jeon Y, Lee SU, Sohn D. Opening and blocking the inner-pores of halloysite. The Royal Society of Chemistry. 2013; 49:4519–21.

[167] Martinez J, Erdmann E. New material as support for nickel boride catalyst. Latin American Applied Research. 2006;36(August 2016):317–20.

[168] Meesuk L, Seammai S. The use of perlite to remove dark colour from repeatedly used palm oil. ScienceAsia ,. 2010;36(1):33–39.

[169] Taxiarchou M, Panias D, Panagiotopoulou C, Karalis a, Taxiarchou R. Study on the Suitability of Volcanic Amorphous Aluminosilicate Rocks (Perlite) for the Synthesis of Geopolymer-Based Concrete. 2013;(July 2016):1–20.

[170] Celik AG, Kilic AM, Cakal GO. Expanded perlite aggregate characterization for use as a lightweight construction raw material. Physicochemical Problems of Mineral Processing. 2013;49(2):689–700.

[171] Roulia M, Chassapis K, Kapoutsis J a., Kamitsos EI, Savvidis T. Influence of thermal treatment on the water release and the glassy structure of perlite. Journal of Materials Science. 2006;41(18):5870–81.

[172] Kabra S, Katara S, Rani A. Characterization and Study of Turkish Perlite. International Journal of Innovative Research in Science, Engineering and Technology. 2013;2(9):4319–26.

[173] Sun D, Wang L, Li C. Preparation and thermal properties of paraffin/expanded perlite composite as form-stable phase change material. Materials Letters. 2013; 108:247–9.

[174] Yang X, Wang X, Yang J, Li J, Wan L. Functionalization of graphene using trimethoxysilanes and its reinforcement on polypropylene nanocomposites. Chemical Physics Letters. 2013; 570:125–31.

[175] Gyoung J, Young S, Jin S, Hyun G, Hyeun J. Composites : Part A Effects of chemical treatments of hybrid fillers on the physical and thermal properties of wood plastic composites. Composites Part A. 2010;41(10):1491–7.

[176] Akin-öktem G, Tincer T. Preparation and characterization of perlite-filled high-density polyethylenes. I. Mechanical properties. Journal of Applied Polymer Science. 1994;54(8):1103–14.

[177] AMRANI S, HALIMI Y, TAHIRI M. Composite Materials Using Expanded Perlite as a Charge and Plastic Wastes as Reinforcement, Elaboration and Properties. GSTF International Journal of Chemical Sciences. 2014;1(2):47–68.

[178] Sahraeian R, Esfandeh M, Hashemi S a. Rheological, Thermal and Dynamic Mechanical Studies of the LDPE/Perlite Nanocomposites. Polymers & Polymer Composites. 2013;21(4):243–9.

[179] Mahkam M, Vakhshouri L. Colon-specific drug delivery behavior of pH-responsive PMAA/perlite composite. International Journal of Molecular Sciences. 2010;11(4):1546–56.

[180] Tian H, Tagaya H. Dynamic mechanical property and photochemical stability of perlite/PVA and OMMT/PVA nanocomposites. Journal of Materials Science. 2008;43(2):766–70.

[181] Krishnamoorti R, Giannelis EP. Rheology of End-Tethered Polymer Layered Silicate Nanocomposites. Macromolecules. 1997;30(14):4097–102.

[182] Jawaid KRHM, Abou el Kacem Qaiss, Rachid Bouhfid. Nanoclay Reinforced Polymer Composites. 2016. 395 p.

[183] Hakeem. KR, Mohammad. J, Y. Alothman Othman. Agricultural Biomass Based Potential Materials: Springer International Publishing Switzerland. 2011. 508 p.

[184] Mansoori Y, Roojaei K, Zamanloo MR, Imanzadeh G. Polymer-clay nanocomposites via chemical grafting of polyacrylonitrile onto cloisite 20A. Bulletin of Materials Science. 2012;35(7):1063–70.

[185] Mejía A, García N, Guzmán J, Tiemblo P. Surface modification of sepiolite nanofibers with PEG based compounds to prepare polymer electrolytes. Applied Clay Science. 2014 Jun [cited 2014 Oct 28]; 95:265–74.

[186] Bhagabati P, Chaki TK, Khastgir D. One step in-situ modification of Halloysite nanotubes: Augmentation in polymer-filler interface adhesion in nanocomposites. 2015;

[187] García-López D, Fernández JF, Merino JC, Santarén J, Pastor JM. Effect of organic modification of sepiolite for PA 6 polymer/organoclay nanocomposites. Composites Science and Technology. 2010 Sep 30 [cited 2014 Oct 28];70(10):1429–36.

[188] Leu CM, Wu ZW, Wei KH. Synthesis and properties of covalently bonded layered silicates/polyimide (BTDA-ODA) nanocomposites. Chemistry of Materials. 2002;14(7):3016–21.

[189] Sánchez-Valdes S, Méndez-Nonell J, Medellín-Rodríguez FJ, Ramírez-Vargas E, Martínez-Colunga JG, Soto-Valdez H, et al. Effect of PEgMA/amine silane compatibilizer on clay dispersion of polyethylene-clay nanocomposites. Polymer Bulletin. 2009;63(6):921–33.

[190] Huda MS, Drzal LT, Mohanty AK, Misra M. The effect of silane treated- and untreated-talc on the mechanical and physico-mechanical properties of poly (lactic acid)/ newspaper fibers / talc hybrid composites. Composites: Part B. 2007;38:367–79.

[191] Zhao Y, Zhang SL, Zhang CF, Zhou Z, Wang GB. Study on poly(ether ether ketone)/organically modified montmorillonite composites. Plastics, Rubber and Composites. 2009;38(7):279–83.

[192] Shanmugharaj a. M, Rhee KY, Ryu SH. Influence of dispersing medium on grafting of aminopropyltriethoxysilane in swelling clay materials. Journal of Colloid and Interface Science. 2006;298(2):854–9.

[193] Herrera NN, Letoffe JM, Putaux JL, David L, Bourgeat-Lami E. Aqueous dispersions of silane-functionalized laponite clay platelets. A first step toward the elaboration of water-based polymer/clay nanocomposites. Langmuir. 2004;20(5):1564–71.

[194] Arrakhiz FZ, El Achaby M, Kakou AC, Vaudreuil S, Benmoussa K, Bouhfid R, et al. Mechanical properties of high density polyethylene reinforced with chemically modified coir fibers: Impact of chemical treatments. Materials & Design. 2012 May; 37:379–83.

[195] Yu-shan XIE, Shao-zao TAN, Ma-hua L, Ren-fu LIU. Structure and Antibacterial Activity of Modified Montmorillonite. CHEM RES CHINESE UNIVERSITIES. 2010;26(4):509–13.

[196] Navrátilová Z, Wojtowicz P, Vaculíková L, Šugárková V. Sorption of Alkylammonium Cations on Montmorillonite. Acta Geodyn Geomater. 2007;4(3):59–65.

[197] Bhattacharya SS, Aadhar M. Studies on Preparation and analysis of Organoclay Nano Particles. Research Journal of Engineering Sciences. 2014;3(3):10–6.

[198] Zhao Y, Abdullayev E, Vasiliev A, Lvov Y. Halloysite nanotubule clay for efficient water purification. Journal of Colloid and Interface Science. 2013;406(June):121–9.

[199] Xie A, Yan W, Zeng X, Dai G, Tan S, Cai X, et al. Microstructure and antibacterial activity of phosphonium montmorillonites. Bulletin of the Korean Chemical Society. 2011;32(6):1936–8.

[200] Szczepanik B, Słomkiewicz P, Garnuszek M, Czech K, Banaś D, Kubala-Kukuś A, et al. The effect of chemical modification on the physico-chemical characteristics of halloysite: FTIR, XRF, and XRD studies. Journal of Molecular Structure. 2015; 1084:16–22.

[201] Frost RL. Fourier transform Raman spectroscopy of Kaolinite, dickite and halloysite. Clays and Clay Minerals. 1995;43(2):191–5.

[202] Ahmed Ben Hassan S, Stojanović DB, Kojović A, Janković-Častvan I, Janaćković D, Uskoković PS, et al. Preparation and characterization of poly(vinyl butyral) electrospun nanocomposite fibers reinforced with ultrasonically functionalized sepiolite. Ceramics International. 2014 Jan;40(1):1139–46.

[203] Alan N, İşçi S. Surface modification of sepiolite particles with polyurethane and polyvinyl alcohol. Progress in Organic Coatings. 2014 Feb;77(2):444–8.

[204] Karataş D, Çelik MS. A Theoretical and Experimental Study on Adsorption of Quaternary Amines onto Sepiolite. 2005;

[205] de Faria EH, Ciuffi KJ, Nassar EJ, Vicente M a., Trujillano R, Calefi PS. Novel reactive amino-compound: Tris(hydroxymethyl)aminomethane covalently grafted on kaolinite. Applied Clay Science. 2010;48(3):516–21.

[206] Carli LN, Daitx TS, Soares G V., Crespo JS, Mauler RS. The effects of silane coupling agents on the properties of PHBV/halloysite nanocomposites. Applied Clay Science. 2014;87(April 2016):311–9.

[207] Basurto FC, García-López D, Villarreal-Bastardo N, Merino JC, Pastor JM. Nanocomposites of ABS and sepiolite: Study of different clay modification processes. Composites Part B: Engineering. 2012 Jul ;43(5):2222–9.

[208] Akin O, Tihminlioglu F. Effect of Organo-Modified Clay Addition on Properties of Polyhydroxy Butyrate Homo and Copolymers Nanocomposite. 2012;(July).

[209] Xie Y, Hill C a S, Xiao Z, Militz H, Mai C. Silane coupling agents used for natural fiber/polymer composites: A review. Composites Part A: Applied Science and Manufacturing. 2010;41(7):806–19.

[210] Kickelbick G. Concepts for the incorporation of inorganic building blocks into organic polymers on a nanoscale. Progress in Polymer Science. 2003;28(1):83–114.

[211] Ganß M, Satapathy BK, Thunga M, Staudinger U, Weidisch R, Jehnichen D, et al. Morphology and mechanical response of S – B star block copolymer – Layered silicate nanocomposites. European Polymer Journal. 2009;45(9):2549–63.

[212] Liu M, Pu M, Ma H. Preparation, structure and thermal properties of polylactide/sepiolite nanocomposites with and without organic modifiers. Composites Science and Technology. 2012 Aug;72(13):1508–14.

[213] Yürüdü C, S I, Ünlü C, Atici O, Ece ö. I, Güngör N. Synthesis and characterization of HDA / NaMMT organoclay. Bull Mater Sci. 2005;28(6):623–8.

[214] Laoutid F, Persenaire O, Bonnaud L, Dubois P. Flame retardant polypropylene through the joint action of sepiolite and polyamide 6. Polymer Degradation and Stability. 2013 Oct [cited 2014 Oct 28];98(10):1972–80.

[215] Guo B, Zou Q, Lei Y, Jia D. Structure and Performance of Polyamide 6 / Halloysite Nanotubes Nanocomposites. Polymer Journal. 2009;41(10):835–42.

[216] Raji M, El M, Mekhzoum M, Rodrigue D, El A, Qaiss K, et al. Effect of silane functionalization on properties of polypropylene/clay nanocomposites. Composites Part B. 2018; DOI: 10.1016/j.compositesb.2018.04.013.

[217] Gupta V. Surface Charge Features of Kaolinite Particles. 2011;(May):236.

[218] Sampaio CH. Novel kaolin / polysiloxane based organic- inorganic hybrid materials: Sol-gel synthesis, characterization and photocatalytic prope .... Journal of Solid-State Chemistry. 2018;260(January):106–16.

[219] Detellier C, Letaief S. Kaolinite-polymer nanocomposites. In: Developments in Clay Science. 2nd ed. Elsevier Ltd.; 2013. p. 707–19.

[220] Aras A. The change of phase composition in kaolinite- and illite-rich clay-based ceramic bodies. Applied Clay Science. 2004;24(3–4):257–69.

[221] Zhao Y, Abdullayev E, Lvov Y. Nanotubular Halloysite Clay as Efficient Water Filtration System for Removal of Cationic and Anionic Dyes. IOP Conference Series: Materials Science and Engineering. 2014;64(1):12043.

[222] Zenasni MA, Meroufel B, Merlin A, George B. Adsorption of Congo Red from Aqueous Solution Using CTAB-Kaolin from Bechar. 2014;(October):332–41.

[223] González J a., Del M. Bleaching of kaolins and clays by chlorination of iron and titanium. Applied Clay Science. 2006;33:219–29.

[224] Mesquita LMS De, Rodrigues T, Gomes SS, de Mesquita LMS. Bleaching of Brazilian kaolins using organic acids and fermented medium. Minerals Engineering. 1996;9(9):965–71.

[225] Hernández RAH, García FL, Cruz LEH, Jacuinde AB. Kaolin bleaching by leaching using phosphoric acid solutions. Journal of the Mexican Chemical Society. 2015;59(3):198–202.

[226] Martínez-Luévanos A, Rodríguez-Delgado MG, Uribe-Salas A, Carrillo-Pedroza FR, Osuna-Alarcón JG. Leaching kinetics of iron from low grade kaolin by oxalic acid solutions. Applied Clay Science ,. 2011;51(4):473–7.

[227] Hernández R a H, García FL, Cruz LEH, Luévanos a M. Iron removal from a kaolinitic clay by leaching to obtain high whiteness index. IOP Conference Series: Materials Science and Engineering ,. 2013;45:12002.

[228] Ambikadevi VR, Lalithambika M. Effect of organic acids on ferric iron removal from iron-stained kaolinite. Applied Clay Science. 2000;16(3–4):133–45.

[229] Acid UP. Kinetics of Iron Leaching from Kaolinitic Clay, Using Phosphoric Acid. 2016;

[230] Zegeye A, Yahaya S, Fialips CI, White ML, Gray ND, Manning DAC. Applied Clay Science Re fi nement of industrial kaolin by microbial removal of iron-bearing impurities. Applied Clay Science. 2013; 86:47–53.

[231] Sultana UK, Gulshan F, Kurny a SW. Kinetics of Leaching of Iron Oxide in Clay in Oxalic Acid and in Hydrochloric Acid Solutions. Materials Science and Metallurgy Engineering. 2014;2(1):5–10.

[232] Lee SO, Tran T, Jung BH, Kim SJ, Kim MJ. Dissolution of iron oxide using oxalic acid. Hydrometallurgy. 2007;87(3–4):91–9.

[233] Zuo X, Wang D, Zhang S, Liu Q, Yang H. Intercalation and Exfoliation of Kaolinite with Sodium Dodecyl Sulfate. Minerals. 2018;8(112):1–11.

[234] Samyn P, Schoukens G, Stanssens D. Kaolinite Nanocomposite Platelets Synthesized by Intercalation and Imidization of Poly(styrene-co-maleic anhydride). Materials. 2015;8(7):4363–88.

[235] Pi Z, Liu Z, Yang C, Tian X, Fei J, Zheng J. Exfoliation of kaolinite by urea-intercalation precursor and microwave irradiation assistance process. Frontiers of Earth Science in China. 2007;1(1):26–9.

[236] Bobos I, Duplay J, Rocha J, Gomes C. Kaolinite to halloysite-7 ?? transformation in the kaolin deposit of S??o Vicente De Pereira, Portugal. Clays and Clay Minerals. 2001;49(6):596–607.

[237] Letaief S, Detellier C. Nanohybrid materials from the intercalation of imidazolium ionic liquids in kaolinite. 2007;1476–84.

[238] Wang D, Liu Q, Hou D, Zhang S, Guo P, Cheng H. Improved Method for Preparation of Methoxy-Modified Kaolinite. J Braz Chem Soc. 2018;29(1):33–7.

[239] Mbey JA, Thomas F, Ngally Sabouang CJ, Liboum, Njopwouo D. An insight on the weakening of the interlayer bonds in a Cameroonian kaolinite through DMSO intercalation. Applied Clay Science. 2013;83–84:327–35.

[240] Gardolinski JE, Carrera LCM, Cantão MP, Wypych F. Layered polymer-kaolinite nanocomposites. Journal of Materials Science. 2000;35(12):3113–9.

[241] Thompson JG, Cuff AC. Crystal Structure of Kaolinite: Dimethylsulfoxide Intercalate. Clays and Clay Minerals. 1985;33(6):490–500.

[242] Caglar B, Afsin B, Tabak A. BENZAMIDE SPECIES RETAINED BY DMSO COMPOSITES AT A KAOLINITE SURFACE. Journal of Thermal Analysis and Calorimetry. 2007; 87:429–32.

[243] Krist NOS. Preparation and characterization of kaolinite nanostructures: reaction pathways, morphology and structural order. 2015;329–40.

[244] Letaief S, Leclercq J, Liu Y, Detellier C. Single kaolinite nanometer layers prepared by an in situ polymerization-exfoliation process in the presence of ionic liquids. Langmuir. 2011;27(24):15248–54.

[245] Xu H, Jin X, Chen P, Shao G, Wang H, Chen D, et al. Preparation of kaolinite nanotubes by a solvothermal method. Ceramics International. 2015;41(5):6463–9.

[246] de Faria EH, Lima OJ, Ciuffi KJ, Nassar EJ, Vicente M a, Trujillano R, et al. Hybrid materials prepared by interlayer functionalization of kaolinite with pyridine-carboxylic acids. Journal of Colloid and Interface Science. 2009;335(2):210–5.

[247] Zhang S, Ou X, Qiang Y, Niu J, Komarneni S. Applied Clay Science Thermal decomposition behavior and de-intercalation mechanism of acetamide intercalated into kaolinite by thermoanalytical techniques. Applied Clay Science. 2015; 114:309–14.

[248] Wang S, Zuo X, Cheng H, Yanga Y, Liu Q. Structural Model and De-Intercalation Kinetics of Kaolinite-Methanol-Sodium Stearate Intercalation Compound. J Braz Chem Soc. 2016;27(7):1311–8.

[249] Cheng H, Hou X, Liu Q, Li X, Frost RL. New insights into the molecular structure of kaolinite-methanol intercalation complexes. Applied Clay Science. 2015;109–110:55–63

[250] Tan D, Yuan P, Annabi-Bergaya F, Dong F, Liu D, He H. A comparative study of tubular halloysite and platy kaolinite as carriers for the loading and release of the herbicide amitrole. Applied Clay Science. 2015; 114:190–6.

[251] Kuroda Y, Ito K, Itabashi K. One-Step Exfoliation of Kaolinites and Their Transformation into Nanoscrolls. :2–8.

[252] Matusik J, Zenon K. Applied Clay Science Characterization of kaolinite intercalation compounds with benzylalkylammonium chlorides using XRD, TGA / DTA and CHNS elemental analysis. 2013;

[253] Sadik C, Amrani I El, Albizane A. Composition and Refractory Properties of Mixtures of Moroccan Silica-Alumina Geomaterials and Alumina. New Journal of Glass and Ceramics. 2013;2013(April):59–66.

[254] Yuan P, Tan D, Annabi-Bergaya F, Yan W, Liu D, Liu Z. From platy kaolinite to aluminosilicate nanoroll via one-step delamination of kaolinite: Effect of the temperature of intercalation. Applied Clay Science. 2013;83–84(May):68–76.

[255] Astm E313 − 10. Standard Practice for Calculating Yellowness and Whiteness Indices from Instrumentally Measured Color Coordinates. Annual Book of ASTM Standards. 2010;6(C):1–6.

[256] SCORZELLI RB, BERTOLINO LC, LUZ AB, DUTTINE M, SILVA FANG, MUNAYCO P. Spectroscopic studies of kaolin from different Brazilian regions. Clay Minerals. 2008;43(1):129–35.

[257] Kuroda Y, Ito K, Itabashi K, Kuroda K. One-step exfoliation of kaolinites and their transformation into nanoscrolls. Langmuir. 2011;27(5):2028–35.

[258] Yang SQ, Yuan P, He HP, Qin ZH, Zhou Q, Zhu JX, et al. Effect of reaction temperature on grafting of γ-aminopropyl triethoxysilane (APTES) onto kaolinite. Applied Clay Science. 2012;62–63(July 2012):8–14.

[259] Zuo X, Wang D, Zhang S, Liu Q, Yang H. Intercalation and Exfoliation of Kaolinite with Sodium Dodecyl Sulfate. 2018;1–11.

[260] He H, Tao Q, Zhu J, Yuan P, Shen W, Yang S. Silylation of clay mineral surfaces. Applied Clay Science ,. 2013;71:15–20.

[261] Sánchez-Fernández A, Peña-Parás L, Vidaltamayo R, Cué-Sampedro R, Mendoza-Martínez A, Zomosa-Signoret V, et al. Synthesization, Characterization, and in Vitro Evaluation of Cytotoxicity of Biomaterials Based on Halloysite Nanotubes. Materials ,. 2014;7(12):7770–80.

[262] Gomari S, Ghasemi I, Karrabi M, Azizi H. An investigation on non-isothermal crystallization behavior and morphology of polyamide 6/ poly(ethylene-co-1-butene)-graft-maleic anhydride/organoclay nanocomposites. Polyolefins Journal. 2015;2(2):99–108.

[263] Klun Ï, Krz A. Degradation of Polyamide-6 by Using Metal Salts as Catalyst. Polymers for Advanced Technologies. 2003;822(2002):817–22.

[264] Liu TX, Liu ZH, Ma KX, Shen L, Zeng KY, He CB. Morphology, thermal and mechanical behavior of polyamide 6/layered-silicate nanocomposites. Composites Science and Technology. 2003;63(3–4):331–7.

[265] Thomas MG, Abraham E, P J, Pothan LA, Maria HJ, Thomas S. Nanocelluloses from jute fibres and their nanocomposites with natural rubber: preparation and characterisation. International Journal of Biological Macromolecules ,. 2015;81:768–77.

[266] El-saied H, El-sherbiny S, Ali O, El-saied W, Rohyem S. Preparation of Modified Kaolin Filler with Cesium and Its Application in Security Paper. 2013;2013.

[267] Cheng H, Liu Q, Cui X, Zhang Q, Zhang Z, Frost RL. Mechanism of dehydroxylation temperature decrease and high temperature phase transition of coal-bearing strata kaolinite intercalated by potassium acetate. Journal of Colloid and Interface Science. 2012;376(1):47–56.

[268] Refaei DA, Abdelrahman MK, Ibrahim IA, Eldears F, Kandil AT. Improvement the Quality of Egyptian Kaolin for Industrial Applications. International Journal of Advancements in Technology. 2017;8(1):1–6.

[269] Gravelle AJ, Barbut S, Marangoni AG. Influence of particle size and interfacial interactions on the physical and mechanical gels. RSC Advances. 2015;5(July):60723–35

[270] Chris DeArmitt, Hancock M. Filled Thermoplastics. In: Particulate-Filled Polymer Composites. p. 357–424.

[271] Calado V, Barreto DW, D'Almeida JRM. The effect of a chemical treatment on the structure and morphology of coir fibers. Journal of materials Science Letters. 2000;2151–3.

[272] Raji V V, Ramakrishnan S, Sukumar R, Brahmakumar M, Menon AR. Kaolin modified with sodium salt of rubber seed oil as a reinforcing filler for blends of natural rubber, polybutadiene rubber and acrylonitrile–butadiene rubber. Polymer International. 2015;(October 2017).

[273] Hoidy WH, Al-mulla EAJ. Study of preparation for co-polymer nanocomposites using PLA/LDPE/CTAB modified clay. Iraqi National Journal of Chemistry. 2013; 49:61–72.

[274] Beauvais M, Serreau L, Heitz C, Barthel E. How do silanes affect the lubricating properties of cationic double chain surfactant on silica surfaces? Journal of Colloid and Interface Science. 2009;331(1):178–84.

[275] Hou G-X, Chen X-G, Liu J-J, Sang X-M. Morphologies and Mechanical Properties of Polyurethane/ Epoxy Resin Interpenetrating Network Composites Modified with Kaolin. Polymer-Plastics Technology and Engineering. 2011; 50:1208–13.

[276] Guessoum M, Nekkaa S. Effects of Kaolin Surface Treatments on the Thermomechanical Properties and on the Degradation of Polypropylene. 2012;2012.

[277] Letaief S, Tonle IK, Diaco T, Detellier C. Nanohybrid materials from interlayer functionalization of kaolinite. Application to the electrochemical preconcentration of cyanide. Applied Clay Science 2008;42(1–2):95–101.

[278] Georgakilas V, Tiwari JN, Kemp KC, Perman JA, Bourlinos AB, Kim KS, et al. Noncovalent Functionalization of Graphene and Graphene Oxide for Energy Materials , Biosensing , Catalytic , and Biomedical Applications. 2016;

[279] Essabir H, Raji M, Essassi EM, Rodrigue D, Bouhfid R, Qaiss A el kacem. Morphological, thermal, mechanical, electrical and magnetic properties of ABS/PA6/SBR blends with Fe3O4 nano-particles. Journal of Materials Science: Materials in Electronics ,. 2017;

SCIENTIFIQUE PRODUCTION:

Articles (Publications in international journals)

1. Morphological, thermal, mechanical, and rheological properties of high density polyethylene reinforced with Illite clay (**Polymers and Polymer Composites. 2016;16(2):101–13**)

   M. Raji, H. Essabir, E. M. Essassi, D. Rodrigue, R. Bouhfid, A. E. K. Qaiss

2. Influence of graphene oxide and graphene nanosheet on the properties of polyvinylidene fluoride nanocomposites (**Polymers and Polymer Composites. 2017. DOI: 10.1002/pc.24292**)

   M. Raji, H. Essabir, D. Rodrigue, R. Bouhfid, A. E. K. Qaiss.

3. Laminated Epoxy Biocomposites Based on Clay and Jute Fibers (**Journal of Bionic Engineering. 2017;14(2):379–89**)

   H. Abdellaoui, H. Bensalah, **M. Raji**, D. Rodrigue, R. Bouhfid, A. E. K. Qaiss

4. Bio-composites based on polylactic acid and argan nut shell: Production and properties (**International Journal of Biological Macromolecules. 2017;104:30–42**)

   S. Laaziz, **M. Raji**, E. Hilali, H. Essabir, D. Rodrigue, R. Bouhfid, A. E. K. Qaiss

5. Morphological, thermal, mechanical, electrical and magnetic properties of ABS/PA6/SBR blends with Fe3O4 nano-particles (**Journal of Materials Science: Materials in Electronics. 2017;28(22):17120–17130**)

   H. Essabir, **M. Raji**, E. M. Essassi, D. Rodrigue, R. Bouhfid, A. E. K. Qaiss

6. Effect of silane functionalization on properties of polypropylene/clay nanocomposites (**Composites Part B. 2018;146(April):106–15**)

   M. Raji, M.E.M, Mekhzoum, D. Rodrigue, R. Bouhfid, A. E. K. Qaiss

7. Thermo-mechanical performances of polypropylene biocomposites based on untreated, treated and compatibilized spent coffee grounds (**Composites Part B (2018), DOI: 10.1016/ j.compositesb.2018.05.020**)

H. Essabir, **M. Raji,** S. Laaziz, D. Rodrigue, R. Bouhfid, A. E. K. Qaiss

8. Utilization of volcanic amorphous aluminosilicate rocks (perlite) as alternative materials in lightweight composites (**Composites Part B: Engineering. 2019, DOI: 10.1016/j.compositesb.2018.11.098**)

   M. Raji, S. Nekhlaoui, I.E. Amrani, E. M. Essassi, H. Essabir, D. Rodrigue, R. Bouhfid, A. E. K. Qaiss

9. Black phosphorus-based polyvinylidene fluoride nanocomposites: Synthesis, processing and characterization (**Composites Part B: Engineering (2019), 175, 107165**)

   G. Tiouitchi, **M. Raji**, O. Mounkachi, M. AitAli, A. Mahmoud, F. Boschini, H. Essabir, R. Bouhfid, A. E. K. Qaiss

10. N-Silylated Benzothiazolium Dye as a Coupling Agent for Polylactic Acid/Date Palm Fiber Bio-composites (**Journal of Polymers and the Environment (2019), 27 (12), 2974-2987**)

    FZSA Hassani**,** W. Ouarhim**, M. Raji**, M.E.M, Mekhzoum, MO. Bensalah, H. Essabir, D. Rodrigue, R. Bouhfid, A. E. K. Qaiss.

Brevet

1. Matériau conducteur électrique à base de mousse de polymère **(MA39099, 2017)**

M. Raji, R. Bouhfid, A. E. K. Qaiss

Chapitre d'ouvrage

1. Nanoclay and Natural Fibers Based Hybrid Composites: Mechanical, Morphological, Thermal and Rheological Properties. In: Nanoclay Reinforced Polymer Composites, 2016. p. 29–49

   H. Essabir, **M. Raji**, R. Bouhfid, A.E.K. Qaiss

2. Nanoclay Modification and Functionalization for Nanocomposites Development: Effect on the Structural, Morphological, Mechanical and Rheological Properties. In: Nanoclay Reinforced Polymer Composites, 2016. p. 1–34

   M. Raji, El M, Mekhzoum , R. Bouhfid, A.E.K. Qaiss

3. Impact of Chemical Treatment and the Manufacturing Process on Mechanical, Thermal, and Rheological Properties of Natural Fibers- Based Composites. In: Handbook of Composites from Renewable Materials, Hoboken, NJ, USA: John Wiley & Sons, Inc.; 2017. p. 225–52

M. Raji, H. Essabir, R. Bouhfid, A.E.K. Qaiss

4. Nanoclay and polymer-based nanocomposites: Materials for energy efficiency. In: Polymer-based Nanocomposites for Energy and Environmental Applications Published Woodhead. 2018. p. 75–103

   N. Zari, **M. Raji**, H El. Mghari, R. Bouhfid, A.E.K. Qaiss

5. Prediction of the cyclic durability of woven-hybrid composites. In: Durability and Life Prediction in Biocomposites, Fibre-Reinforced Composites and Hybrid Composites Publieshed Woodhead Publishing Series in Composites Science and Engineering . 2019, Pages 27-62

   M. Raji, H. Abdellaoui, H. Essabir, C.A. Kakou, R. Bouhfid, A.E.K. Qaiss

6. Rheological Properties of Functionalized Graphene and Polymeric Matrices–Based Nanocomposites. In: Functionalized Graphene Nanocomposites and Their Derivatives Synthesis, Processing and Applications Micro and Nano Technologies. 2019, Pages 109-120

   H. Essabir, **M. Raji**, R. Bouhfid, A.E.K. Qaiss

7. Durability of composite materials during hydrothermal and environmental aging. In : Durability and Life Prediction in Biocomposites, Fibre-Reinforced Composites and Hybrid Composites. Published Woodhead Publishing Series in Composites Science and Engineering. 2019, Pages 83-119

   M. Raji, N. Zari, R. Bouhfid, A.E.K. Qaiss

8. Chemical Preparation and Functionalization Techniques of Graphene and Graphene Oxide. In: Functionalized Graphene Nanocomposites and Their Derivatives Synthesis, Processing and Applications Micro and Nano Technologies. 2019, Pages 0-20

   M. Raji, N. Zari, R. Bouhfid, A.E.K. Qaiss

9. Functionalized Graphene and Thermoset Matrices Based Nanocomposites: Mechanical and Thermal Properties. In: Functionalized Graphene Nanocomposites and Their Derivatives Synthesis, Processing and Applications Micro and Nano Technologies. 2019, Pages 47-94

   N. Bouhfid, **M. Raji**, MO.Bensalah, A.E.K. Qaiss

10. Investigation of the deformation behavior of epoxy-based composite materials. In: Failure Analysis in Biocomposites, Fibre-Reinforced Composites and Hybrid Composites. Published: Woodhead Publishing Series in Composites Science and Engineering. 2019, Pages 29-49

H. Abdellaoui, **M. Raji**, R. Bouhfid, A.E.K. Qaiss

11. Mechanical behavior of carbon/natural fiber-based hybrid composites. In: Mechanical and Physical Testing of Biocomposites, Fibre-Reinforced Composites and Hybrid Composites. Published : Woodhead Publishing Series in Composites Science and Engineering. 2019, Pages 103-122.

    H. Abdellaoui, **M. Raji**, H. Essabir, R. Bouhfid, A.E.K. Qaiss

12. Numerical modeling of hybrid composite materials.In: Modelling of Damage Processes in Biocomposites, Fibre-Reinforced Composites and Hybrid Composites. Published: Woodhead Publishing Series in Composites Science and Engineering. 2019, Pages 57-101

    N. Bouhfid, **M. Raji**, R. Boujmal, H. Essabir, MO.Bensalah, R. Bouhfid ,A.E.K. Qaiss

13. Properties of Nano-composites Based on Different Clays and Polyamide 6/Acrylonitrile Butadiene Styrene Blends: Preparation, Processing, Properties & Performance. In book: Bio-based Polymers and Nanocomposites; Preparation, Processing, Properties & Performance, springer International Publishing. 2019, Pages 107-128

    M. Raji, E. M. Essassi, H. Essabir, D. Rodrigue, A.E.K. Qaiss, R. Bouhfid.

14. Nanofibrillated Cellulose-Based Nanocomposites: Preparation, Processing, Properties & Performance. In book: Bio-based Polymers and Nanocomposites; Preparation, Processing, Properties & Performance, springer International Publishing. 2019, Pages 67-86

    H. Abdellaoui, **M. Raji**, H. Essabir, R. Bouhfid, A.E.K. Qaiss

Communications

1. Oral presentation “Effect of clay structure and clay content on thermoplastic composites properties” at 1st International UPM-MAScIR-FSR Symposium “Composites Nanocomposites Materials” (ISymposite 2019), 08/10-04-2019, Rabat, Morocco.

2. poster presentation “Effect of clay type and clay surface modification on the thermoplastic composites properties” at 1st International UPM-MAScIR-FSR Symposium “Composites Nanocomposites Materials” (ISymposite 2019), 08/09-04-2019, Rabat, Morocco.

3. Oral presentation “Preparation and characterization of composites filled with bleached and functionalized kaolinite nano-particles” at Workshop MSN-UM6P & CNC-MAScIR), 25-02-2019, benguerir, Morocco.